The University of Osaka
Institutional Knowledge Archive

Title	Neural and Behavioral Dynamics within the Dynamical System with Complex Networks
Author(s)	朴, 志勲
Citation	大阪大学, 2019, 博士論文
Version Type	VoR
URL	https://doi.org/10.18910/73463
rights	
Note	

The University of Osaka Institutional Knowledge Archive : OUKA

https://ir.library.osaka-u.ac.jp/

The University of Osaka

Doctoral Dissertation

Neural and Behavioral Dynamics within the Dynamical System with Complex Networks

Jihoon Park

March 2019

Graduate School of Engineering
Osaka University

Supervisor: Dr. Minoru Asada

Title: Neural and Behavioral Dynamics within the Dynamical System with Complex Networks

Committee: Dr. Minoru Asada, Chair
Dr. Koh Hosoda
Dr. Yusuke Doi

Copyright © 2019 by Jihoon Park
All Rights Reserved.

Abstract

Diverse behaviors of animals and their transitions emerge from the complex interactions between the brain and the body, leads to self-organization of attractors and their transitions in the dynamical system with constraints of the structure of the body and the brain. This thesis investigates how the brain activities relate to the macroscopic structure of the brain and affect to behavioral dynamics using computational model with complex network theory. First, simulations are conducted using a spiking neural network model to examine how the macroscopic network in the brain is related to the complexity of activity in each region and to functional networks, which is estimated by phase coherence between neural activity in each region. The results of the study showed the following. Local over-connectivity of a neuron group in the network model (1) increases the firing rate of neurons, and therefore, enhances the strength of the connections from excitatory to inhibitory neurons; (2) decreases the complexity of neural activity, while increasing the intensity of specific frequency components of neural activity in a neuron group; (3) increases functional connectivity derived from the synchronization of neural activity.

Second, we conducted a series of simulations using non-linear oscillator networks with different macroscopic networks and a musculoskeletal model (i.e., a snake-like robot) as a physical body, to understand how the coupled neural and behavioral dynamics affect the emergence as well as transitions of behaviors. A behavior analysis (behavior clustering) and network analysis for the classified behavior were then applied. The former consisted of feature vector extraction from the motions and classification of the behaviors that emerged from the coupled dynamics. The coupled dynamics underlying the classified behaviors were revealed by estimating the functional networks using mutual information and transfer entropy. The results showed the following. (1) The number of behaviors and their duration depended on the sensor ratio to control the balance of strength between the body

and brain dynamics, as well as on structural properties of certain non-linear oscillator networks. (2) Two types of functional networks underlie two types of behaviors, with different durations, by utilizing complex network theory, a clustering coefficient, and the shortest path length with a negative and a positive relationship with the duration periods of behaviors. Finally, we discuss relationship of our results with those of previous studies and propose future directions.

Acknowledgments

This thesis would not have been possible without the support of many mentors, colleagues, friends, and my family. I wish to express my gratitude to all of them. I want to thank my supervisor professor Minoru Asada who gave me the opportunity to do study in Japan. I am sure I could not have completed PhD course without his great guidance and valuable comments throughout many years. I am thankful to professor Koh Hosoda and Assistant Professor Yusuke Doi for serving as members of my thesis committee, and for their valuable comment to greatly improve the quality of this thesis. I greatly thank Associate Professor Hiroki Mori in Waseda University. He introduced me to the interesting topics about constructive approach with complex system for cognitive developmental science, and I learned a lot from working with him. I am sure I could not have finished the this thesis without his help on so many levels. I also thanks to Dr. Joschka Boedecker. I learned a lot of knowledge and programming skills about the neural network from him and it was useful to do researches during the master and PhD courses. I'd also like to thank many friends, colleagues and former member in the lab: Dr. Yuji Kawai, Dr. Takato Horii, Dr. Tomoyo Morita, Dr. Hisashi Ishihara, Dr. Yuji Sasamoto, Dr. Jimmy Baraglia, Dr. Takumi Kawasetsu, Ryo Iwaki, Dr. Takashi Ikeda, Dr. Hideyuki Takahashi, Dr. Nobutsuna Endo, Dr. Hiroki Yokoyama, Dr. Yukie Nagai. Valuable discussions at the meeting and enjoyable daily life with theme helped to complete this thesis. Further, I'd like to thank Yuji Okuyama, Junichi Suzuki and Koki Ichinose who played a valuable role to complete the journal papers as a co-author and former student in the lab. Also, I would like to express my gratitude to Woori Bae, Jongbeom Park, Junghwa Park who advised me to have a good life in Japan. In fact, all members of the Asada lab and many people have surely supported me, and I'd like to thank them. Last but certainly not least, I would like to thank to my family in Korea.

Contents

1 Introduction **3**

1.1 Background 3

1.2 Problem Statement and Thesis Objectives 5

1.3 Structure of the Thesis 6

2 Related works **9**

2.1 Anatomical and Functional Network Structures in the Brain 9

2.2 Complexity of Brain Activities 10

2.2.1 Imaging Studies 10

2.2.2 Computational Model for Relationship between Connectivity and the Complexity of Neural Activities 11

2.3 Dynamics between the Brain and Body 12

2.3.1 Relationship with Diverse Behaviors 12

2.3.2 Dynamical System and Chaotic Itinerancy 13

2.3.3 Computational Model for Emergence of Behaviors 14

3 Complexity of Neural Activity in Macroscopic Cluster Organization **17**

3.1 Problem Statement 17

3.2 Spike Neural Network Model 19

3.2.1 Neuron Model 19

3.2.2 Construction of a Fundamental Network using the Watts and Strogatz Model 20

3.2.3 Self-organization in a Spike Neural Network Model 21

3.2.4 Parameters and Simulation Setting 22

3.3 Analysis method for neural activity 23

3.3.1 The Complexity of Neural Activity 23

3.3.2 Neural Activation in Neuron Groups 24
3.3.3 Graph Analysis of Network Structure 25
3.4 Results 27
3.4.1 Relationship between MSE and the WS Model 28
3.4.2 Neural Activities in Neuron Groups with Different Levels of the Complexity 29
3.4.3 Relationship between Neural Activity and Structural Properties 33
3.5 Discussion 37
3.5.1 Hypothetical Mechanism of Low Complexity Caused by Local Over-connectivity 38
3.5.2 Relationship to Studies on ASD 40

4 Chaotic Itinerancy from the Coupled Dynamics 41
4.1 Problem Statement 41
4.2 Model 44
4.2.1 Synaptic Network with Nonlinear Oscillators 44
4.2.2 Complex Networks for Fundamental Network 47
Small-world Network 47
Scale-free Network 47
4.2.3 Network Structures of Nonlinear Oscillators 47
4.2.4 Snake-like Robot 48
4.2.5 Parameters and Simulation Setting 51
4.3 Method for analysis of the Neural and Behavioral Dynamics 51
4.3.1 Analysis of the Behavior Pattern 51
4.3.2 Functional Network within Behaviors 53
4.4 Results 55
4.4.1 Movement of the Snake-like Robot 55
4.4.2 Relationship between Various Movements and the Synaptic Network 56
4.4.3 Analysis of the Functional Network 56
4.5 Discussion 60

4.5.1 Role of the Body and Brain Dynamics in Bodily Chaotic Itinerancy 60
4.5.2 Network Structure of Functional Network Underlying Behaviors and Transition of Behaviors 64
4.5.3 Influence of the Network Types on the Number and Duration of Behaviors 65

5 Conclusion **67**
5.1 Summary and Contributions 67
5.2 Directions for Future work 68
5.2.1 Extension of Parameters of Macro- and Microscopic Network Model 68
5.2.2 Role of Subnetworks and Dynamical Changing 69
5.2.3 Learning Method and Self-organization of Networks for Tasks using Coupled Dynamics 69
5.2.4 Effect of Morphology of Body and Environment 70

A Data for all p_{WS} **73**

B Effect of tonic input for emergence of behaviors **79**

Bibliography **87**

List of Figures

1.1 Overview of research topic in the thesis 6

2.1 Graphical representation of previously proposed models [67, 78, 66, 119]. (a) No connectivity is found between the interface neurons [67, 78]. Furthermore, the hidden neurons, which are considered as a cortex to represent brain dynamics, are missing. (b) Hidden neurons are observed, but there is no connectivity is found between the interface neurons [66]. (c) Constant input from the hidden neurons is provided to the interface neurons, and the hidden neurons have no influence on the body to generate motor behavior [119]. 15

3.1 Hypothesis and assumptions about relationships among the fundamental network, synaptic network, the complexity of neural activity. The black node and empty black circle represent a neuron group and a neuron in the group, respectively. The black and green lines indicate an intraconnection between neurons in a neuron group, and an interconnection between neurons in different neuron groups, respectively. The red and blue dots show neuron groups with and without high clustering coefficient and high shortest path length, respectively 18

3.2 Overview of spiking neural network model. A network is created using 100 neuron groups with macroscopic connections between neuron groups based on the Watts and Strogatz model [118]. The black nodes and green edge represent the neuron groups and macroscopic connections, respectively. (a) A lattice network, where each node is connected with neighboring nodes, has local over-connectivity. All connections are rewired with rewiring probability p_{WS}, and p_{WS} increases randomness. (b) A small-world network with a large number of clusters and shorter path length compared with other networks. (c) A random network where nodes are completely randomly connected to each other. (d) Each neuron group contains 800 excitatory (red dots) and 200 inhibitory (blue dots) spiking neurons, and each neuron has intra- (black line with arrow) and inter-connections (green line with arrow). 19

3.3 Time schedule for simulation. Each colored area indicates the time at which the event occurred. Neural activities during 1110 s to 1200 s were analyzed to determine the relationship among the structural properties of the synaptic network, neural activity, and the functional network. 23

3.4 Examples of the clustering coefficient, degree centrality, and path length. (a) Clustering coefficient of the ith node. The clustering coefficient indicates the density of the number of closed triplet connections (red and blue connections) between nodes in a network (Section 3.3.3). Here, the dashed line indicates a possible connection. (b) The path length from the ith node to the jth node. Path length represents the distance of an arbitrary route from node i to node j, and the shortest path length represents the distance of the shortest route from i to j (red line). (c) Degree centrality of the ith node. Degree centrality refers to the number of connections of a node (red connections). 25

3.5 The relationship between sample entropy and p_{WS} of the WS model. The x-axis in all graphs represents p_{WS} (the rewiring probability of the Watts and Strogatz model [118]). (a)-(f) Average sample entropy of all neuron groups with ten independent simulations at scale factors (€ in equation 3.7) of MSE at 1, 10, 20, 40, 60, and 80. The error bars indicate the standard deviation. 28

3.6 Amplitude of each frequency spectrum sampled from the LAP of the 10 neuron groups with low complexity (blue) and high complexity (red) in a network. The peak envelopes are used to plot the curve in the figure. Color curves and color-shaded areas represent average and standard deviation values for ten simulations, respectively. (a) The lattice network ($p_{WS} = 0.0$) during self-organization by STDP (0-100 s). (b) The random network ($p_{WS} = 1.0$) during self-organization by STDP (0-100 s). (c) The lattice network ($p_{WS} = 0.0$) after self-organization by STDP (1100-1200 s). (d) The random network ($p_{WS} = 1.0$) after self-organization by STDP (1100-1200 s). 29

3.7 The difference in summation of MSE for 80 scale factors between the band-phase-surrogate LAP signal in specific frequency bands and the original LAP signal. The x-axis indicates the frequency band for the surrogate, and the y-axis indicates the difference in summation of MSE for 80 scale factors between surrogate and original data. The number on above each violin plot denotes the average value. Surrogate was performed 100 times for each neuron group that has the lowest complexity in the lattice network for each of the 10 simulations. See Table. A.1 for statistical differences, based on the Tukey-Kramer test. 30

3.8 Autocorrelation of the number of fired neurons sampled in non-overlapping time windows of $\Delta t_w = 5$ ms in a lattice network ($p_{\mathrm{WS}} = 0.0$). The x-axis represents the lag of the window, and the y-axis represents the autocorrelation. The black curves and blue shaded area represent the average and standard deviation for ten simulations, respectively. (a) Autocorrelation of fired excitatory neurons in a neuron group with the lowest complexity during the later period (1100-1102 s). (b) Autocorrelation of fired inhibitory neurons in a neuron group with the lowest complexity during the later period (1100-1102 s). (c) Autocorrelation of fired excitatory neurons in a neuron group with the highest complexity during the later period (1100-1102 s). (d) Autocorrelation of fired inhibitory neurons in a neuron group with the highest complexity during the later period (1100-1102 s). The dashed line and solid line represent the 95% and 99% confidence intervals, respectively. 32

3.9 Relationship between the connectivity structure and the complexity of neural activity. Each marker corresponds to a neuron group in the network, and its color indicates the summation of the sample entropy for all 80 scale factors. The x-axis indicates the degree centrality, and the y-axis indicates the clustering coefficient. 33

3.10 Relationship between the peak frequency and complexity of neural activity. (a) Relationship in the 0-20 Hz band. (b) Relationship in the 20-40 Hz band. (c) Relationship in the 40-60 Hz band. Each marker corresponds to a neuron group in the network, and its color indicates the summation of the sample entropy for all 80 scale factors. The x-axis indicates the peak frequency of neural activity, and the y-axis indicates the amplitude. 35

3.11 Relationship between the connectivity structure and firing rate of excitatory and inhibitory neurons. Each marker corresponds to a neuron group in the network, and its color indicates the average firing rate of excitatory and inhibitory neurons. The x-axis indicates the degree centrality, and the y-axis indicates the clustering coefficient. (a) Relationship between structural properties and firing rate of excitatory neurons. (b) Relationship between structural properties and firing rate of inhibitory neurons. 35

3.12 Relationship among the weight of intraconnection, structural properties of the synaptic network, and the complexity of neural activity. (a) Relationship among the weight of intraconnection from excitatory to excitatory neuron, clustering coefficient based on the interconnection, and the complexity. (b) Relationship among the weight of intraconnection from excitatory to inhibitory neuron, clustering coefficient based on the interconnection, and the complexity. (c) Relationship among the weight of intraconnection from excitatory to excitatory neuron, degree centrality based on the interconnection, and the complexity. (d) Relationship among the weight of intraconnection from excitatory to inhibitory neuron, degree centrality based on the interconnection, and the complexity. Each marker corresponds to a neuron group in the network, and its color indicates the summation of the sample entropy for all 80 scale factors. The x-axis indicates the average weight of interconnection, and the y-axis the structural properties of interconnection. 36

3.13 Schematic representation of a possible mechanism of reduction of complexity of neural activity in a neuron group with local over-connectivity. The red and blue solid circles represent excitatory and inhibitory neurons, respectively. The transparency of color of solid circles represents the firing rate of neurons. The black and green lines with arrows represent intraconnection between neurons in the same neuron group and interconnection between neurons in different neuron groups, respectively. The thickness of a line with an arrow represents the weight of connectivity. (a) A fundamental network and a neuron group with local over-connectivity. The green line without an arrow represents the edge between neuron groups. (b) Relationship between the strength of connectivity from inhibitory neurons to excitatory neurons, with the firing time of neurons. The vertical black bar on the time axis indicates the firing of a neuron. The firing rate of inhibitory neurons with a strong connectivity from excitatory neurons increases, and therefore, inhibitory neurons strongly affect other excitatory neurons. The excitatory neurons that are strongly influenced by inhibitory neurons show a synchronous firing pattern and therefore induce periodical oscillation of neural activity; (c) A LAP signal of neural activity in a neuron group and the amplitude of frequency spectrum of the LAP signal. 39

4.1 Hypothesis and assumptions about relationship among the synaptic and functional network, body, emergence of behaviors, and their transitions in this study. The black node represents non-linear oscillator, signifying the dynamics of brain regions. The green and orange lines indicate synaptic and functional connections between oscillators, respectively. The blue dots and their black lines with arrow represent attractors, which self-organized behaviors from the coupled dynamics, and their transitions. The curved arrows in (c) indicate a ratio between the brain and body dynamics on the coupled dynamics. 43

4.2 Overview of snake-like robot with a synaptic network with nonlinear oscillator. (a) Snake-like robot. (b) Physical model of the snake-like robot. (c) A graphical representation of the model in this study. The sensor and actuator connect with the interface neurons. Additionally, interface and hidden neurons (oscillator) are interacting with each other and other neurons in the same layer, through synaptic connections. That is, brain dynamics (hidden neurons) affect the behavior of the body, and body dynamics also affect brain dynamics through interface neurons. The variable of α adjusts the ratio of body dynamics to brain dynamics in coupled dynamics. 45

4.3 Complex network properties of synaptic networks employed in the experiments. The number in each box plot denotes the value of the median of 100 measurements for different experimental settings for each network type. (a) Average clustering coefficient for the uniform weights. (b) Average clustering coefficient for the randomly distributed weights. (c) Average shortest path length for the uniform weights. (d) Average shortest path length for the randomly distributed weights. . 49

4.4 Maximum node degree of the synaptic network employed in the experiments. The number in each box plot denotes the value of the median of 100 measurements for different experimental settings for each network type. (a) Uniform weights and (b) randomly distributed weights. 50

4.5 Example of forward crawling movement of the robot. 55

4.6 Example of bending movement of the robot. 55

4.7 Example of the feature vector and transitions of the state vector in the dimensionally-reduced space by Laplacian eigenmaps (WS model ($p = 0.05$) with randomly distributed weights, a tonic input of 0.4, and a sensor ratio of 0.3). (a) The blue dots represent an unstable behavior. The dots with other colors represent stable behaviors. The bar graphs show the histogram of data points along the x and y axes. (b) The black circle represents current state in the feature space. 57

4.8 Number of behaviors and maximum duration of behavior for a uniform weight. The tonic input is 0.45. (a) Number of behaviors, (b) number of stable behaviors, and (c) maximum duration of behaviors. The x-axis indicates the sensor ratio required α in Eq (4.3) to control the proportional influences between the body and the network. *** $p < 0.001$, ** $p < 0.01$, * $p < 0.05$, · $p < 0.1$ indicate statistically significant differences between the synaptic networks through the ANOVA test. 58

4.9 Number of behaviors and maximum duration of behavior for a randomly distributed weight. The tonic input is 0.45. (a) Number of behaviors, (b) number of stable behaviors, and (c) maximum duration of behaviors. The x-axis indicates the sensor ratio required α in Eq (4.3) to control the proportional influences between the body and the network. *** $p < 0.001$, ** $p < 0.01$, * $p < 0.05$, · $p < 0.1$ indicate a statistically significant differences between the synaptic networks through the ANOVA test. 59

4.10 Estimated functional network structures for different movement durations: 329.5 s (longer) and 32.5 s (shorter). (a), (b) Number of neurons in each subnetwork for 329.5 s and 32.5 s, respectively. The red and black bars indicate hidden and interface neurons. (c) Synaptic network with a musculoskeletal movement and two different functional networks. Each node indicates an IRM-extracted subnetwork, and the node sizes indicate the number of neurons in each subnetwork. 61

4.11 Structural property of the functional network for the uniform weights. Each red line in the figure indicates a correlation. (A) Average clustering coefficient and (B) average shortest path length. 62

4.12 Interaction between the body and the network in terms of the duration of periodic movements for the uniform weights. The red line in the figure indicates a correlation: average of transfer entropy from the interface neurons to hidden neurons. 63

A.1 Multiscale entropy (MSE)-based complexity curves of each neuron group in a synaptic network. (a) Lattice network ($p_{\mathrm{WS}} = 0.0$). (b) A small-world network ($p_{\mathrm{WS}} = 0.1$). (c) A random network ($p_{\mathrm{WS}} = 1.0$). The y-axis indicates sample entropy, and the x-axis indicates scale factor € 73

A.2 The differences of peak amplitude of spontaneous neural activity in some frequency bands between neuron groups with low and high complexity when $p_{WS} = 0.0$. We used 10 neuron groups with high and low complexity in each simulation as comparison data. The number on above each violin plot denotes the average value for ten simulations. Wilcoxon signed-rank test was used for statistical test. (a) Amplitude in the 20-40 Hz band (Wilcoxon signed-rank test, statistic=6.0, p-value=4.6706e-18); (b)) Amplitude in the 40-60 Hz band (Wilcoxon signed-rank test, statistic=11.0, p-value=5.4302e-18). 74

A.3 Relationship between the connectivity structure and the complexity of neural activity. Each marker corresponds to a neuron group in the network, and its color indicates the summation of the sample entropy for all 80 scale factors. The x-axis indicates the degree centrality, and the y-axis indicates the clustering coefficient. 74

A.4 Relationship between the peak frequency and the complexity of neural activity. (a) Relationship in the 0-20 Hz band. (b) Relationship in the 20-40 Hz band. (c) Relationship in the 40-60 Hz band. Each marker corresponds to a neuron group in the network, and its color indicates the summation of the sample entropy for all 80 scale factors. The x-axis indicates the peak frequency of the neural activity, and the y-axis indicates the amplitude. 75

A.5 Relationship between the connectivity structure and the firing rate of excitatory and inhibitory neurons. Each marker corresponds to a neuron group in the network, and its color indicates the average firing rate of excitatory and inhibitory neurons. The x-axis indicates the degree centrality, and the y-axis indicates the clustering coefficient. (a) Relationship between structural properties and firing rate of excitatory neurons. (b) Relationship between structural properties and firing rate of inhibitory neurons. 75

A.6 Relationship among the weight of intraconnection, structural properties, and complexity of neural activity. (a) Relationship among the weight of intraconnection from excitatory to excitatory neuron, clustering coefficient based on the interconnection, and complexity. (b) Relationship among the weight of intraconnection from excitatory to inhibitory neuron, clustering coefficient based on the interconnection, and complexity. (c) Relationship among the weight of intraconnection from excitatory to excitatory neuron, degree centrality based on the interconnection, and complexity. (d) Relationship among the weight of intraconnection from excitatory to inhibitory neuron, degree centrality based on the interconnection, and complexity. Each marker corresponds to a neuron group in the network, and its color indicates the summation of the sample entropy for all 80 scale factors. The x-axis indicates the average of weight of interconnection, and the y-axis the structural properties of interconnection. 76

A.7 Relationship between shortest path length and complexity for each neuron group. The x-axis is the shortest path length, and the y-axis is the summation of the sample entropy for all 80 scale factors. 77

A.8 Relationship between the connectivity structure without STDP and the complexity of neural activity with the tonic input. Duration for tonic input was set as 100 s. Here, we used the same initial weights of the synaptic networks in the Figure A.3 and fixed the weights during the tonic input. Each marker corresponds to a neuron group in the network, and its color indicates the summation of the sample entropy for all 80 scale factors. The x-axis indicates the degree centrality, and the y-axis indicates the clustering coefficient. There is no clear relationship between the complexity and structural properties of synaptic network compared to the Figure A.3 78

B.1 Number of movement patterns for uniform weights. The tonic input for each graph is 0.4 (A), 0.45 (B), 0.5 (C),or 0.55 (D). The x-axis indicates the sensor ratio necessary α in Eq (4.3) to control the proportional influences between the body and the network. *** $p < 0.001$, ** $p < 0.01$, * $p < 0.05$ and $\cdot$ $p < 0.1$ indicate a statistically significant differences between the wired networks through the ANOVA test. . . 80

B.2 Number of movement patterns for randomly distributed weights. The tonic input for each graph is 0.4 (A), 0.45 (B), 0.5 (C),or 0.55 (D). The x-axis indicates the sensor ratio necessary α in Eq (4.3) to control the proportional influences between the body and the network. *** $p < 0.001$, ** $p < 0.01$, * $p < 0.05$ and $\cdot$ $p < 0.1$ indicate a statistically significant differences between the wired networks through the ANOVA test. . . 81

B.3 Number of stable movement patterns for uniform weights. The tonic input for each graph is 0.4 (A), 0.45 (B), 0.5 (C),or 0.55 (D). The x-axis indicates the sensor ratio necessary α in Eq (4.3) to control the proportional influences between the body and the network. *** $p < 0.001$, ** $p < 0.01$, * $p < 0.05$ and $\cdot$ $p < 0.1$ indicate a statistically significant differences between the wired networks through the ANOVA test. . . 82

B.4 Number of stable movement patterns for randomly distributed weights. The tonic input for each graph is 0.4 (A), 0.45 (B), 0.5 (C),or 0.55 (D). The x-axis indicates the sensor ratio necessary α in Eq (4.3) to control the proportional influences between the body and the network. *** $p < 0.001$, ** $p < 0.01$, * $p < 0.05$ and $\cdot$ $p < 0.1$ indicate a statistically significant differences between the wired networks through the ANOVA test. 83

B.5 Maximum duration of the movement pattern for uniform weights. The tonic input for each graph is 0.4 (A), 0.45 (B), 0.5 (C),or 0.55 (D). The x-axis indicates the sensor ratio necessary α in Eq (4.3) to control the proportional influences between the body and the network. *** $p < 0.001$, ** $p < 0.01$, * $p < 0.05$ and $\cdot$ $p < 0.1$ indicate a statistically significant differences between the wired networks through the ANOVA test. 84

B.6 Maximum duration of the movement patterns for randomly distributed weights. The tonic input for each graph is 0.4 (A), 0.45 (B), 0.5 (C),or 0.55 (D). The x-axis indicates the sensor ratio necessary α in Eq (4.3) to control the proportional influences between the body and the network. *** $p < 0.001$, ** $p < 0.01$, * $p < 0.05$ and $\cdot$ $p < 0.1$ indicate a statistically significant differences between the wired networks through the ANOVA test. 85

List of Tables

3.1 Parameters of the simulation model used in this study. 22

4.1 Setting of the snake-like robot. 51

A.1 Statistical comparisons with Tukey–Kramer test among MSE of LAP signals and MSE of band-pass randomized surrogate LAP signals in a specific frequency bands. In the table, Meandiff indicates the difference in mean value between the compared groups. Lower and Upper mean lower limit and upper limit of confidence interval, respectively. 77

A.2 Correlation coefficient among the complexity, structural properties of synaptic and functional networks for all values of p_{WS} of ten simulations. In the table, Clustering_S and Clustering_F represent clustering coefficient of synaptic and functional networks in each frequency bands, respectively. Degree_S and Degree_F represent degree centrality of synaptic and functional networks in each frequency bands, respectively. In all cases, p-value < 2.2e-16. 78

Chapter 1

Introduction

1.1 Background

The brain is a complex network, comprised of anatomical connections between brain regions. It shows various dynamics, which causes different rhythmic synchronized and desynchronized patterns among brain regions. Diverse behaviors and behavioral transitions emerge from the coupling of dynamics between the body and such neural dynamics in the environment. Additionally, recent studies have implied that cognitive functions and behaviors arise from the dynamically changing interactions between brain regions, rather than from neural activity in only one specific area in the brain [29, 15]. How these complex and nonlinearly coupled dynamics between the neural dynamics in the network and body dynamics relates to emergence of behaviors is fundamental question in neuroscience and developmental science. To address this issue, we have to understand what kind of neural activity in the network is organized and how it contributes the emergence of behaviors through interaction with body dynamics from the perspective of the complex system.

The brain can be considered as a complex network that consists of anatomical connections between brain regions (i.e., an anatomical network). Many studies using brain-imaging technique with complex network theory have shown that the anatomical network has specific complex network structural properties [101, 30, 55]. On the contrary, several studies about the brain of autism spectrum disorder (ASD) show that the structures in anatomical network [95], and the brain activity itself [14, 43] are atypical. ASD is a neurodevelopmental disorder characterized by impairments in social interaction, repetitive behavior, and sensory abnormalities.

Altogether, these studies have been suggesting that the unique structural properties of the brain are closely related to the brain activity itself. However, it remains unclear how the macroscopic network structure affects neural activity and relates to the emergence of behaviors.

Several studies discuss the importance of brain dynamics for the emergence of varied and complex behaviors from the perspective of the development of fetus and infant. Hadders-Algra [48, 49, 47] discussed the importance of subplate, which contributes to building thalamocortical pathways, for development of diverse behaviors based on the similarity of the timing of appearance of the subplate and the timing of emergence of general movement (GM), which is the various and complex spontaneous whole-body movement of the fetus. Further, Spittle et al. [99] showed that the infant with an abnormality in the volume of white matter has an abnormality on the GM. These studies imply that the brain dynamics in the cortex may contribute to emergence of diverse behaviors through interaction with body dynamics. However, it is still not clear how the diverse behaviors and their transitions emerge through the interaction between the brain and the body dynamics, which have different constraints and time scales.

Several studies have proposed a computational model to understand how the network structure of the brain relates to brain activities [79, 90, 120, 58]. For instance, Izhikevich and Edelman [58] constructed a large-scale model using spiking neurons, based on detailed data of mammalian thalamocortical systems, to investigate the complex dynamics caused by a neuronal process in the brain. They showed that, in the model, brain-like spontaneous activity occurs over various frequency bands. However, since these models were constructed based on detailed brain data, which involves a large number of parameters, it is difficult to understand which factors are dominant in inducing complex brain dynamics. Furthermore, models do not involve a physical body; therefore, it is difficult to use a model to gain understanding of the relation between change in neural activity within behaviors that emerge from the coupled dynamics between the brain and body.

A dynamical system approach has been used to explain the complex interaction between the brain and the body in an environment for artificial intelligence [9], cognitive science [92, 88, 106], and developmental psychology [93, 10, 110]. Kuniyoshi

and Suzuki [67] constructed a computational model consisting of musculoskeletal and neural systems based on chaotic dynamics. This model showed that the emergence of adaptive behaviors through interaction with the environment. As an extensional of their model [67], a detailed infant [66] and fetus models [78, 119] have also been proposed. These studies showed that the interaction between the body and the neural system within the environment is important for emergence of infant- or fetus-like whole-body movements. However, these studies did not focus on the coupled dynamics between the brain and body that underline these emergent behaviors and their transitions. Furthermore, some models have not expressed coupled dynamics between the brain and body (detailed in Section 2.2.2).

1.2 Problem Statement and Thesis Objectives

In this thesis, we address the following main question from a dynamical system approach by using information theory and complex network theory.

How do coupled dynamics between the neural dynamics in the complex network and the body dynamics affect to emergence of behaviors?

We break this main question into two sub-questions which will be addressed in the main part of this thesis:

- How is the macroscopic structure of the brain related to neural dynamics?
- How does the interaction between neural dynamics in the network and body dynamics affect the emergence of behaviors?

In order to address each of the above questions, we construct simulation models to express the dynamic properties of the brain and the body, and their interactions under the constraints of a macroscopic network. We then adjust the structural properties of the macroscopic network in the brain and ratio of the brain to body dynamics affecting the coupled dynamics. This approach would enable us to understand more clearly how different macroscopic networks affect neural activity and how this neural activity influences the emergence of behaviors through interaction with the body. The first question is addressed using a spiking neural network model, which

can express the complex neural activities consisting of multiple frequency components (orange area in Figure 1.1), in Chapter 3. In this model, we control the structural properties of the macroscopic network structure using Watts and Strogatz (WS) model [118], which can gradually modify the structural properties of the network by changing one parameter. The second question is addressed by using non-linear oscillator networks and a musculoskeletal model, which together represent the coupled dynamics of the brain and body (green area in Figure 1.1) in Chapter 4. Here, we control the sensory ratio to control the degree of interaction between the brain and body. Different macroscopic network structures are also applied to elucidate how structural properties of the brain affect the coupled dynamics and the emergence of behaviors.

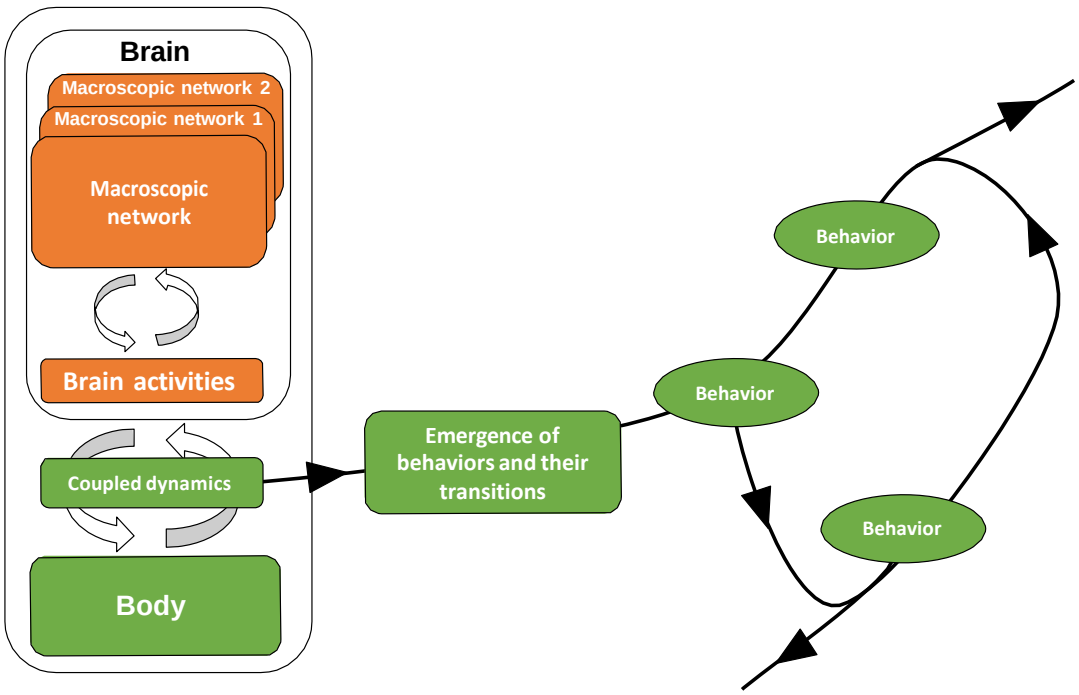

Figure 1.1: Overview of research topic in the thesis

1.3 Structure of the Thesis

In Chapter 2, an overview of previous related work is given. This includes relevant studies on the structural and dynamic properties of the brain, the relationship between the brain and body in terms of the emergence of behaviors, and a computational model for the brain dynamics or the emergence of behaviors. Chapter 3

presents our work on the computational model, using spiking neurons, to explain how the macroscopic anatomical network relates to the complexity of brain activities and the functional network. Chapter 4 addresses the issue of how structural properties of the anatomical network relates to the emergence of the behaviors and their transitions, which arise from the interaction between the network and the body in an environment, using oscillator networks and a musculoskeletal model. Furthermore, in this chapter, we showed how functional networks underlying the coupled dynamics between the brain and body changes according to the behaviors themselves and transitions between these behaviors. In Chapter 5, we summarize our results and contributions to understanding the relationship among the structural properties of the network, emergence of behaviors, and their dynamics. Finally, we discuss the future directions and conclude our work. Appendices give additional data for a deeper understanding about the results presented in Chapters 3 and 4.

Chapter 2

Related works

2.1 Anatomical and Functional Network Structures in the Brain

The brain is a complex network composed of a numerous neuron and their connections, which are modified based on activation of these neurons. Complex network theory shows that a macroscopic anatomical brain network, which is constructed based on the anatomical connections between brain regions, has the structural properties of a complex network, such as a small-world network [102, 18, 52]. A small-world network has a high clustering coefficient and low shortest path length. The clustering coefficient refers to the density of the number of closed triangles constructed by connections between nodes in the network, and the shortest path length indicates the averaged shortest distance between arbitrary nodes in the network (detailed in Section 3.3.3). Several studies have shown that a high clustering coefficient and low shortest path length in the network contributed to local and global information transmission from one node to other nodes [69, 75, 76]. Therefore, the brain has an efficient structure for transmitting information to local and global brain regions using the properties of a small-world network [8]. Furthermore, several studies have shown that the anatomical network have other structural properties such as being scale-free network [6], which has a heavy-tailed distribution of the degree of nodes, or being rich-club network [117], which has connections between the nodes of high degree, and not only the small-world network [1, 31, 116, 103]. However, it is unclear how the structural properties of such types of complex networks affect the macroscopic activity of a brain region, the microscopic activities of individual neurons, and emergence of behaviors.

The relationship between brain activities in the different brain regions, which can be estimated by various statistical methods (e.g., phase coherence, mutual information, and many other statistical indexes), results in a functional network, which differer from the anatomical network [86, 25, 24, 3]. Several studies have shown that the functional network dynamically changes spontaneously or according to tasks at hand or the situation [13, 25, 12, 91, 98]. Spadone et al. [98] compared the functional network between during a visuospatial attention task and the resting state, using functional magnetic resonance imaging (fMRI), and showed increased connectivity between visual cortex and dorsal attention regions. Furthermore, Betti et al. [13] showed the increased functional connectivity between visual and language networks while watching a movie using magnetoencephalography (MEG). Therefore, the structure of the functional network may express changes in the coupled dynamics, including in the sensory-motor system and nervous system. However, how this functional network relates to the emergence of behaviors and behavioral transitions, which result from the from the coupled dynamics between the body and brain, with different macroscopic network structures, is not clear.

2.2 Complexity of Brain Activities

2.2.1 Imaging Studies

The brain shows various dynamics from in spatiotemporally complex interactions among the neurons or regions in the brain. Buzsaki and Draguhn [20] and Buzsaki and Watson [21] showed that the brain exhibits rhythmic neural activities (oscillations) with different frequencies and scales, which cause various rhythmic patterns, such as synchronized and desynchronized patterns among brain activities.

Complexity has been used to characterize the dynamics of biological signals that consists of multiple frequency components. This complexity represents the unpredictability of time-series signals on multiple time scales, based on sample entropy, which is called multiscale entropy (MSE). Studies on autism spectrum disorder (ASD) have suggested that the complexity of the brain activity is closely related to certain structural properties of anatomical and functional networks. Bosl et al. [14] showed that the complexity of EEG signals during the resting state in ASD children

is lower than that of typical developing (TD) children in certain brain regions. Several studies have discussed that this atypical dynamical property can be due to an atypical structure. Solso et al. [95] showed that ASD brain have excessive connection in certain local regions. Moreover, Courchesne [28] have discussed disconnection of the long-range shortcut paths between regions, based on the existing studies (i.e., the ASD brain has a high clustering coefficient and high shortest path length).

2.2.2 Computational Model for Relationship between Connectivity and the Complexity of Neural Activities

Computational studies have shown the relationship between the complexity of a brain activity and an anatomical network. Friston [37] observed that the complexity of neural activity was reduced if the strength of the connections between neuron groups in a network is increased. Nakagawa et al. [79] showed that MSE at slow time scales decreased with the reduction in the strength of connections between neuron groups in a network. However, these studies did not consider any macroscopic network structures. Sporns et al. [100] showed that a small-world-like network structure emerges through the optimization of connections between neuron models, to maximize the functional segregation of network activity. However, since they used a simple linear neuron model, it is difficult to determine how the structural properties of a complex network relate to the complexity of neural activity that consists of multiple frequency components. Furthermore, they did not consider the neural plasticity in the network model. Synaptic connections can be modified by spiking the activities of neurons, e.g., spike timing-dependent plasticity (STDP) [96], in biological neural networks. Therefore, neural activity leads to changes in macroscopic structural properties, and this changed structure then affect brain activities.

A computational model, based on an actual anatomical structure, has also been used to understand brain activities. Schmidt et al. [90] constructed a network model using Kuramoto oscillators [68], where their connectivity was in accordance with the diffusion tensor imaging (DTI) data of human brains. They showed that a brain region with a high degree of anatomical connectivity exhibits high synchronization with other brain regions. However, such an oscillator model tends to converge to a specific frequency; thus, it is difficult to express brain signals composed of multiple

frequency bands. In contrary, a spiking neural network model can express various frequency signals more naturally. Izhikevich and Edelman [58] created a large-scale corticostriatal model, using spiking neurons based on detailed brain data to understand the dynamics of the brain. They observed brain-like spontaneous activity over various frequency bands. However, the network models based on detailed brain data cannot be standardized because they contain a large number of parameters. Hence, it is difficult to understand which factors are important to induce complex brain dynamics.

2.3 Dynamics between the Brain and Body

2.3.1 Relationship with Diverse Behaviors

From an organism to survive in the complex environments, it is important to use appropriate behaviors from among a diverse repertoire of behaviors. Moreover, from the viewpoint of the motor development, the diversity of spontaneous movement patterns observed in early childhood affects subsequent motor development. Hadders-Algra [50] showed that children with atypical motor development have limited movement variability. They argued that it may be due to differences in cerebral connectivity.

Many studies have addressed the importance of anatomical and functional networks to understand how cognitive functions and motor behaviors develop [7, 17, 59, 34, 111, 81]. Connectivities in networks change during brain development, and changed connectivity induces a different relationship of dynamics between the brain and the body. The first movement of the fetus is starting at 7 week postmenstrual age (PMA) with the development of the spinal cord [82]. This movement changes to use whole part but slow and simple movement pattern [72]. At 9 to 10 weeks PMA, the general movement (GM), which is a varied and complex spontaneous whole-body movements, can be observed [72]. This period coincides with the appearance of synaptic activity in the cortical subplate, which contributes to building thalamocortical pathways [104, 64]. Based on these studies, Hadders-Algra [49, 48] has discussed the relationship between the emergence of the GM of the fetus and the cortical subplate. These studies imply that the emergence of behaviors from body

dynamics be changed by forming coupled dynamics through the interaction with brain dynamics. However, the understanding of how diverse behaviors and their transitions emerge from the dynamics of the brain and the body is not clear.

2.3.2 Dynamical System and Chaotic Itinerancy

As a dynamical system approach, Kelso [61] used the metastability concept to explain the emergence of behavior patterns and their transitions. From this viewpoint, behavioral patterns are self-organized as an attractor from the interaction between the brain and body in an environment. Furthermore, transitions between behavioral patterns correspond to the trajectories of attractors in a state space.

Chaotic itinerancy, which represents the transitions among multiple attractors in a high-dimensional state space, has been proposed to explain the dynamics of the brain. This concept is similar to metastability but is more theoretical and focuses on the instability of attractors. Chaotic itinerancy is observed in coupled map lattice (CML) and global coupled map (GCM) models, which have been proposed to constitute complex nonlinear systems [60]. Based on these phenomena, Tsuda et al. proposed a computational model to describe chaotic itinerancy in the brain [115, 114, 83], which shows that these transitory dynamics can be regarded as a chaotic switch between the synchronized and desynchronized states of neurons. Their model is also used to explain the relationship between chaotic itinerancy and cognitive functions at the conceptual level [113, 112]. Several studies have shown that the dynamics of the olfactory systems of animals and EEG signals of the human brain during sleep exhibit chaotic itinerancy [36, 35]. The model proposed in these studies provides a theoretical infrastructure for the one of the issues of dynamic interaction in this thesis for emergence of behaviors and transitions of behaviors, from the coupled dynamics of the brain and body. However, it is unclear how chaotic itinerancy can emerge from the interaction between the brain and body, and how chaotic itinerancy influences transitions behaviors.

2.3.3 Computational Model for Emergence of Behaviors

Inspired by the concept of chaotic itinerancy, Kuniyoshi and Suzuki [67] showed the emergence of adaptive behaviors from the coupled chaotic elements throughout the body in an environment. In their model, adaptive behaviors emerge through a mathematical model of the CML and GCM of chaotic elements. Each CML receives feedback signals from the muscles of the body and sends output signals to these muscles. These CMLs globally interact through a GCM. Furthermore, they show different movement patterns, including a goal-directed behavior that emerged through body constraints, such as the alignment of muscles or an object attached to the body. As extensions this model, Kuniyoshi and Sangawa [66] and Mori and Kuniyoshi [78] constructed more complicated models, i.e., that of the body of a fetus consisting of 198 muscles with tactile sensors. In these models, the musculoskeletal and neural systems interact with each other in the uterine environment. As a result, certain types of ordered movements and their transitions were observed. The abovementioned studies [67, 66, 78] showed the importance of embodiment with regard to the spontaneous emergence of both behaviors and their transitions.

Yamada et al. [119] constructed a detailed brain-body-environment system of a fetus to understand cortical learning via sensorimotor experience in a uterine environment. In this model, more detailed anatomical and physiological data were used for a musculoskeletal system, tactile sensor, vision sensors, a uterine environment, and a cortical model. The cortical model was constructed using 2.6 million spiking neurons and 5.3 billion synaptic connections, based on DTI data. They showed that biologically reasonable whole-body movement and cortical dynamics emerge from the interaction among the brain, body, and environment.

However, the abovementioned models have not been sufficient to explain the relationship between the brain and body for emergence behaviors. Figure 2.1 shows the differences in the network structure of the proposed model from that of these existing models. In previous studies [67, 78], there was no connectivity exists between the interface neurons. Furthermore, hidden neurons, which are considered as a cortex to represent brain dynamics, are missing (Figure 2.1(a)). Hidden neurons are present, but no connectivity is observed between the interface neurons in the model

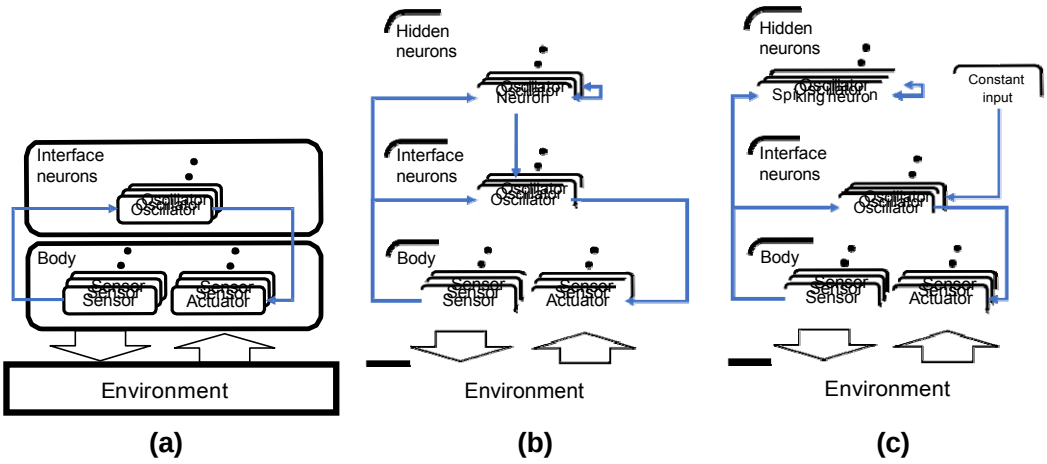

Figure 2.1: Graphical representation of previously proposed models [67, 78, 66, 119]. (a) No connectivity is found between the interface neurons [67, 78]. Furthermore, the hidden neurons, which are considered as a cortex to represent brain dynamics, are missing. (b) Hidden neurons are observed, but there is no connectivity is found between the interface neurons [66]. (c) Constant input from the hidden neurons is provided to the interface neurons, and the hidden neurons have no influence on the body to generate motor behavior [119].

proposed by Kuniyoshi and Sangawa [66] (Figure 2.1(b)). In the case of a detailed fetal simulation [119], constant input is provided to the interface neurons, which means that there is no influence from the hidden neurons on the body to generate a motor behavior (Figure 2.1(c)). The neural architectures described in previous models [66, 119] consider biological brain structure. Therefore, the difference between the interface and the hidden neurons is not clear, which could make analysis of the network analysis underlying the emerging behavior intractable because of complicated connections among neurons. For this reason, this issue has not been addressed to date.

Chapter 3

Complexity of Neural Activity in Macroscopic Cluster Organization

3.1 Problem Statement

In this chapter, we address the issue of how the macroscopic network in the brain is related to the complexity of neural activity for each region. As we mentioned in Chapter 2, several studies have discussed about the relationship between the complex dynamics of brain activities, which has multiple frequency components, and structural properties of the macroscopic network of the brain. Several studies have shown the relationship between connections and complexity of neural activity of the brain using computation models [37, 79, 100]. However, these studies have not allowed investigation of the relationship among the macroscopic network structure, the complexity of brain activities and functional networks, due to the inability to express the multiple frequency components of neural activities, absence of macroscopic structure, or lack of plasticity of connections in the brain.

In order to overcome the abovementioned problems, we construct a network model consisting of multiple neuron groups, each of which consists of spiking neurons, and their macroscopic connections. We then self-organize the network model under different structural properties of a macroscopic network, based on the WS model. The WS model can control the clustering coefficient and path length of the network without changing the number of connections. This approach allows us to identify dominant structural properties that may affect the complexity of brain activity. We hypothesize that a macroscopic network with high clustering coefficient

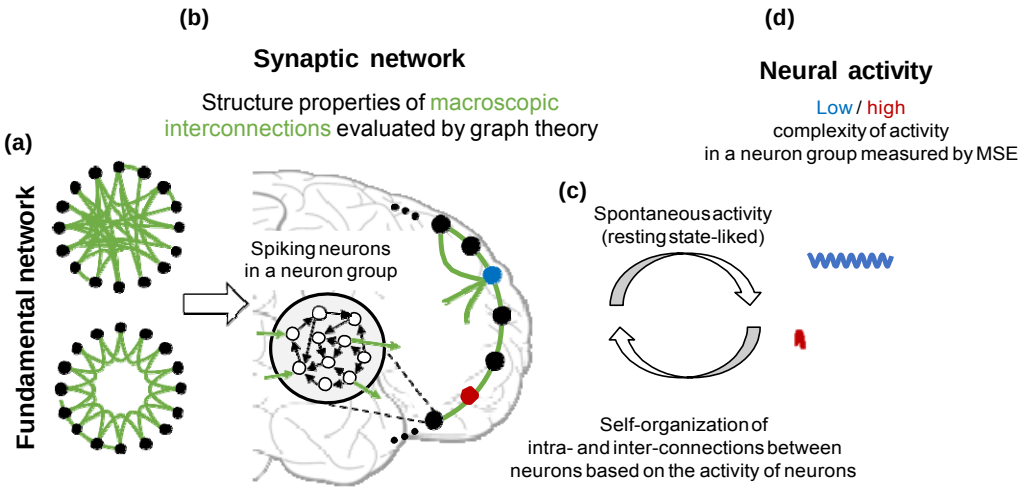

Figure 3.1: Hypothesis and assumptions about relationships among the fundamental network, synaptic network, the complexity of neural activity. The black node and empty black circle represent a neuron group and a neuron in the group, respectively. The black and green lines indicate an intraconnection between neurons in a neuron group, and an interconnection between neurons in different neuron groups, respectively. The red and blue dots show neuron groups with and without high clustering coefficient and high shortest path length, respectively.

and high shortest path length causes low complexity of brain activity in each region. The main procedures and analyses for verifying our hypothesis are as follows (see Figure 3.1):

1. Construct neuron groups consisting of spiking neurons that have weighted connections to randomly selected neurons in the same neuron group (intraconnections). We assume that a neuron group and the intraconnections inside it correspond to a brain region and its intraconnections within the regions, respectively.

2. Determine the initial macroscopic network structure of neuron groups (fundamental network) based on the WS model (Figure 3.1(a)). Then, if an edge exists between two neuron groups in the fundamental network, construct synaptic connections from the neurons in the group to the neurons in another group (interconnections). We assume that the average of interconnections between neuron groups correspond to the long-range interconnectivity between brain regions (synaptic network, Figure 3.1(b)).

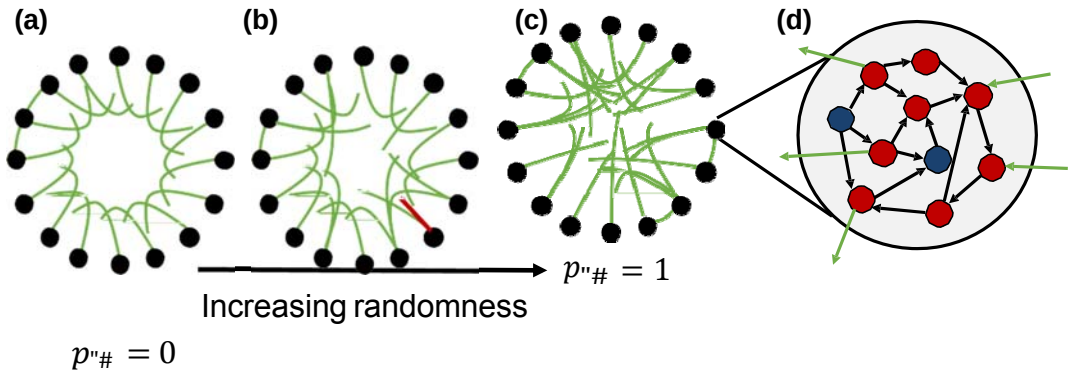

Figure 3.2: Overview of spiking neural network model. A network is created using 100 neuron groups with macroscopic connections between neuron groups based on the Watts and Strogatz model [118]. The black nodes and green edge represent the neuron groups and macroscopic connections, respectively. (a) A lattice network, where each node is connected with neighboring nodes, has local over-connectivity. All connections are rewired with rewiring probability p_{WS}, and p_{WS} increases randomness. (b) A small-world network with a large number of clusters and shorter path length compared with other networks. (c) A random network where nodes are completely randomly connected to each other. (d) Each neuron group contains 800 excitatory (red dots) and 200 inhibitory (blue dots) spiking neurons, and each neuron has intra- (black line with arrow) and inter-connections (green line with arrow).

3. Apply a plasticity rule to synaptic weights and self-organize the network (Figure 3.1(c)). If an edge does not exist between two neuron groups in the fundamental network, the weights between them remain zero to retain the given small-world structure.

4. Analyze the complexity of the activity and structural properties of the self-organized synaptic network using MSE and complex network theory to show their relationship (Figure 3.1(d)).

5. Investigate the frequency characteristics, firing rate, and intraconnections in each neuron group to explore the possible mechanisms of decrease in the complexity of neural activity (Figure 3.1).

3.2 Spike Neural Network Model

3.2.1 Neuron Model

In this study, we utilize the Izhikevich spiking neuron model. This model can reproduce various firing patterns of cortical neurons, and their synchronization can

produce activity patterns on various frequencies. Moreover, since this model has a low computation cost, a large-scale network can be constructed. The equations for the neuron model are given by

$$\frac{dv}{dt} = 0.04v^2 + 5v + 140 - u + I_{tonic} + I_{synapse}, \tag{3.1}$$

$$\frac{du}{dt} = a(bv - u), \tag{3.2}$$

$$\text{if } v \geq 30\,\text{mV, then} \begin{cases} v \leftarrow c \\ u \leftarrow u + d, \end{cases} \tag{3.3}$$

where v and u denote the membrane potential and a recovery variable, respectively. Variables a and b represent the time scale and sensitivity of the recovery variable u, respectively. Variables c and d denote the reset value of membrane potential and the recovery variable after spiking, respectively. Furthermore, I_{tonic} and $I_{synapse}$ represent a tonic input and a synaptic current, respectively. Here, synaptic current, which corresponds to a weight of the connection of presynaptic neuron, is injected if a presynaptic neuron is fired. In this study, the firing of excitatory and inhibitory neurons increases and suppresses the firing of postsynaptic neurons, respectively. These parameters are the same as used in a previous study [57].

3.2.2 Construction of a Fundamental Network using the Watts and Strogatz Model

The interconnections in the synaptic network are generated based on the edges of the fundamental network. In order to modify the structural properties of interconnections without changing the number of connections, the WS model was used to construct the fundamental network. The WS model is one of the methods used to construct a small-world network, and it can generate a network with different clustering coefficients and the average of shortest path length by changing one parameter, p_{WS}. The procedure to construct fundamental network was as follows:

1. Begin with a lattice (regular) network, where each neuron group is connected

to k nearest neuron groups (Figure 3.2(a)). The lattice network has large number of clusters and a long path length.

2. Rewire each edge randomly according to the rewiring probability, p_{WS}. This procedure creates a shortcut between neuron groups (the red line in Figure 3.2(b)). The network structure becomes random, and the number of clustering and average path length decrease if p_{WS} increases (Figure 3.2(c)). The value of p_{WS} for a small-world network is typically between 0.01 and 0.1.

3.2.3 Self-organization in a Spike Neural Network Model

In this study, we assume that intra and interconnections between neurons have plasticity; therefore, the synaptic network is self-organizing. Here, we apply an STDP [97] rule to update the weights of connections. The STDP rule, which is considered a biologically plausible rule [74], modify the connection weights w, based on the firing times of pre and postsynaptic neurons. The update value of weight, Δw, is given as

$$\Delta w = \begin{cases} A_+ \exp(-\Delta t/\tau_+) & \text{if } \Delta t \geq 0 \\ A_- \exp(\Delta t/\tau_-) & \text{if } \Delta t < 0, \end{cases} \tag{3.4}$$

$$\Delta t = t_{post} - t_{pre}, \tag{3.5}$$

where Δt represents the difference between the firing times of presynaptic, t_{pre}, and postsynaptic neurons, t_{post}. This difference is calculated when a neuron fires, and the connection weight between neurons is updated based on equation (3.4). Here, $\Delta t \geq 0$ and $\Delta t < 0$ denote long-time potentiation (LTP) and long-time depression (LTD), respectively. Time constant τ_+ (τ_-) controls the LTP (LTD) decay, and A_+ (A_-) represents the LTP (LTD) intensity constant.

Table 3.1: Parameters of the simulation model used in this study.

parameters	values	descriptions	notes
$D_{\text{intra,exc}}$	[0,20]	Transfer delay of excitatory synapse in neuron group	(uniform dist., ms)
$D_{\text{intra,inh}}$	1	Transfer delay of inhibitory synapse in neuron group	(ms)
I_{tonic}	20	Tonic input	(mV)
τ_+	20	Time constant of LTP	(ms)
τ_-	20	Time constant of LTD	(ms)
A_+	0.1	Amplitude of update weight (LTP)	-
A_-	-0.12	Amplitude of update weight (LTD)	-
$w_{\text{init,exc}}$	6.0	Initial weight of excitatory synapse	-
$w_{\text{init,inh}}$	-5.0	Initial weight of inhibitory synapse	-
w_{upper}	10.0	Maximum value of weight	-
N_{E}	800	Number of excitatory neurons in a neuron group	-
N_{I}	200	Number of inhibitory neurons in a neuron group	-
N	1000	Number of neurons in a neuron group	$= N_E + N_I$
C_{intra}	100	Number of intraconnections of a neuron	-
$D_{\text{inter,exc}}$	[10,30]	Transfer delay of excitatory synapse between neuron groups	(uniform dist., ms)
N_{group}	100	Number of neuron groups	-
k	6	Number of edges for each neuron group	-
C_{inter}	3	Number of interconnections of a excitatory neuron	-
p_{WS}	[0.0,1.0]	Rewiring probability	-
t_{step}	1	Time step	(ms)
T_{total}	1200	Total simulation time	(s)
T_{tonic}	1100	Time length of tonic input	(s)
T_{STDP}	1000	Time length of self-organization through STDP	(s)
N_{sim}	10	Number of independent simulations	-

3.2.4 Parameters and Simulation Setting

Table. 3.1 shows model parameters used in this study. We set the parameters based on previous studies [57, 121, 56]. The model consists of N_{group} (= 100) neuron groups, and each neuron group has N_{E} (= 800) excitatory neurons and N_{I} (= 200) inhibitory neurons. Here, an excitatory neuron is intraconnected with C_{intra} (= 100) randomly selected neurons in the same group and interconnected with C_{inter} (= 3) randomly selected neurons of the connected neuron group. An inhibitory neuron is intraconnected with C_{intra} (= 100) randomly selected excitatory neurons in the same group; however, there are no interconnections for inhibitory neurons. C_{intra} and C_{inter} are fixed through simulation. N_{group} and k (= 6) are experimentally determined, so that the fundamental network differs in its structural properties according to the rewiring probability p_{WS}. In this study, we conducted simulations using {0.0, 0.002, 0.005, 0.01, 0.02, 0.05, 0.1, 0.2, 0.3, 0.4, 0.5, 0.6, 0.7, 0.8, 0.9, 1.0} as the values of p_{WS}.

Figure 3.3 shows the schedule of simulation. The total simulation time was 1200 s, and one time step was 1 ms. The duration for self-organization through STDP was 1000 s. Furthermore, the tonic input duration, T_{tonic}, was 1100 s, to drive neural

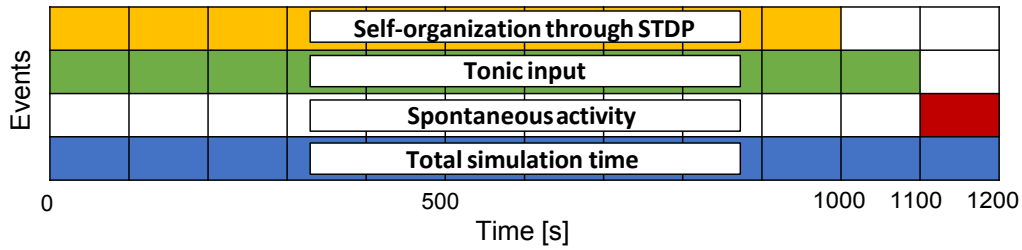

Figure 3.3: Time schedule for simulation. Each colored area indicates the time at which the event occurred. Neural activities during 1110 s to 1200 s were analyzed to determine the relationship among the structural properties of the synaptic network, neural activity, and the functional network.

activity after self-organization. Then, the activity without any external inputs, such as a resting state, for a period of 1100 s to 1200 s was analyzed as the neural activity of the network model. The simulation was independently conducted ten times for each p_{WS}.

3.3 Analysis method for neural activity

3.3.1 The Complexity of Neural Activity

In this study, the neural activity of a neuron group is represented by the local averaged potential (LAP) [19]. LAP is the average of the membrane potentials of the excitatory neurons within a neuron group. The LAP is not directly equivalent to the local field potential, which is recorded in the extracellular space around neurons, or to the EEG signals in the brain, which are typically used as an index for electric potentials. Nevertheless, LAP directly reflects the group activity of neurons, therefore, it can be used to indicate the synchronous activity of a neuron group. LAP is calculated as

$$LAP_i(t) = \frac{1}{N_E} \sum_{j=1}^{N_E} v_{i,j}(t), \tag{3.6}$$

where $v_{i,j}$ indicates the membrane potential of the jth excitatory neuron in the ith neuron group.

MSE analysis was proposed to discern the complexity (degree of irregularity) of biological signals composed of multiple time scales [27, 26]. The procedure for

calculating the MSE was as follows:

1. An original signal $x(t)$, is down sampled by multiple time scales to obtain coarse-grained signals, $y(t)$.

$$y(t) = \frac{1}{€} \sum_{i=(t-1)€+1}^{i=t€} x(i) \quad (1 \leq t \leq N/€), \tag{3.7}$$

   where € indicates the scale factor.

2. Sample entropy is calculated for each coarse-grained signal.

$$SampEn(r, m, N) = -\ln[C_{m+1}(r)/C_m(r)], \tag{3.8}$$

$$C_m(r) = \frac{\text{number of pairs}(i, j)\,(|z_i^m - z_j^m| < r,\ i /= j)}{(N - m + 1)(N - m)}, \tag{3.9}$$

   where $z_i^m = \{y_i, y_{i+1}, \cdots, y_{i+m-1}\}$ denotes a subsequence of the coarse-grained signals from the ith to the $(i + m - 1)$th data point of $y(t)$, m denotes the length of the subsequence, $Y = \{y_1, \cdots, y_i, \cdots, y_N\}$ denotes the coarse-grained signals, and N denotes the length of Y.

In this study, a LAP signal is used for $x(t)$, and MSE is calculated for each neuron group. Furthermore, we used $m = 2$ and $r = 0.15$, which are commonly used for MSE analysis.

3.3.2 Neural Activation in Neuron Groups

We analyzed the frequency properties of LAP signals to determined how different frequency components of neural activity influence the functional network or MSE values. We obtained the peak frequency with the highest intensity as robust frequency components in neural activity through the decomposition of the LAP signals into the frequency domain using fast Fourier transform (FFT). Furthermore, we use a band-phase-randomized surrogate method [70] to clarify which frequency bands mainly contribute to a decrease in MSE (i.e., sample entropy increases if a specific frequency component that mainly contributes to a decrease in complexity

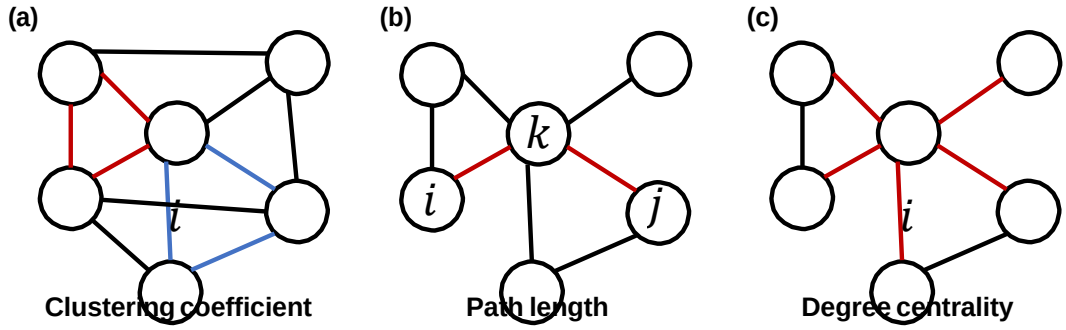

Figure 3.4: Examples of the clustering coefficient, degree centrality, and path length. (a) Clustering coefficient of the ith node. The clustering coefficient indicates the density of the number of closed triplet connections (red and blue connections) between nodes in a network (Section 3.3.3). Here, the dashed line indicates a possible connection. (b) The path length from the ith node to the jth node. Path length represents the distance of an arbitrary route from node i to node j, and the shortest path length represents the distance of the shortest route from i to j (red line). (c) Degree centrality of the ith node. Degree centrality refers to the number of connections of a node (red connections).

is surrogated). In order to obtain surrogate signals, FFT is used to transform the time series into frequency domains, and then, the amplitude adjusted Fourier transform method (AAFT) [108] is used to randomize the phase relationship in specific frequency bands. Thereafter, a surrogate time series with the original amplitude is obtained through inverse FFT.

Moreover, we evaluated the firing rates and a periodic firing pattern to understand how the microscopic activation of neurons affects the complexity of the neural activity in a neuron group. Here, periodicity was evaluated by autocorrelation of the number of fired neurons within a non-overlapped time-window of 5 ms.

3.3.3 Graph Analysis of Network Structure

In order to elucidate how the structural properties of the synaptic network affect the complexity of neural activity, we considered the following features of the network, using complex network theory. The graph to be analyzed consisted of 100 nodes that correspond to neuron groups. The average weight of the interconnections of neurons between neuron groups corresponds to the weight of the edge between nodes in the

graph. We investigated the clustering coefficient, shortest path length, and degree centrality of the weighted directed networks.

- Clustering coefficient: The proportion of connections with the shape of a closed triplet over all possible combinations of triplets formed by three nodes in a network (Figure 3.4(a)). This is defined as follows:

$$C_i = \frac{\text{number of closed triangles}}{\text{number of possible triangles}}. \tag{3.10}$$

As we consider a directed weighted network, we use the following extended equation [33]:

$$C_i(E) = \frac{[R^{1/3} + (R^T)^{1/3}]^3_{ii}}{2[d_i^{tot}(d_i^{tot} - 1) - 2d_i^{\leftrightarrow}]}, \tag{3.11}$$

where $R = \{r_{ij}\}$ is the weight matrix of the connectivity of nodes, r_{ij} represents the weight of the connection from the ith node to the jth node, $d_i^{tot} = d_i^{in} + d_i^{out}$ denotes the total of the in-degree and out-degree of the ith node, and $d_i^{\leftrightarrow}$ denotes the number of bilateral connections of the ith node. A node with a high clustering coefficient indicates that the node interacts with neighboring nodes more locally, which may induce a synchronized behavior between nodes [75, 76].

- Average shortest path length: The shortest path length is defined as the minimum number of steps required to pass from one node to another node in a network (Figure 3.4(b)). We use the following equation to calculate the average shortest path length:

$$L = \sum_{i \neq j} \frac{S(i,j)}{N(N-1)}, \tag{3.12}$$

$$s_{ij} = \frac{1}{r_{ij}}, \tag{3.13}$$

where $s_{i,j}$ and $S(i,j)$ represent the path length and shortest path length from the ith node to the jth node, respectively. N denotes number of nodes.

- Degree centrality: This refers to the number of connections of a node (Figure 3.4(c)). The equation for a directed weighted connection is as follows:

$$G_i = \sum_{i/=j} r_{ij}. \tag{3.14}$$

We show the relationship between these complex network measures and MSE. In addition, intraconnections are organized under inputs from interconnections, which are specified in accordance with the fundamental network. Hence, this self-organization of interconnections and intraconnections may affect the complexity of the activity of a neuron group. Therefore, we investigated the average intraconnection in a neuron group and examined its relationship with the structural properties and MSE of activity for each neuron group after self-organization.

3.4 Results

In our model, we observed spontaneous activity in the self-organized synaptic network even after stopping the tonic input. However, the network did not show spontaneous activity if we did not use STDP for self-organization; these were also reported in previous studies [56, 58]. In this study, we assumed that the spontaneous activity corresponds to the brain activity in the resting state. Hereafter, we mainly analyzed the spontaneous activity.

We present the result of the analyses in this section. The main results are as follows:

1. The analysis of MSE showed that the different levels of complexity in each neuron group and the average complexity of all neuron groups in the a network decreased if p_{WS} of the fundamental network decreased.

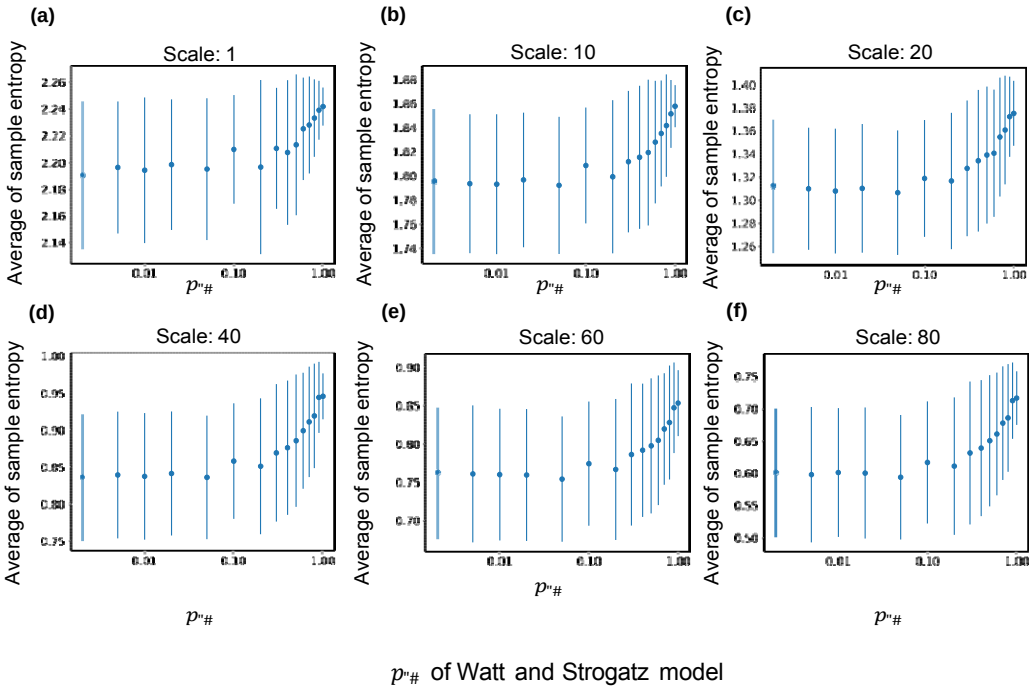

Figure 3.5: The relationship between sample entropy and p_{WS} of the WS model. The x-axis in all graphs represents p_{WS} (the rewiring probability of the Watts and Strogatz model [118]). (a)-(f) Average sample entropy of all neuron groups with ten independent simulations at scale factors (€ in equation 3.7) of MSE at 1, 10, 20, 40, 60, and 80. The error bars indicate the standard deviation.

2. The analysis of neural activity in neuron groups with different levels of complexity showed that a neuron group with low complexity has a periodical firing pattern and increased signal amplitude in two frequency bands (20-40 and 40-60 Hz) of neural activity (Section 3.4.2).

3. The complex network analyses for each neuron group showed that the complexity of a neuron group is negatively related to the local over-connectivity (the clustering coefficient and degree centrality were high) (Section 3.4.3).

3.4.1 Relationship between MSE and the WS Model

Figure 3.5 shows the relationship between the average sample entropy of a LAP signal and the p_{WS} of the fundamental network (see Section 3.3.1 for the method). As shown in the figure, the average of sample entropy of all neuron groups increased if p_{WS} increased at any time scale, and decreased if the scale factor of MSE is large (see Figure A.1 for curves of sample entropy on all scale factors). Therefore, the average

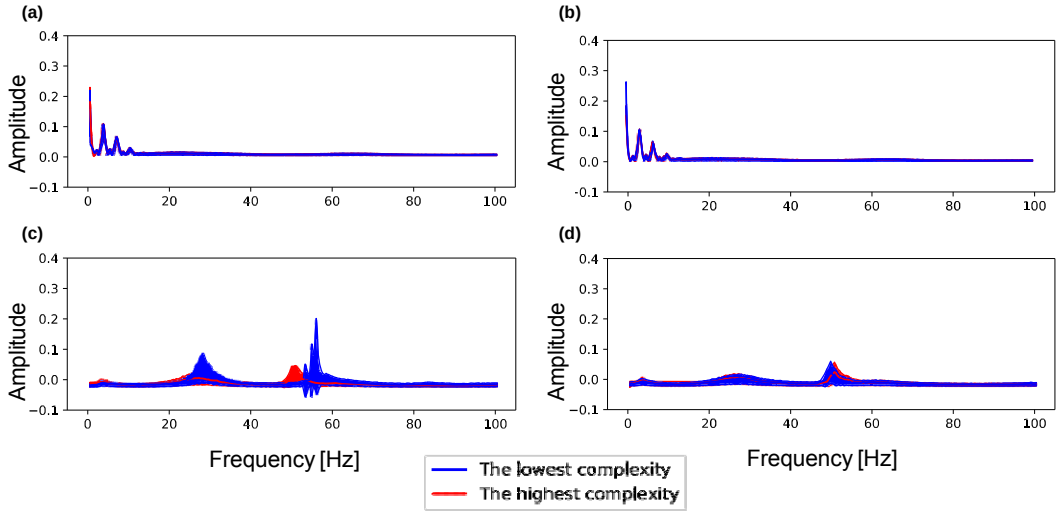

Figure 3.6: Amplitude of each frequency spectrum sampled from the LAP of the 10 neuron groups with low complexity (blue) and high complexity (red) in a network. The peak envelopes are used to plot the curve in the figure. Color curves and color-shaded areas represent average and standard deviation values for ten simulations, respectively. (a) The lattice network ($p_{\mathrm{WS}} = 0.0$) during self-organization by STDP (0-100 s). (b) The random network ($p_{\mathrm{WS}} = 1.0$) during self-organization by STDP (0-100 s). (c) The lattice network ($p_{\mathrm{WS}} = 0.0$) after self-organization by STDP (1100-1200 s). (d) The random network ($p_{\mathrm{WS}} = 1.0$) after self-organization by STDP (1100-1200 s).

of sample entropy decreased if the fundamental network has a high clustering coefficient and a large shortest path length. Furthermore, since the down sampling with a large scale factor in equation (3.7) acts as a low-pass filter, the lower frequency components have lower complexity than the higher frequency components of the neural activity. Moreover, as shown in Figure 3.5, variance of the average sample entropy of the synaptic network appears even, although the same fundamental network is used for the lattice network. This result indicates that the interconnections and neural activities in several neuron groups differ from those in the initial network through self-organization.

3.4.2 Neural Activities in Neuron Groups with Different Levels of the Complexity

The frequency components of neural activity and the complexity of surrogate data in specific frequency bands are shown in Figures 3.6 and 3.7, respectively (see the first paragraph in Section 3.3.2 for the method). These figures shows a robust frequency

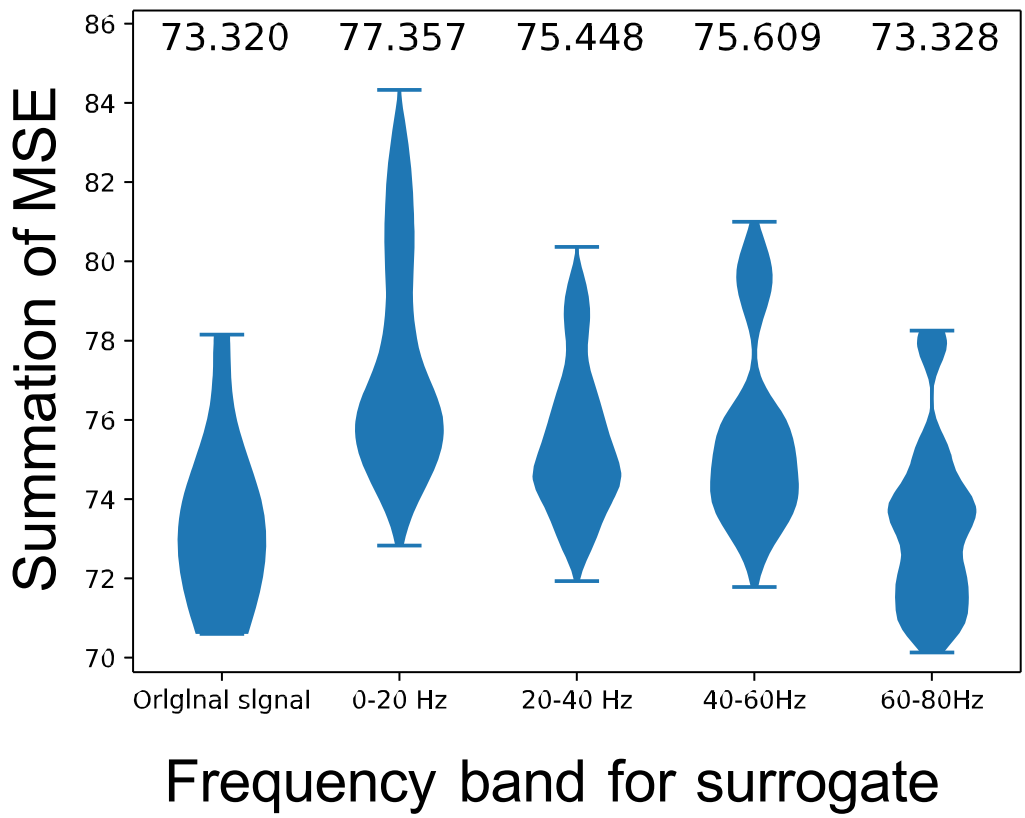

Figure 3.7: The difference in summation of MSE for 80 scale factors between the band-phase-surrogate LAP signal in specific frequency bands and the original LAP signal. The x-axis indicates the frequency band for the surrogate, and the y-axis indicates the difference in summation of MSE for 80 scale factors between surrogate and original data. The number on above each violin plot denotes the average value. Surrogate was performed 100 times for each neuron group that has the lowest complexity in the lattice network for each of the 10 simulations. See Table. A.1 for statistical differences, based on the Tukey-Kramer test.

of neural activity and their relationship with complexity of neural activity. Figure 3.6 shows the spectra in neuron groups with high and low complexity (summation of MSE for 80 scale factors) during (0-100 s) and after self-organization (1100-1200 s) in a lattice and random network. As shown in Figure 3.6(a) and (b), both networks show similar frequency distributions during self-organization. However, as shown in Figure 3.6(c), after self-organization, neuron groups with low complexity in the lattice network show increased signal amplitude in two frequency bands (20-40 and 40-60 Hz), as compared with the neuron group with high complexity in the network (see Figure A.2 for data distribution and statistical differences). In contrast, as shown in Figure 3.6(d), increased signal amplitude appears in both neuron groups in the random network but has similarly shaped curves to the neuron groups with high complexity in the lattice network. Therefore, frequency properties in neuron groups in a random network, which shows higher average and lower standard deviation of sample entropy than the lattice network (see Figure 3.5), is similar to those of neuron group with high complexity in the lattice network. This result indicates that the self-organization of synaptic connections is affected by the initial macroscopic network structure, as result of neural activities in different frequency bands.

We show the relationship between the complexity and peak frequency of neural activity in all neuron groups in Figure A.4. The figure shows the peak frequency and their amplitude in the three frequency bands (0–20, 20–40 and 40–60 Hz) in which many changes occurred in Figure 3.6. We observed the same tendency with Figure 3.6 that amplitude increases as the complexity of neural activity decreases in 20–40 Hz and 40–60 Hz bands.

Figure 3.7 shows the summation of MSE for 80 scale factors between the original LAP signals and the band-phase-randomized surrogate signals using AAFT in different frequency bands (see the first paragraph in Section 3.3.2 for the method). In this study, the surrogates were conducted 100 times for each LAP signal in a neuron group with the lowest complexity in the lattice network for each of the 10 simulations (i.e., 10 original signals and 1000 surrogate signals). As shown in the figure, the surrogate signals in 0-20 Hz, 20-40 Hz and 40-60 Hz bands had larger complexity than the original signal and surrogate signals in 60-80 Hz bands. This result indicated that frequency bands under 60 Hz, especially, the 0-20 Hz frequency

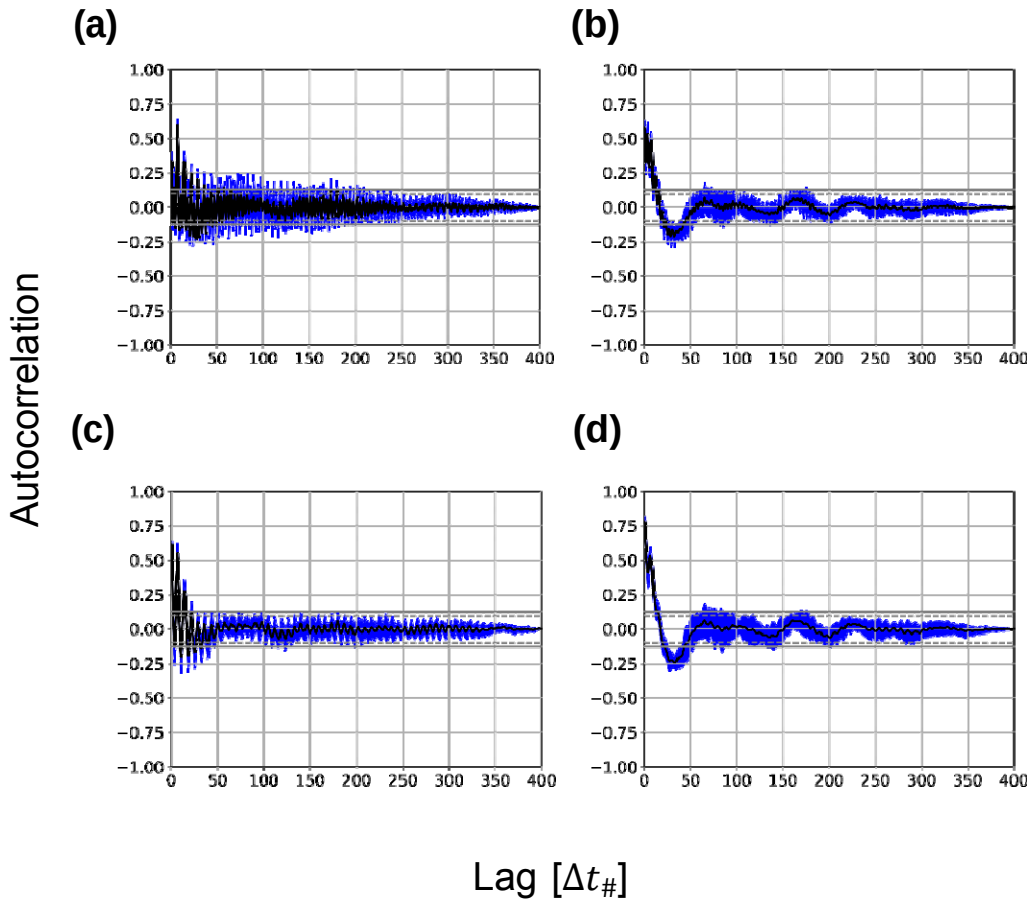

Figure 3.8: Autocorrelation of the number of fired neurons sampled in non-overlapping time windows of $\Delta t_w = 5$ ms in a lattice network ($p_{\mathrm{WS}} = 0.0$). The x-axis represents the lag of the window, and the y-axis represents the autocorrelation. The black curves and blue shaded area represent the average and standard deviation for ten simulations, respectively. (a) Autocorrelation of fired excitatory neurons in a neuron group with the lowest complexity during the later period (1100-1102 s). (b) Autocorrelation of fired inhibitory neurons in a neuron group with the lowest complexity during the later period (1100-1102 s). (c) Autocorrelation of fired excitatory neurons in a neuron group with the highest complexity during the later period (1100-1102 s). (d) Autocorrelation of fired inhibitory neurons in a neuron group with the highest complexity during the later period (1100-1102 s). The dashed line and solid line represent the 95% and 99% confidence intervals, respectively.

bands, largely contributed to a decrease in MSE (see Table. A.1 for statistical differences with Tukey–Kramer test for unequal sample sizes). Figure 3.8 shows the autocorrelation of the numbers of firing excitatory and inhibitory neurons to compare the degree of periodicity of the firing pattern between different neuron groups with the highest and lowest MSE in the lattice network (see the second paragraph in Section 3.3.2 for the method). As shown in the figure, curves of autocorrelation in the neuron group with the lowest complexity showed more periodic pattern with

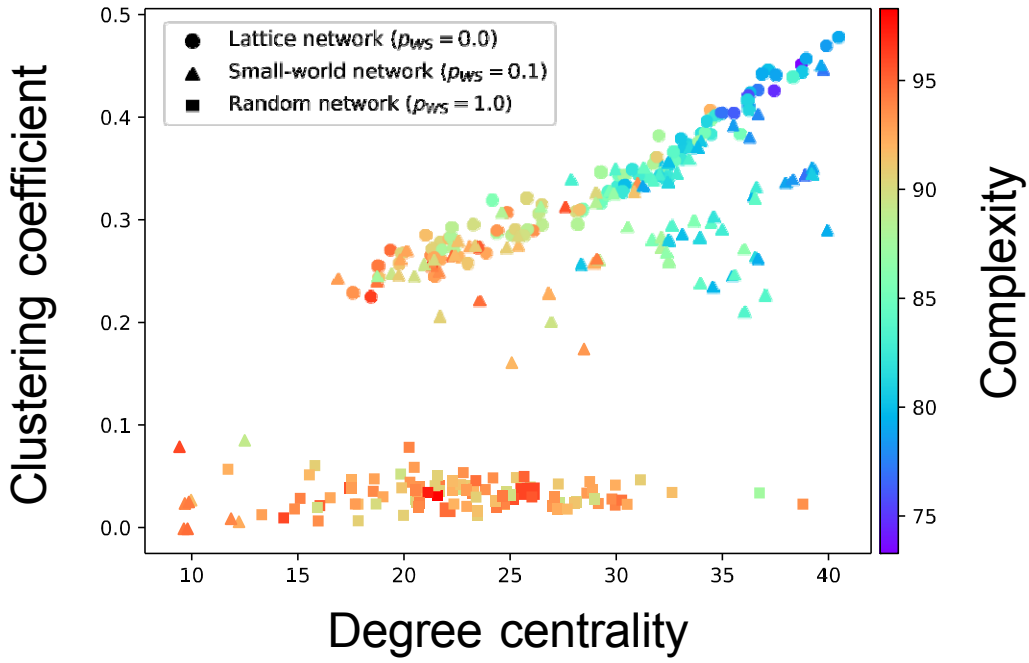

Figure 3.9: Relationship between the connectivity structure and the complexity of neural activity. Each marker corresponds to a neuron group in the network, and its color indicates the summation of the sample entropy for all 80 scale factors. The x-axis indicates the degree centrality, and the y-axis indicates the clustering coefficient.

higher value than that of the neuron group with the highest complexity, in both neuron types (Figures 3.8(c) and (d)). These results indicate that the neuron group with low complexity not only has higher signal amplitude in the two frequency bands, but also has a more periodical firing pattern of neurons than the neuron group with high complexity.

3.4.3 Relationship between Neural Activity and Structural Properties

In order to clarify the factor that induced different values of the complexity of neural activity among neuron groups, we used complex network analysis for each neuron group after self-organization (see Section 3.3.3 for the method). Here, we only showed the results of one simulation when the p_{WS} of fundamental network was 0.0, 0.1, and 1.0; see Figures A.3-A.7 for all values of p_{WS} of ten simulations. Figure 3.9 shows the relationship between the structural properties and complexity of neural activity for each neuron group in the synaptic network. As shown in the

figure, the complexity of neural activity decreases if the clustering coefficient and degree centrality are increased. Since the cluster organizations of neuron groups originate from the lattice network in the WS model, they are constructed by neighboring (or local) neuron groups. Hereafter, we define the local over-connectivity for the structural property in which the clustering coefficient and degree centrality are large. In contrast, the shortest path length is not related to the complexity (see Figure A.7). Furthermore, we conducted experiments on the complexity index for the network before the self-organization by STDP to clarify the role of the self-organization, when no spontaneous activity without tonic input occurs prior to self-organization. We analyzed the activity for all network structures that we adopted above, with the random tonic inputs and the fixed initial weights. We show the results of the complexity index with clustering coefficient and degree centrality in Figure A.8. We found no clear relationship between the complexity of neural activity with tonic input (i.e., neural activities in the network are induced by external input instead of by spontaneous activation) and structural properties of the synaptic network without STDP as compared to the activity after self-organization by STDP (Figure A.3). Therefore, the relationship between the structural properties and complexity must be induced by the self-organization under the macroscopic structure via STDP.

Figure 3.10 shows how complexity relates to peak frequency of neural activity (see Section 3.3.1 and 3.3.2 for the method). Since LAP signals had two intensity peaks, around 30 and 50 Hz (see Figure 3.6), and the surrogate test showed a large difference in the 0-20 Hz band (see Figure 3.7), we investigated peak frequency in three frequency bands (0-20 Hz, 20-40 and 40-60 Hz). As shown in Figure 3.10(b) and (c), amplitude increased when the complexity of neural activity decreased in the 20-40 Hz and 40-60 Hz bands. Moreover, in the 40-60 Hz band, the peak frequency increased if the complexity of neural activity decreased. However, as shown in Figure 3.10(a), amplitude decreased if the complexity of neural activity decreases in the 0-20 Hz. Therefore, the robust frequency components of neural activity in the neuron groups with low complexity shifted from the low frequency bands (0-20 Hz) to the high frequency bands (20-40 Hz and 40-60 Hz).

Hereafter, we focus on the activation of neurons and intraconnections in a neuron

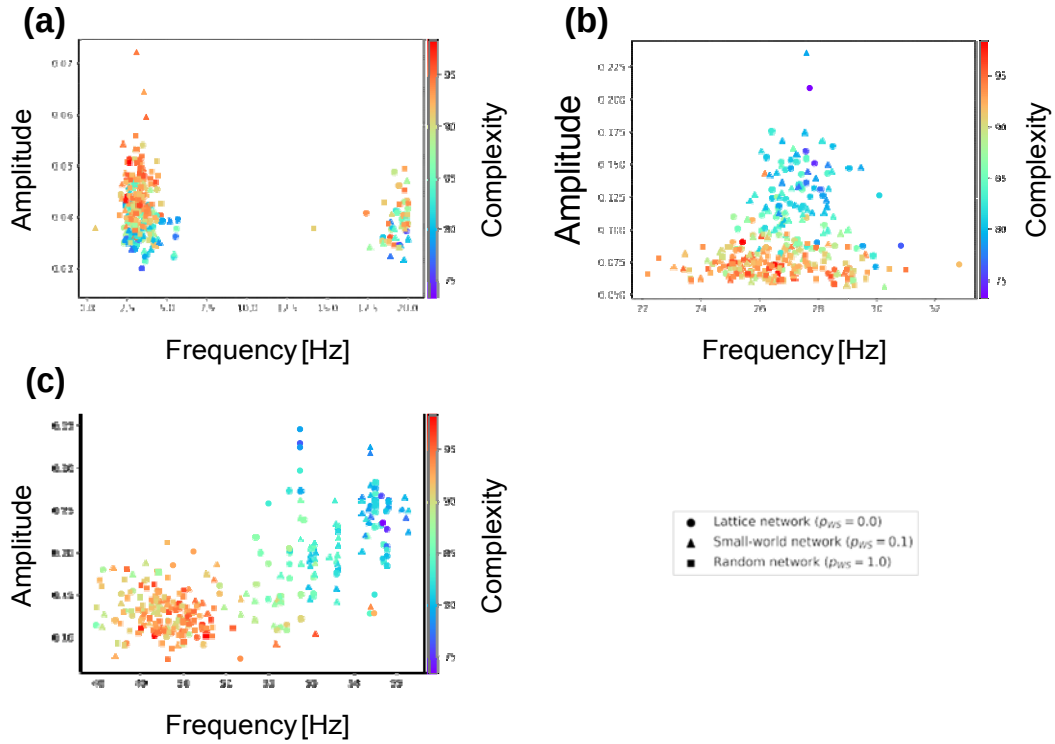

Figure 3.10: Relationship between the peak frequency and complexity of neural activity. (a) Relationship in the 0-20 Hz band. (b) Relationship in the 20-40 Hz band. (c) Relationship in the 40-60 Hz band. Each marker corresponds to a neuron group in the network, and its color indicates the summation of the sample entropy for all 80 scale factors. The x-axis indicates the peak frequency of neural activity, and the y-axis indicates the amplitude.

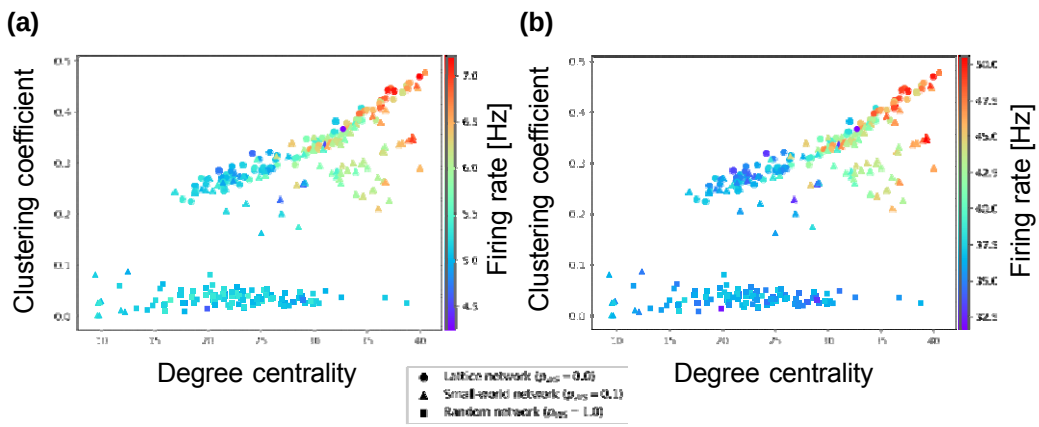

Figure 3.11: Relationship between the connectivity structure and firing rate of excitatory and inhibitory neurons. Each marker corresponds to a neuron group in the network, and its color indicates the average firing rate of excitatory and inhibitory neurons. The x-axis indicates the degree centrality, and the y-axis indicates the clustering coefficient. (a) Relationship between structural properties and firing rate of excitatory neurons. (b) Relationship between structural properties and firing rate of inhibitory neurons.

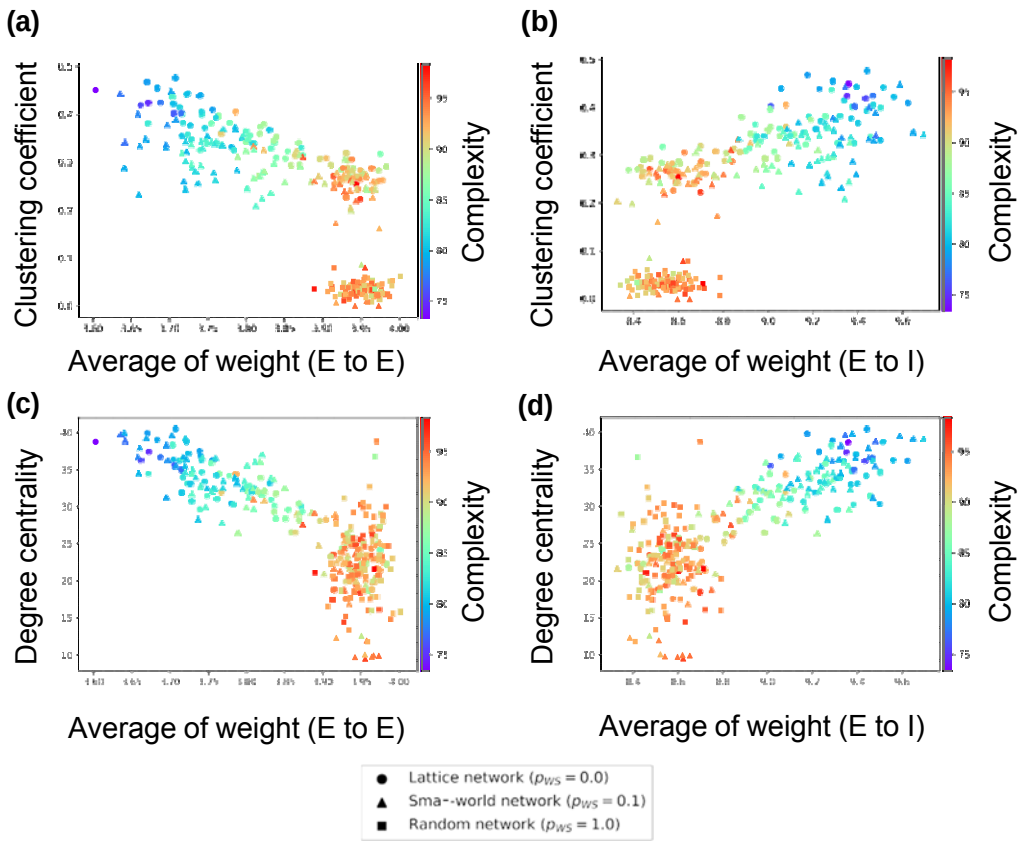

Figure 3.12: Relationship among the weight of intraconnection, structural properties of the synaptic network, and the complexity of neural activity. (a) Relationship among the weight of intraconnection from excitatory to excitatory neuron, clustering coefficient based on the interconnection, and the complexity. (b) Relationship among the weight of intraconnection from excitatory to inhibitory neuron, clustering coefficient based on the interconnection, and the complexity. (c) Relationship among the weight of intraconnection from excitatory to excitatory neuron, degree centrality based on the interconnection, and the complexity. (d) Relationship among the weight of intraconnection from excitatory to inhibitory neuron, degree centrality based on the interconnection, and the complexity. Each marker corresponds to a neuron group in the network, and its color indicates the summation of the sample entropy for all 80 scale factors. The x-axis indicates the average weight of interconnection, and the y-axis the structural properties of interconnection.

group. As shown in Figure 3.11, the firing rates of excitatory and inhibitory neurons in a neuron group with local over-connectivity increased. Figure 3.12 shows the average of the weights of intraconnections from excitatory neurons to excitatory neurons and the intraconnections from excitatory neurons to inhibitory neurons. Here, we omit a value for the average weight of intraconnections from the inhibitory neurons to excitatory neurons because the weight of those connections were not changed by STDP. According to Figure 3.12, the average of the weights of the connections from excitatory neuron to another excitatory (inhibitory) neuron positively (negatively) relates to the average sample entropy and negatively (positively) relates to local over-connectivity of the synaptic network. Therefore, the neuron groups with low complexity with local over-connectivity have increased firing rates of both type of neurons, and have a small weight of intraconnections from excitatory to excitatory neurons and a large weight of intraconnections from excitatory to inhibitory neurons.

3.5 Discussion

We constructed a spiking neural network model which consisted of multiple spiking neuron groups, to understand how the macroscopic fundamental network structure (inter-neuron groups) affects its self-organization of the microscopic (synaptic) network and its activity using complexity of neural activity. We only modulated the rewiring probability of the WS model to control the structural properties of the macroscopic fundamental network. Our simulation showed that the complexity of the neural activity decreased with changed intraconnections in a neuron group, through the self-organization under the macroscopic structure. Our complex network analyses implied that a higher clustering coefficient and degree centrality (local over-connectivity) of a neuron group caused the lower complexity of neural activity.

3.5.1 Hypothetical Mechanism of Low Complexity Caused by Local Over-connectivity

According to Figure 3.9, the complexity of neural activity in a neuron group decreases if the degree of local over-connectivity (the clustering coefficient and degree centrality) increases. We suppose that this can be ascribed to changes in intraconnections through self-organization under the macrostructure cause this result. As shown in Figure 3.12, intraconnections of a neuron group with low complexity of neural activity have increased average weight from excitatory to inhibitory neurons and decreased average weights from excitatory to excitatory neurons. This implies that a microstructure that suppresses the activity of excitatory neurons appears through a self-organization under local over-connectivity in the macroscopic network. However, as shown in Figure 3.11, a neuron group with local over-connectivity shows increased firing rates of excitatory and inhibitory neurons, i.e., a neuron group takes excessive input from other neuron groups. We speculate that intraconnections might be self-organized through STDP to sustain a certain amount of neural activity (homeostasis) against excessive input from other neuron groups. As a result of self-organization, the activation of the inhibitory neurons increases, which might cause periodical activity, with two peaks, within frequency bands (see Figure 3.6 and 3.8). Several studies have shown that inhibitory activation induces periodic patterns of brain activity [45, 89].

Based on these results, we speculate a possible mechanism for low complexity of neural activity in a neuron group with local over-connectivity, as follows (see Figure 3.13):

1. The firing rates of neurons in a neuron group with local over-connectivity is increased by excessive input from the connected neuron groups (see Figures 3.11). Consequently, to sustain a certain amount of the activation of neurons in the neuron group, strong intraconnection from excitatory to inhibitory neurons and weak intraconnections from excitatory neuron to excitatory neurons are self-organized through STDP (see Figures 3.12 and 3.13(a)).

2. The increased activation of inhibitory neurons induces the oscillation of excitatory neurons, and therefore, the intensity of the several specific frequency

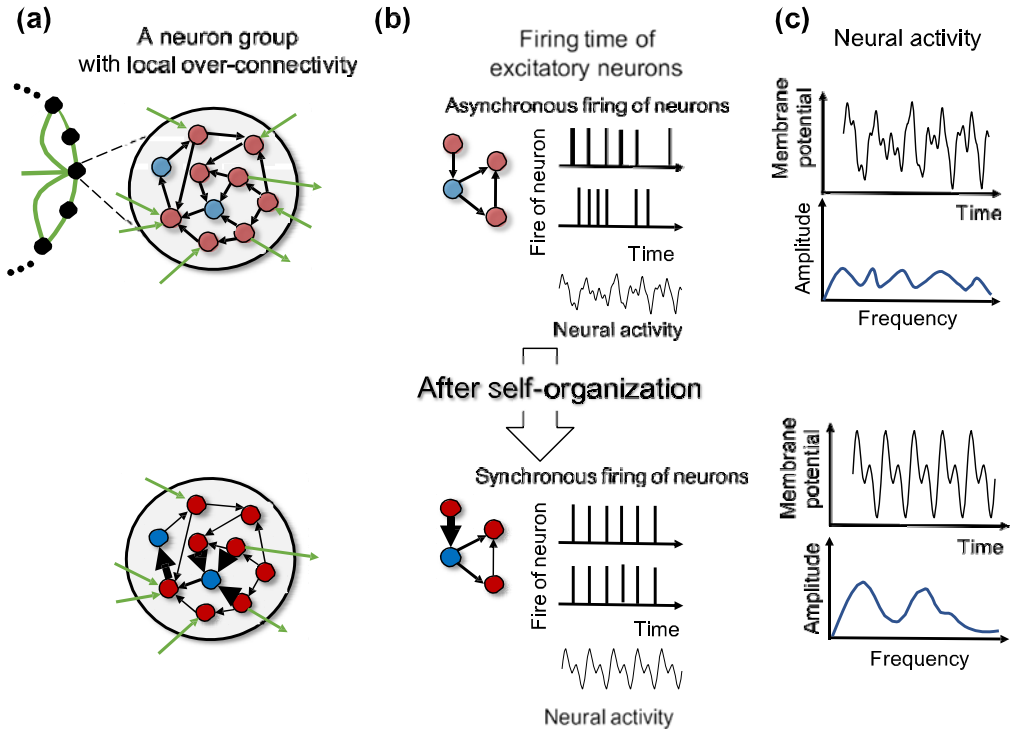

Figure 3.13: Schematic representation of a possible mechanism of reduction of complexity of neural activity in a neuron group with local over-connectivity. The red and blue solid circles represent excitatory and inhibitory neurons, respectively. The transparency of color of solid circles represents the firing rate of neurons. The black and green lines with arrows represent intraconnection between neurons in the same neuron group and interconnection between neurons in different neuron groups, respectively. The thickness of a line with an arrow represents the weight of connectivity. (a) A fundamental network and a neuron group with local over-connectivity. The green line without an arrow represents the edge between neuron groups. (b) Relationship between the strength of connectivity from inhibitory neurons to excitatory neurons, with the firing time of neurons. The vertical black bar on the time axis indicates the firing of a neuron. The firing rate of inhibitory neurons with a strong connectivity from excitatory neurons increases, and therefore, inhibitory neurons strongly affect other excitatory neurons. The excitatory neurons that are strongly influenced by inhibitory neurons show a synchronous firing pattern and therefore induce periodical oscillation of neural activity; (c) A LAP signal of neural activity in a neuron group and the amplitude of frequency spectrum of the LAP signal.

components of neural activity increases (see Figures 3.6 and 3.13(b)).

3. The specific frequency components of signals become robust, and neural activity becomes periodic (see Figure 3.8). As a result, complexity decreases (Figures 3.10 and 3.13(c)).

The results of the band-phase-randomized surrogate test (see Figure 3.7) supports our speculation that the specific frequency components of neural activity contribute to reducing the complexity of neural activity.

3.5.2 Relationship to Studies on ASD

In this study, we found the reduced complexity of neural activity in a neuron group with local over-connectivity in the synaptic network. This result may relate to the lower complexity of EEG signals in ASD children (2 to 24 months) [14]. Therefore, in our model, a neuron group with local over-connectivity in the synaptic network shows the ASD-like low complexity of neural activity, as shown in Figure 3.9. However, another study showed that MEG signals in several regions of the brains of ASD children (6-15 years) have high complexity [43]. We speculate that developmental changes in the anatomical network structure cause this discrepancy. Solso et al. [95] showed that over-connectivity was mainly observed in the extremely early stages of development of ASD children, but not in ASD children aged 3-4 years. Hence, our model shows the possibility that the reduction of complexity of neural activity in ASD children aged 2-24 months is caused by local over-connectivity. On the other hand, in ASD children aged 6-15 years, who were the research targets in the study of Ghabari et al. [43], fluctuations in the complexity of brain activity may be caused by other factors other than local over-connectivity. Future studies may clarify the exact relationship between the complexity of brain activity and the anatomical network in ASD by using a computational model that includes the developmental changes.

Chapter 4

Chaotic Itinerancy from the Coupled Dynamics within an Embodiment System

4.1 Problem Statement

The main objective of this section is to comprehend the coupled dynamics underlying emerging behaviors and their transitions, which occur through the interaction between the brain and the body, in an environment. In particular, in this study, we focus on how structural properties of a synaptic network and the ratio of the brain to the body, affecting coupled dynamics, influence the diversity of emergence of behaviors. Further, we analyze the functional network within the coupled dynamics in each behavior from the perspective of the information theory and the complex network theory to understand how the coupled dynamics induce the emergence of behaviors and their transitions. As we mentioned in Section 2.3.1, several studies discussed the importance of anatomical and functional networks for the emergence of behaviors or cognitive functions [7, 17, 59, 34, 111, 81]. Additionally, some studies have suggested the importance of organization of connections between the body and brain for generating diverse behaviors during development [50, 49].

The complex relationship between the brain and body can be expressed as a nonlinear dynamical system. This complex system often shows a phenomenon, called chaotic itineracy, in a state space, where the state of the system transits along a

certain trajectory consisting of stable and unstable attractors, as mentioned in Section 2.3.2. From this perspective, the diverse behavior of animals and the spontaneous transitions between behaviors could be explained by a complex coupled dynamical system consisting of the brain and physical body. Inspired by this concept, several studies have shown the importance of the interaction between the body and brain in the environment using computational models [67, 78, 66, 119]. However, as mentioned in Section 2.3.3, these models only partially succeed in representing the coupled dynamics between the brain and the body. That is, these models are not sufficient to investigate the relationship between the brain and body for emerging behaviors.

In this study, we conduct simulations using a synaptic network with a nonlinear oscillator (brain) and a musculoskeletal model (body), which are connected to each other to induce coupled dynamics between the brain and body. To focus on the role of the brain and body dynamics for emergence of behaviors and transition of behaviors, we use a simple body structure (i.e., a snake-like robot) and a nonlinear oscillator model, without self-organization, instead of a spiking neural network with self-organization as we used in the previous chapter. Using this approach, the coupled dynamics between a network and a body is feasible and can be informatively analyzed. We suppose that the number of emerged behaviors is affected by the structural properties of the synaptic networks under different macroscopic structural properties and the ratio of the brain to the body for coupled dynamics. Further, we hypothesize that different interactions within the functional network induce stable or unstable behaviors. Herein, the functional network is estimated based on the causality between the neurons in the synaptic network.

The main procedures and analyses for verifying our hypothesis are as follows (see Figure 4.1):

1. Determine the structure of the fundamental network based on the complex network model (Figure 4.1(a)). Then, if an edge exists between two nodes in the fundamental network, construct synaptic connections between nonlinear oscillators (synaptic network, Figure 4.1(b)). We assume that a nonlinear oscillator and their connections correspond to a brain region and the connectivity

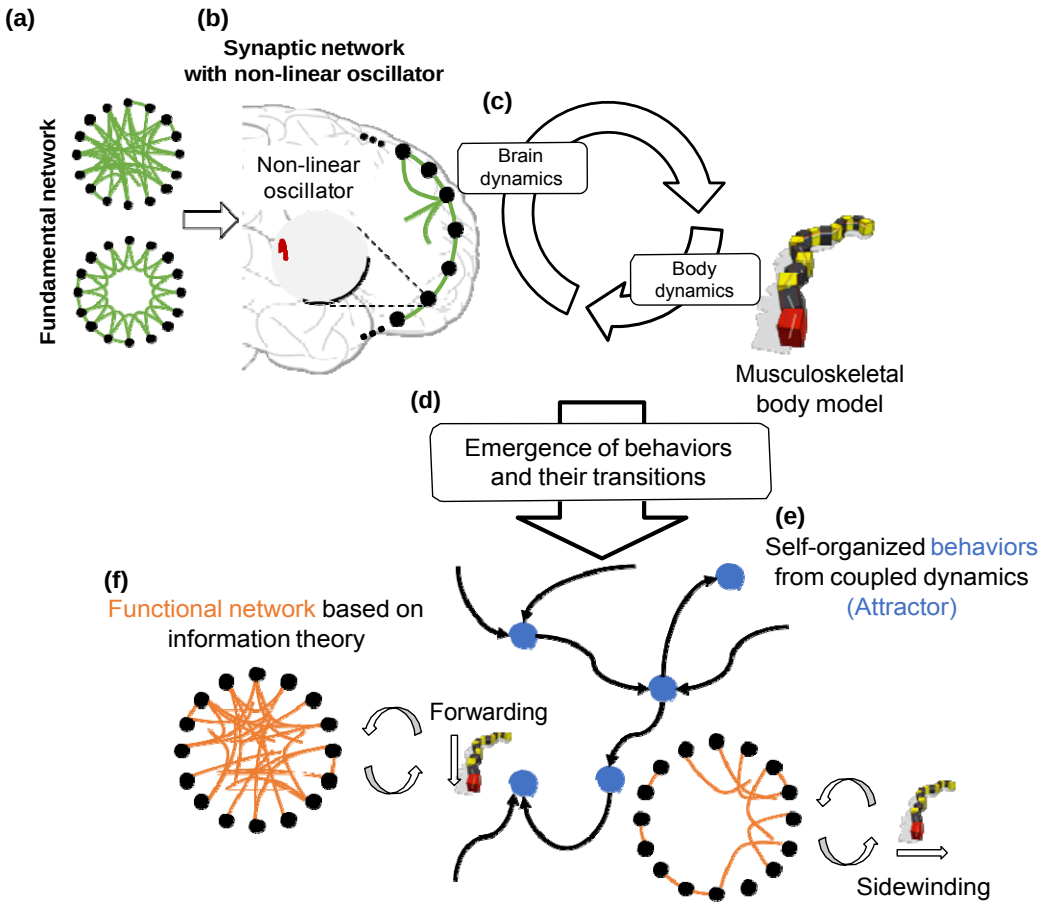

Figure 4.1: Hypothesis and assumptions about relationship among the synaptic and functional network, body, emergence of behaviors, and their transitions in this study. The black node represents non-linear oscillator, signifying the dynamics of brain regions. The green and orange lines indicate synaptic and functional connections between oscillators, respectively. The blue dots and their black lines with arrow represent attractors, which self-organized behaviors from the coupled dynamics, and their transitions. The curved arrows in (c) indicate a ratio between the brain and body dynamics on the coupled dynamics.

between regions. Furthermore, we suppose that the initial weight of connection in the synaptic network is given and is fixed.

2. Interact the network model with the musculoskeletal model to allow emergence of behaviors and transitions of behaviors (Figure 4.1(d)). The sensory ratio is modified to adjust the ratio between the brain and body dynamics for coupled dynamics (Figure 4.1(c)).

3. Classify behaviors, which are characterized by the clustering method, as the stable or unstable behaviors based on relative stability (defined per duration of behavior). We assume these stable and unstable behaviors correspond to a behavioral attractor and the transition between attractors (Figure 4.1 (e)), respectively.

4. Analyze the functional network for each classified behavior using transfer entropy and complex network theory to determine the coupled dynamics underlying these behaviors and their transitions (Figure 4.1(f)).

4.2 Model

4.2.1 Synaptic Network with Nonlinear Oscillators

Figure 4.2 (c) shows the overview of the network model and their connections with the body in this study. The network consists of multiple nonlinear oscillators, which are connected to each other based on the fundamental network (synaptic network). In this study, we utilize the Bonhoeffer-van der Pol (BVP) equation as a nonlinear oscillator to express the synchronized and desynchronized dynamics between the rhythmic activities of the brain regions. A previous study has shown that the interaction between BVP equations induce chaotic dynamics [4]. The oscillators are separated into interface neurons, which are directly connected to the robot muscle and other neurons, and the hidden neurons, which are only connected to other neurons. The interface neurons receive and send sensory feedback on muscle lengths

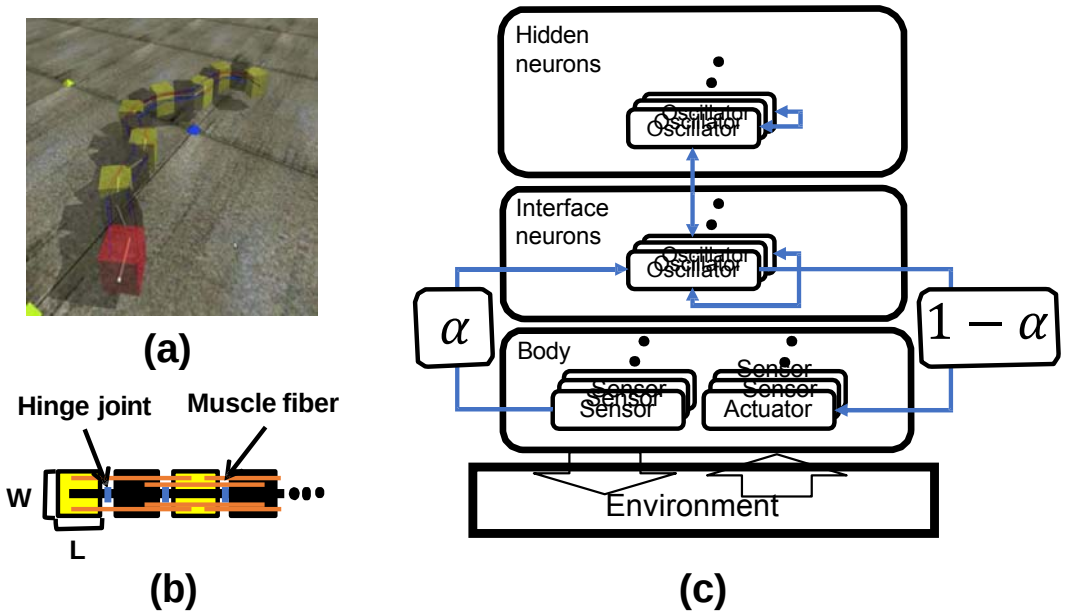

Figure 4.2: Overview of snake-like robot with a synaptic network with nonlinear oscillator. (a) Snake-like robot. (b) Physical model of the snake-like robot. (c) A graphical representation of the model in this study. The sensor and actuator connect with the interface neurons. Additionally, interface and hidden neurons (oscillator) are interacting with each other and other neurons in the same layer, through synaptic connections. That is, brain dynamics (hidden neurons) affect the behavior of the body, and body dynamics also affect brain dynamics through interface neurons. The variable of α adjusts the ratio of body dynamics to brain dynamics in coupled dynamics.

and signals to adjust the length of the muscle, respectively. The dynamics of oscillators and their interactions are expressed as follows:

$$\tau \frac{dx}{dt} = c\left(x - \frac{1}{3}x^3 - y + z\right) + \delta(S_f - x), \tag{4.1}$$

$$\tau \frac{dy}{dt} = \frac{1}{c}(x - by + a) + \epsilon S_f, \tag{4.2}$$

$$S_f = \begin{cases} \alpha I + (1-\alpha)\frac{1}{K}\sum_{j=1, j\neq i}^{N} w_{ji}x_j & \text{if interface neuron, or} \\ \frac{1}{K}\sum_{j=1, j\neq i}^{N} w_{ji}x_j & \text{else.} \end{cases} \tag{4.3}$$

where a, b, and c control the dynamics of neuron; z is a tonic input; and δ and ϵ control the strength of the excitatory and inhibitory influences from other neurons, respectively. Each neuron has a connection weight w, and K represents the number of connections for each neuron. Finally, α controls the strength of the ratio between the body and the network, while I is the sensory feedback value from the musculoskeletal model. The movement of the robot is generated by spontaneous activation of the synaptic network without sensory input, if $\alpha = 0.0$. Each interface neuron is independently activated using the sensory feedback from the body only (i.e., no interaction in the network) if $\alpha = 1.0$. In our simulation, we use $a = 0.7$, $b = -0.2$, $c = 2.0$, $\delta = 0.01$, $\epsilon = 0.015$, $\alpha = \{0.0, 0.1, 0.3, 0.5, 0.7, 0.9, 1.0\}$, and $z = 0.4$, 0.45, 0.5, or 0.55. The network consists of 26 interfaces and 174 hidden neurons. In this study, we utilized the following weight types for w:

- Uniform weights: $w_{j,i} = \begin{cases} 1 & \text{if } j, i \textit{ are connected, or} \\ 0 & \text{else} \end{cases}$
- Randomly distributed weights: the weights are randomly distributed in $[-1.0; 1.0]$ and normalized to $\sum_{i=1, i\neq j}^{N} |w_i| = 1$.

4.2.2 Complex Networks for Fundamental Network

In this study, we utilize different structure of complex networks for fundamental network.

Small-world Network

See Section 3.2.2.

Scale-free Network

A scale-free network is defined as a network in which the number of node connections follows the power-law distribution given by $P(k) \sim k^{-\gamma}$, where k is the number of connections for each node, and γ is typically between 2 and 3. In this study, we constructed a scale-free network based on the BarabasiAlber (BA) [6] model as follows:

1. Begin with an initial number of nodes (m_0).
2. Add a new node with $m(< m_0)$ connections to the already existing nodes with probability $P(k_i)$, where

$$P(k_i) = \frac{k_i + 1}{\sum_k k_j + 1} \tag{4.4}$$

3. Repeat Step 2 until the prespecified number of nodes has been added.

4.2.3 Network Structures of Nonlinear Oscillators

We utilized the following network types and parameters of the fundamental networks in our experiments.

1. Regular network: $m = 2$;
2. Small world network (WS model): $p = 0.01$ or 0.05;
3. Random network (based on WS model): $p = 1.0$; and
4. Scale-free network (BA model): $m_0 = 2$.

In order to know structural properties of the synaptic network in this study, we investigated the clustering coefficient, shortest path length, and degree centrality as we explained in Section 3.3.3. In this study, we assumed that information is transmitted from one neuron to another, regardless of whether the weight between the oscillator has a positive or negative value. Hence, we use the absolute value of weights to calculate the clustering coefficient and the shortest path length. Figure 4.3 shows the clustering coefficient and shortest path length of each synaptic network in this study. As shown in the figure, a randomly distributed weighted network shows a longer shortest path length and a smaller clustering value, implying that randomly distributed weighted networks require more time to transmit information from one node to another node using less interaction among the neighboring nodes. Figures 4.4 presents the maximum degree centraility of each synaptic network. A larger value implies that the network has a hub node, which has more degrees than other nodes. Several studies have showed that a hub node plays an important role in maintaining the connectivity of the network [2] and in efficiently model (p=0. information [63]. We expected that there. would be a difference in information transmission within the network caused by structural differences which influence the stability of the behavior in chaotic itinerancy.

4.2.4 Snake-like Robot

We utilized a snake-liked robot for our simulations because the model has a simple body which makes it possible to analyze the relationship between the emergent behavior and the underlying network structure, but still it shows variational behaviors. We constructed a model of the snake-like robot using open dynamics engine [94]. Figure 4.2 shows the model and the appearance of the snake-like robot. The robot consists of multiple links connected by hinge joints and two-joint muscles, allowing it to exhibit synchronized behaviors. Each muscle fiber is stretched and compressed to move the robot body based on the muscle model shown in a previous study [51]. Each muscle is connected to an interface neuron that receives the muscle lengths as sensory feedback values. Furthermore, we restricted the movement of the robot to two dimensions using a hinge joint to simplify the analysis of the behaviors and its

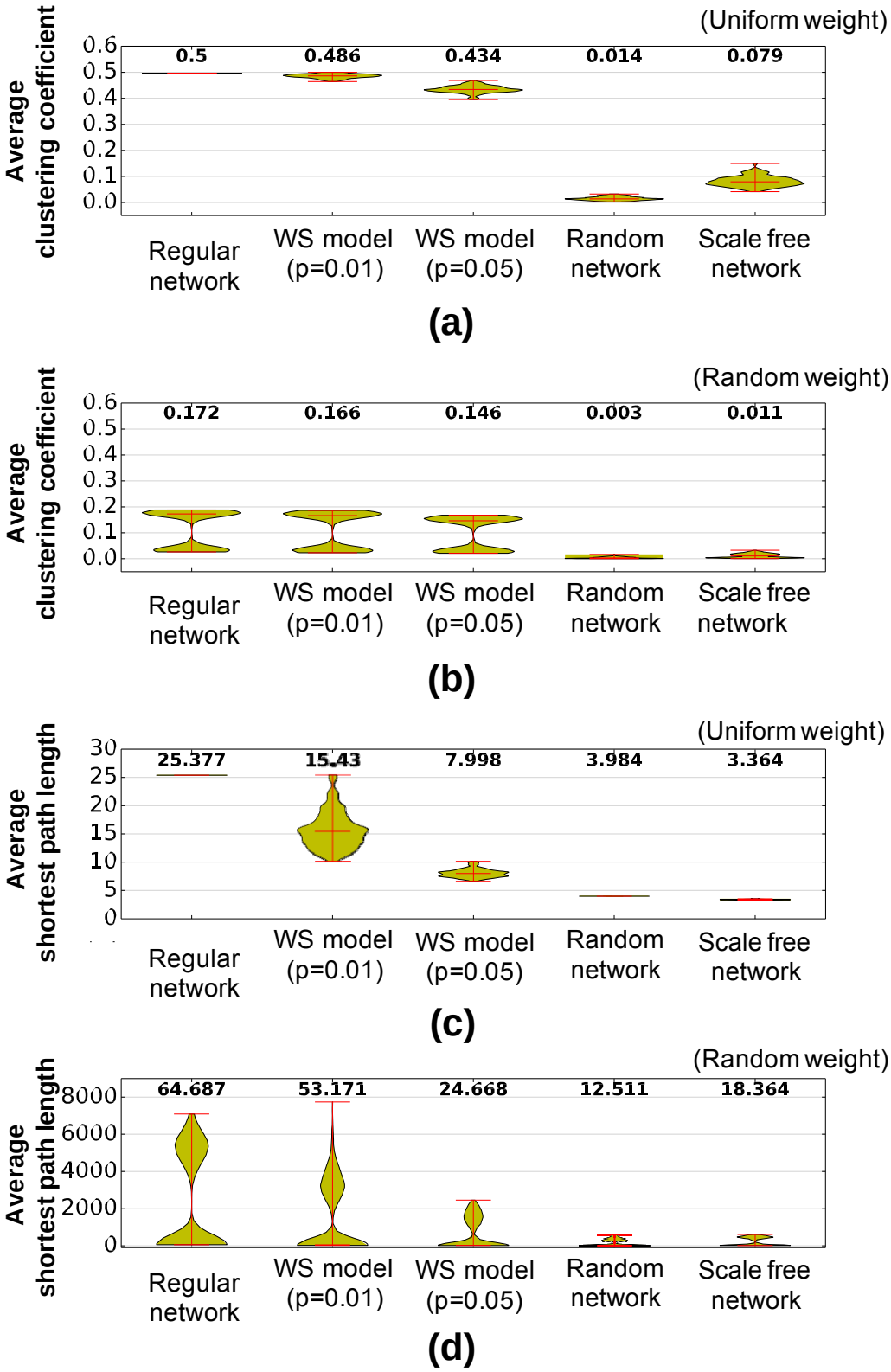

Figure 4.3: Complex network properties of synaptic networks employed in the experiments. The number in each box plot denotes the value of the median of 100 measurements for different experimental settings for each network type. (a) Average clustering coefficient for the uniform weights. (b) Average clustering coefficient for the randomly distributed weights. (c) Average shortest path length for the uniform weights. (d) Average shortest path length for the randomly distributed weights.

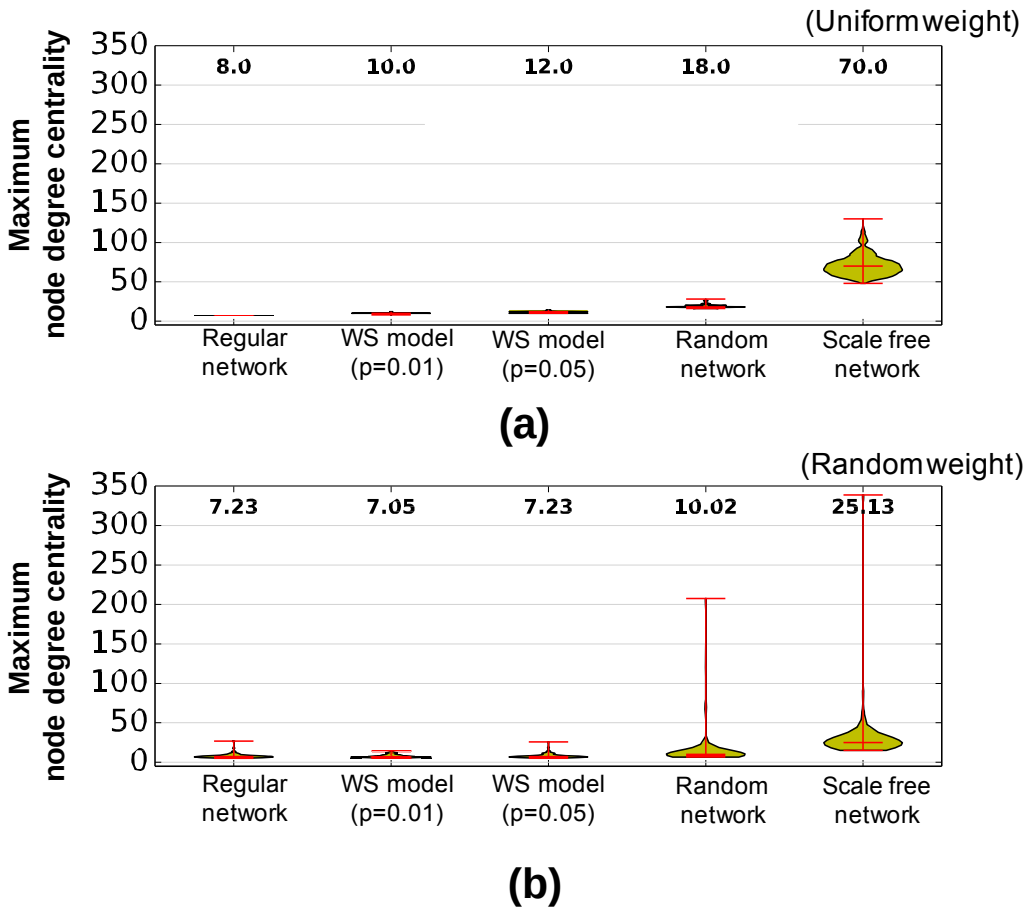

Figure 4.4: Maximum node degree of the synaptic network employed in the experiments. The number in each box plot denotes the value of the median of 100 measurements for different experimental settings for each network type. (a) Uniform weights and (b) randomly distributed weights.

interpretations. The parameters of this snake-like robot are shown in Table 4.1 shows the parameters of this snake-like robot.

Table 4.1: Setting of the snake-like robot.

Link height	Link width	Link length	Gap between two bodies
0.1 [m]	0.1 [m]	0.1 [m]	0.02 [m]
Link mass	Number of links	No. of single-joint muscles	No. of double-joint muscles
0.6 [kg]	15	0	26

4.2.5 Parameters and Simulation Setting

We conducted experiments using the above-mentioned network structure. Sensor ratio α in Eq (4.3) is set as $\{0.0, 0.1, 0.3, 0.5, 0.7, 0.9, 1.0\}$. Furthermore, we used $\{0.4, 0.45, 0.5, 0.55\}$ as the values of tonic input. The simulation was independently conducted 100 times for each condition, and the simulation time was 2000 s for each condition. In this study, we excluded the first 50 s from the analysis to avoid excessive unstable behaviors of the snake-like robot.

4.3 Method for analysis of the Neural and Behavioral Dynamics

4.3.1 Analysis of the Behavior Pattern

In order to distinguish repetitive behaviors, we constructed a feature vectors using correlation coefficients between the hinge joint angles within overlapped time windows, and then, applied a clustering method to the feature vectors. The procedure is presented as follows:

1. Calculate a feature vector that consists of correlation coefficients for all possible joint angle combinations within an overlapped time window. This vector is calculated as follows:

$$\mathbf{R} = [\mathbf{r}^{1,2}, \mathbf{r}^{1,3}, \ldots \mathbf{r}^{1,k}, \mathbf{r}^{2,3}, \mathbf{r}^{2,4}, \ldots, \mathbf{r}^{k,k-1}], \tag{4.5}$$

$$\mathbf{r}^{\mathbf{i,j}} = [\mathbf{r}_{\mathbf{1}}^{\mathbf{i,j}}, \mathbf{r}_{\mathbf{2}}^{\mathbf{i,j}}, \ldots, \mathbf{r}_{\mathbf{n-1}}^{\mathbf{i,j}}, \mathbf{r}_{\mathbf{n}}^{\mathbf{i,j}}], \tag{4.6}$$

where r is a correlation coefficient; k is the number of joint angles; and i and j are the indices of the joint angles.

$$r_n^{i,j} = \frac{\sum_{l=n*t_s}^{t+\Delta t} (\theta_l^i - \bar{\theta}^i)(\theta_l^j - \bar{\theta}^j)}{\sqrt{\sum_{l=n*t_s}^{t+\Delta t} (\theta_l^i - \bar{\theta}^i)} \sqrt{\sum_{l=n*t_s}^{t+\Delta t} (\theta_l^j - \bar{\theta}^j)}}, \tag{4.7}$$

where θ is the joint angle; $\bar{\theta}$ is the mean of the joint angles in a time window; n is an index of the window position; and Δt and t_s denote the sizes of the time window and the shifting time, respectively.

2. Reduce the number of the dimensions of the feature vectors using the Laplacian eigenmaps for clustering [11]. Laplacian eigenmaps are manifold unsupervised learning algorithms for nonlinear dimension reduction, which projects each sample point into a low-dimensional space based on Laplacian eigenmaps to retain the local geometric properties in the k-nearest neighbor points for each point.

3. Apply the density-based spatial clustering of applications with noise (DBSCAN) [32] to find clusters.DBSCAN can determine the arbitrary number of clusters with arbitrary shapes based on the density of a given set of points in space.This algorithm considers it as one cluster if the distance between the data is less than a parameter ε, and the number of data points is more than a minimum number of points.

4. Measure the duration of each behavior and classify the behavior pattern based on whether the durations are shorter or longer than a threshold value, which is determined by the Otsu method [84]. Hereafter, we classify these behaviors as unstable (less than the threshold) or stable (longer than the threshold).

4.3.2 Functional Network within Behaviors

We estimated the functional network for each behavior in order to understand the dynamic properties of the synaptic network for emergence and transitions of behaviors. In this study, we used transfer entropy to estimate a functional network and information flows between the neurons or the brain (nonlinear oscillator) and body (musculoskeletal model).

The transfer entropy (TE) from one neuron y to another neuron x is given as follows:

$$T_{y\to x} = \sum p(x_{n+1}, x_n^{(k)}, y_n^{(l)}) \log \frac{p(x_{n+1}|x_n^{(k)}, y_n^{(l)})}{p(x_{n+1}|x_n^{(k)})}, \tag{4.8}$$

where l and k denote the given historical lengths used to predict the future state and t indicates the current time step. In this study, $l = k = 1$. The Java Information Dynamics Toolkit (JIDT) [71] was used to calculate the TE using the Kraskov, Stogbauer, and Grassberger (KSG) method [65]. The KSG method has a greater accuracy for a smaller number of samples than does other methods. The extracted functional network structure was then analyzed to answer the following three questions: (1) What is the nature of the spatial interactions between the neurons (local or global)? (2) How complex is the network structure (high or low complexity)? (3) How strongly are the neurons connected to the environment through the body?

The procedures used to answer to these questions are as follows:

1. Apply the infinite relational model (IRM) [62] to visualize the structure of functional network. The IRM is nonparametric Bayesian model to discover clusters in the observed relational data. The generative model for the IRM is defined as below:

$$\begin{aligned} z|\gamma \sim &\quad \mathrm{CRP}(\gamma) \\ \eta(a,b)|\beta \sim &\quad \mathrm{Beta}(\beta, \beta) \\ R(i,j)|z,\eta \sim &\quad \mathrm{Bernouli}(\eta(z_i, z_j)), \end{aligned} \tag{4.9}$$

here, $R(i, j)$ is a relationship between two elements of i and j in a relational data R. The variable z is latent variable and $\eta(a, b)$ is a relationship between two clusters of a and b. The CRP, Beta and Bernouli in the equation represent Chinese Restaurant Process [85], Beta distribution and Bernoulli distribution, respectively. The variable γ and β represent hyper-parameter for frequency of the new cluster using the Dirichlet process and the noise of the relationship among the elements in a cluster, respectively. In this study, we use $\gamma = 1$ and $\beta = 7$. The procedures used to visualize the structure of functional network using IRM are as follows:

(a) Estimate mutual information to extract subnetworks, such as brain regions. The mutual information (MI) between two neurons (x and y) can be calculated as follows:

$$I(X;Y) = \sum_{x,y} P_{XY}(x,y) \log \frac{P_{XY}(x,y)}{P_X(X)P_Y(Y)} \tag{4.10}$$

The KSG method using JIDT was used to estimate MI.

(b) Binarize the result of (a) to apply the IRM, as this model handle binary values. The value of the threshold to be binarized is determined by the Otsu method [84].

(c) Rearrange a matrix consisting of relational data variables to a diagonal sequence of submatrices (cluster), which may correspond to the subnetworks.

(d) Overlay TE values on the result of (c) to extract the final subnetwork structure.

2. Calculate the complex network properties for the functional network to determine the global properties of the network.

3. Calculate the average of the two TEs from (to) the hidden neurons to (from) the interface neuron to understand the relationship between the body and the functional network.

4.4 Results

4.4.1 Movement of the Snake-like Robot

In our simulation, the model shows more than four different stable behaviors: crawling movement (forward crawling, backward crawling) and bending (hold a position, sidewinding). Figures 4.5 and 4.6 show examples of these behavior. These behaviors and their transitions emerged with different durations.

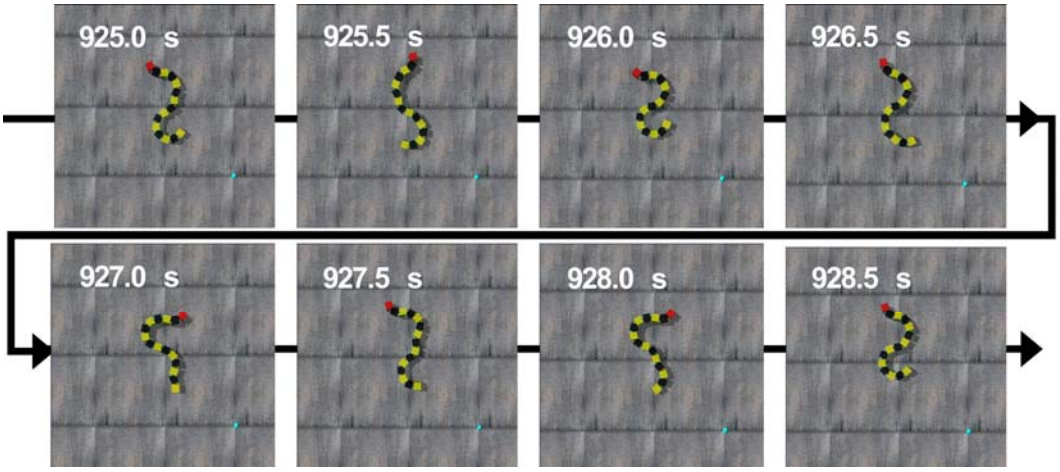

Figure 4.5: Example of forward crawling movement of the robot.

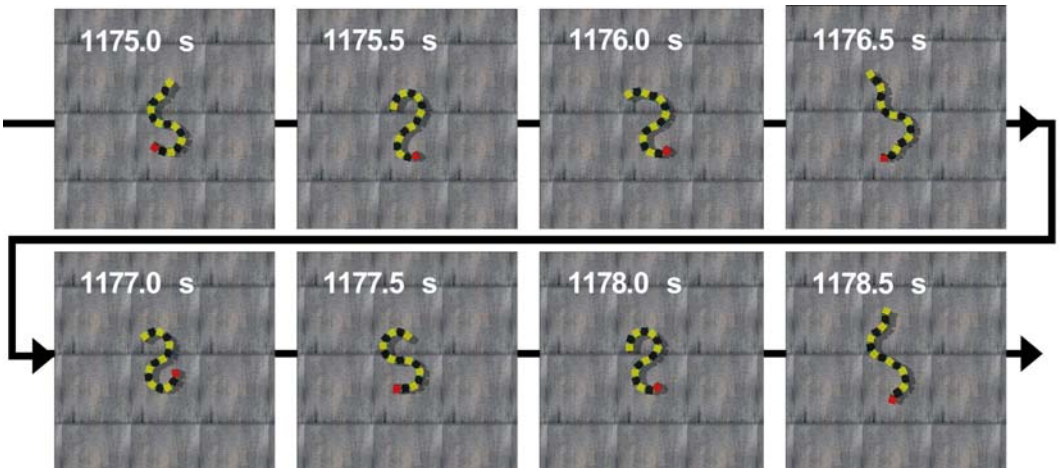

Figure 4.6: Example of bending movement of the robot.

In this study, we reduced the 91 dimensions of the feature vector to three dimensions using 350 k-nearest points to avoid curse of dimensionality. After dimensionality reduction, we clustered each point with $\varepsilon = 0.16$, and the minimum number of points was set to 10. We observed the clusters that correspond to one behavior in the

low-dimensional space of behaviors and their transitions, as chaotic itinerancy (see Figure 4.7).

4.4.2 Relationship between Various Movements and the Synaptic Network

Figures 4.8 and 4.9 show the average number of behaviors, average number of stable behaviors, and the maximum duration of one behavior in each network structure for the uniform and randomly distributed weights, respectively. Since there is no marked differences resulted from using different tonic input values, we only show the results for tonic input = 0.45 (see Figures B -B for the effect of the tonic input). The threshold to determine the stable or unstable movement was determined as 101.5 s according to Otsu method. The x-axis indicates the sensor ratio α in Eq (4.3). Different peak positions were observed according to the network type.

As shown in Figures 4.8(a) and 4.9(a), the number of behaviors decreased if the sensor ratio increased. However, as shown in Figures 4.8(b) and 4.9(b), the peak of number of stable behaviors appeared near the center of the sensor ratio range, whereas only a small number of behaviors emerged if the sensor ratio = 1.0 or = 0.0. Furthermore, as shown in Figures 4.8(c) and 4.9(c), more stable behaviors emerged when the value of the sensor ratio was high.

These results indicated that network dynamics facilitate the emerge of diverse behaviors, but too strong dynamics of a network destabilizes the body, making it unable to sustain the current behavior. This result suggests the importance of balance between the synaptic network and the body of the robot for the emergence of diverse behaviors. Furthermore, there were statistically significant differences between network types.

4.4.3 Analysis of the Functional Network

Figure 4.10 shows the differences between a synaptic network and two functional networks for a stable and unstable behavior in one simulation. As shown in the figure, different network structures emerged with different behaviors, even though the structure of the synaptic network was fixed. A longer (shorter) behavior has

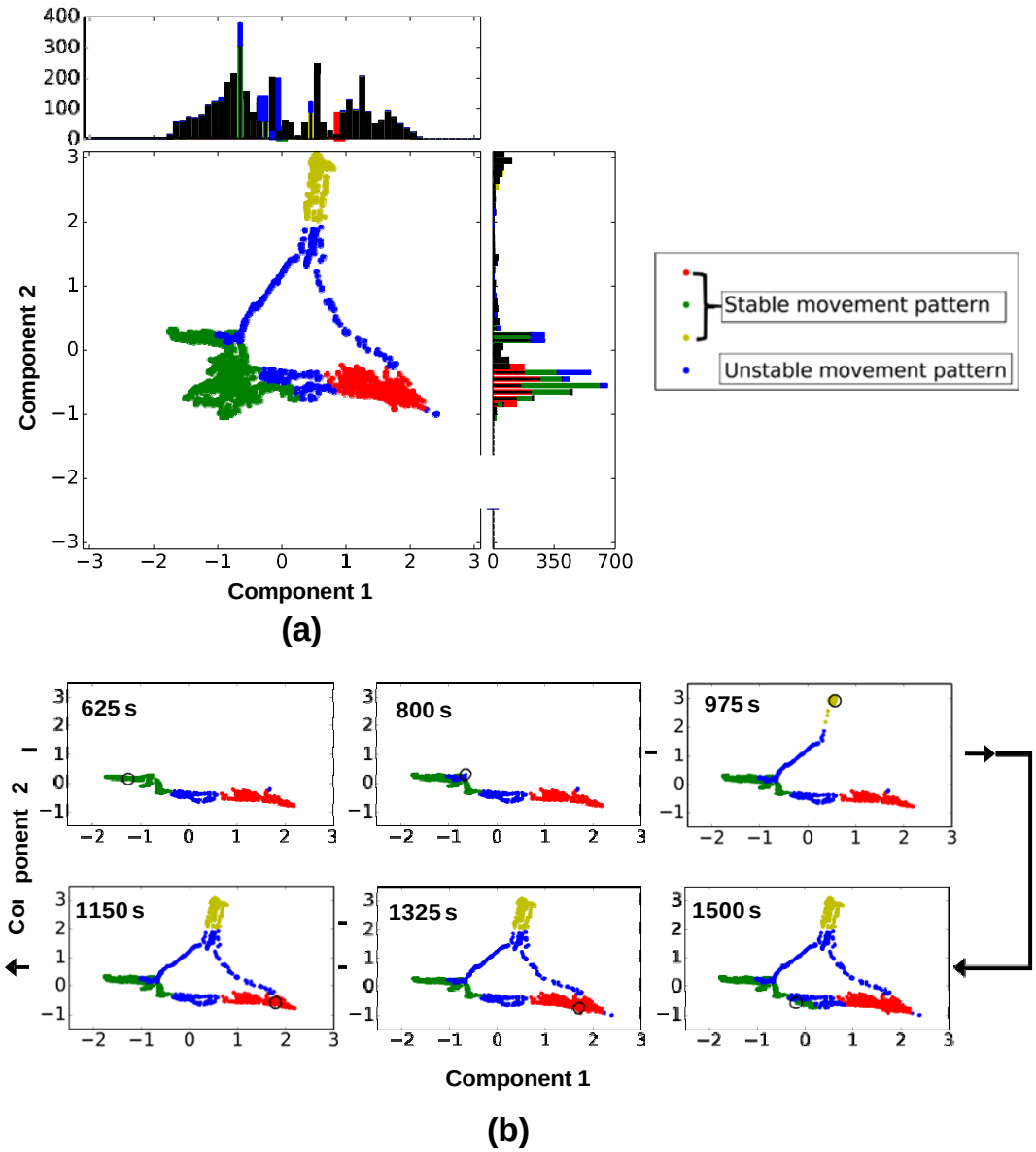

Figure 4.7: Example of the feature vector and transitions of the state vector in the dimensionally-reduced space by Laplacian eigenmaps (WS model ($p = 0.05$) with randomly distributed weights, a tonic input of 0.4, and a sensor ratio of 0.3). (a) The blue dots represent an unstable behavior. The dots with other colors represent stable behaviors. The bar graphs show the histogram of data points along the x and y axes. (b) The black circle represents current state in the feature space.

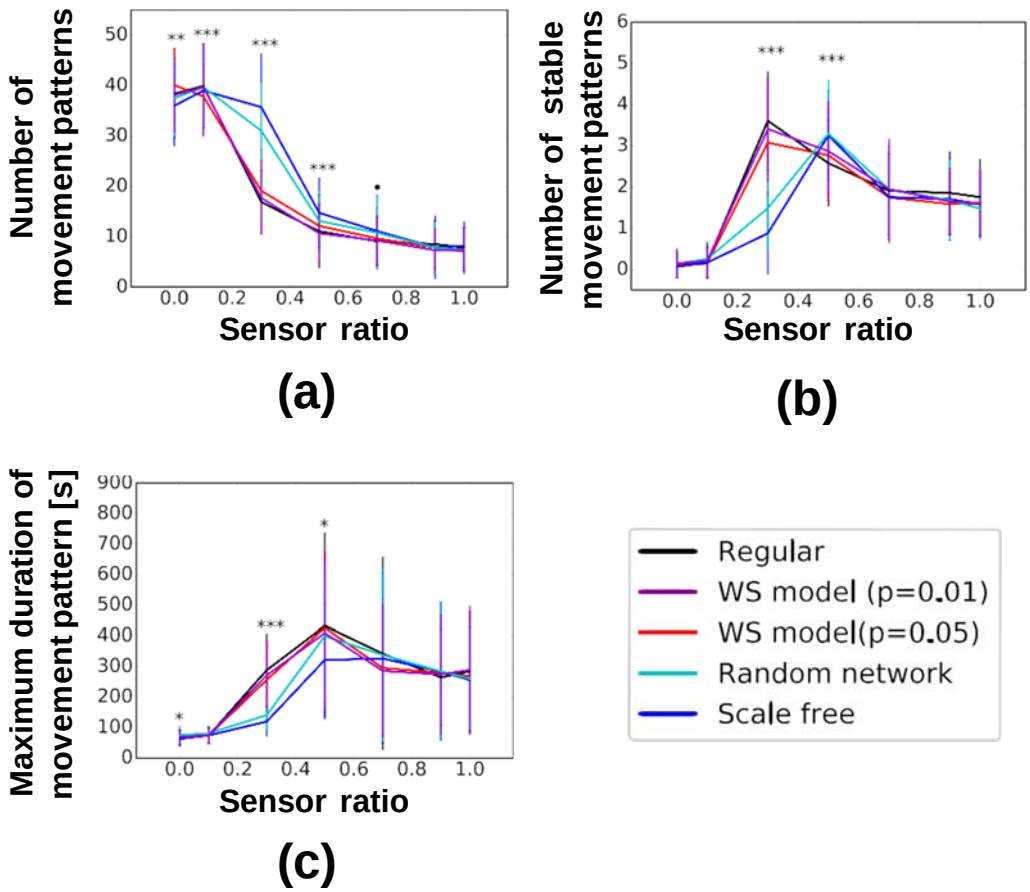

Figure 4.8: Number of behaviors and maximum duration of behavior for a uniform weight. The tonic input is 0.45. (a) Number of behaviors, (b) number of stable behaviors, and (c) maximum duration of behaviors. The x-axis indicates the sensor ratio required α in Eq (4.3) to control the proportional influences between the body and the network. *** $p < 0.001$, ** $p < 0.01$, * $p < 0.05$, · $p < 0.1$ indicate statistically significant differences between the synaptic networks through the ANOVA test.

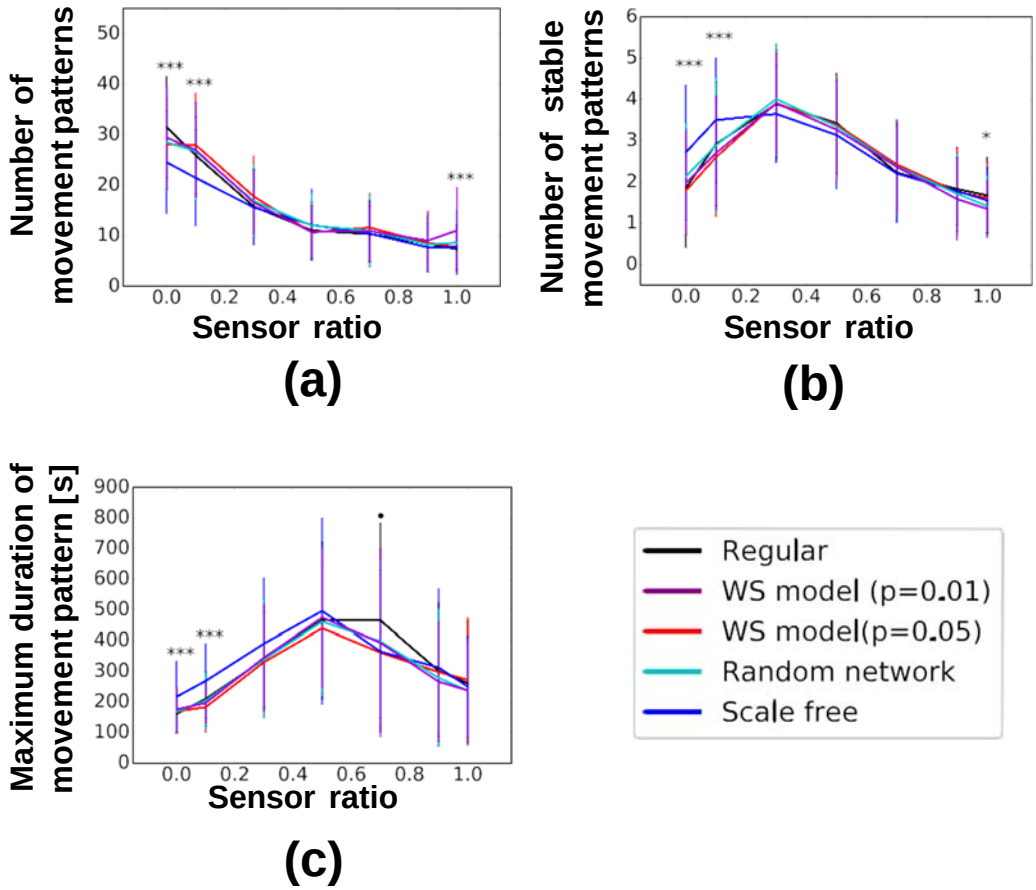

Figure 4.9: Number of behaviors and maximum duration of behavior for a randomly distributed weight. The tonic input is 0.45. (a) Number of behaviors, (b) number of stable behaviors, and (c) maximum duration of behaviors. The x-axis indicates the sensor ratio required α in Eq (4.3) to control the proportional influences between the body and the network. *** $p < 0.001$, ** $p < 0.01$, * $p < 0.05$, · $p < 0.1$ indicate a statistically significant differences between the synaptic networks through the ANOVA test.

small (large) subnetworks with less (large) interaction among them. Furthermore, the interface neurons were sparsely (densely) distributed in the subnetworks.

Figures 4.11 and 4.12 show the structure properties of the functional network and the interaction between the interface and hidden neurons in terms of the stability of the periodic behavior. Since tendency was same, regardless of whether the synaptic network was used with a uniform or random weight, we only plot the results of a synaptic network with a uniform weight.

Figure 4.11 shows the relationship between the sustainability of the periodic behavior and structural properties of functional network, regardless of the structure of the synaptic network. As shown in the figure, sustainability shows a positive and negative relationship with the shortest path length and clustering coefficient, respectively. The high value of shortest path length and a small value of the clustering coefficient in the network indicate that the network is not a complex network. Figure 4.12 shows the transfer entropy from the hidden to the interface neurons regardless of the structure of the synaptic network, indicating how the body dynamics influence on the network.

Since there were no differences in terms of transfer entropy from hidden neurons to interface neuron and from interface neurons to hidden neurons, we only plot the transfer entropy from hidden neurons to interface neurons. As shown in the figure, the transfer entropy between the interface and hidden neurons decreases if duration of the movement increases. The above results indicate that a vigorous interaction between many hidden neurons may induce a transition from the current behavior to another behavior. Moreover, the absence of differences may indicate that a common structural feature of the functional network is related to the sustainability of the behavior, irrespective of the structure of the synaptic network.

4.5 Discussion

4.5.1 Role of the Body and Brain Dynamics in Bodily Chaotic Itinerancy

Our simulation showed that emergence of behaviors and their transitions occur with interactions between the musculoskeletal model and synaptic network. Figures 4.8 and 4.9 shows how the sensor ratio and the type of the synaptic network structure

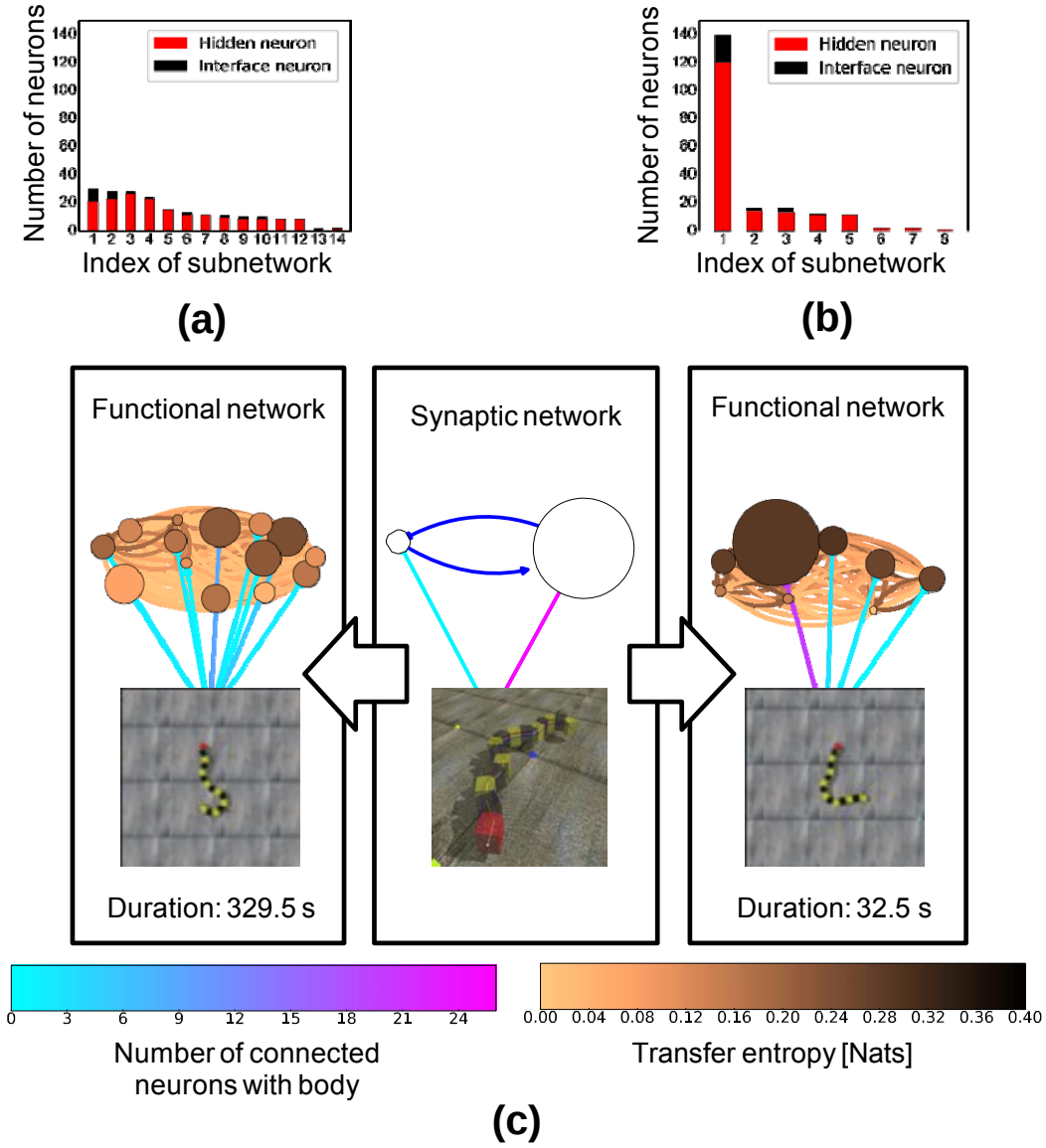

Figure 4.10: Estimated functional network structures for different movement durations: 329.5 s (longer) and 32.5 s (shorter). (a), (b) Number of neurons in each subnetwork for 329.5 s and 32.5 s, respectively. The red and black bars indicate hidden and interface neurons. (c) Synaptic network with a musculoskeletal movement and two different functional networks. Each node indicates an IRM-extracted subnetwork, and the node sizes indicate the number of neurons in each subnetwork.

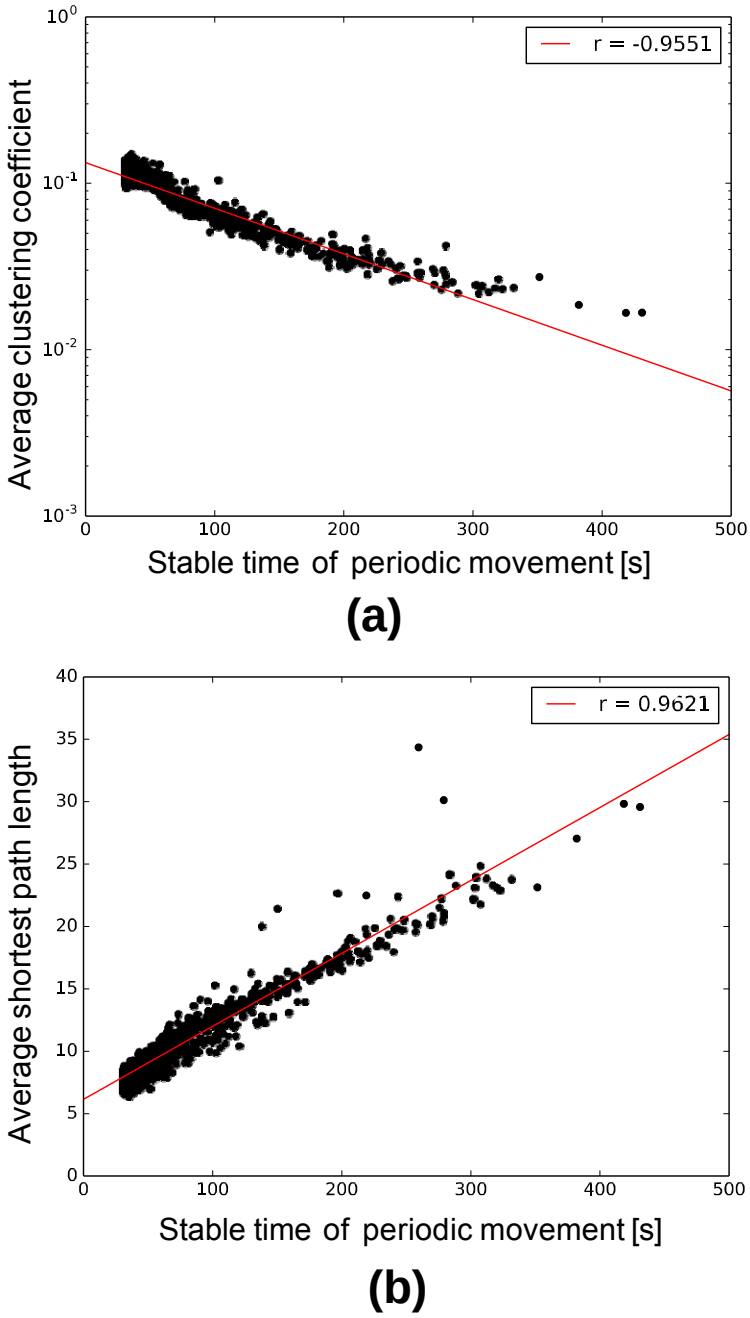

Figure 4.11: Structural property of the functional network for the uniform weights. Each red line in the figure indicates a correlation. (A) Average clustering coefficient and (B) average shortest path length.

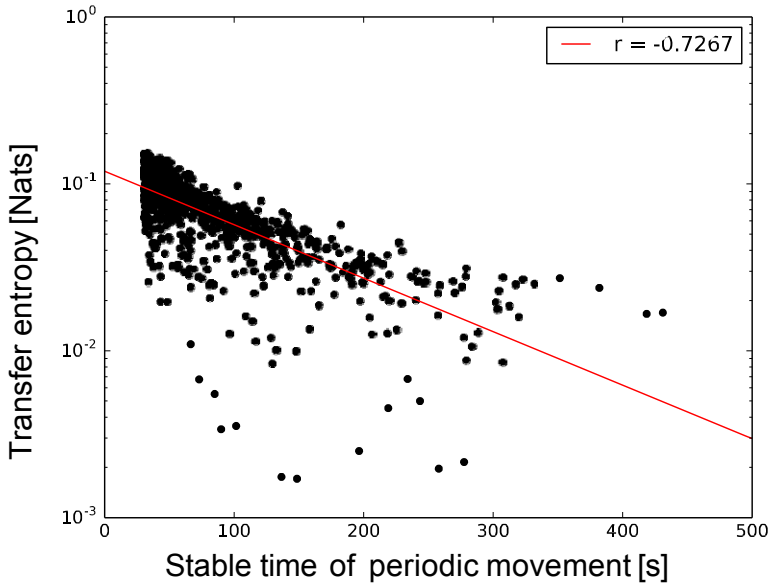

Figure 4.12: Interaction between the body and the network in terms of the duration of periodic movements for the uniform weights. The red line in the figure indicates a correlation: average of transfer entropy from the interface neurons to hidden neurons.

influence the number of movements and the duration of the most stable movement. As shown in Figures 4.8(a), (b) and 4.9(a), (b), many unstable behaviors emerged if the sensor ratio was 0.0. However, the number of unstable behaviors decreased, while the number of stable behaviors increased, if the sensor ratio increased. These results indicate that the network dynamics contribute to generating various behaviors, while the dynamics per se cannot stabilize the movements because of the strong chaotic dynamics of the network. Additionally, the body dynamics from the sensory feedback may provide stability to sustain the current behavior. The maximum duration of the behavior shown in Figures 4.8(c) and 4.9(c) may support this concept. However, as shown in the Figures 4.8(b), (c) and 4.9(b), (c), the maximum duration and number of stable behaviors decrease if the sensor ratio exceeds 0.5. We speculate that the attractor for convergence to one behavior is weakened, because synchronicity is weakened by loose connections between neurons if the sensor ratio is high. The findings of a study of spontaneous activation in the neocortex [73] might be related to the above interpretation of the role of the body and the brain for the emergence of behaviors. They showed that the activation pattern for encoding sensor information

is already observed in the spontaneous activations of neocortical activities in rat experiments, and proposed that neocortical activation is constrained by sensory input. Therefore, the sensory feedback may act as a trigger for self-organization of stable behaviors into a subspace in one of the possible states determined by a non-linear oscillator network.

4.5.2 Network Structure of Functional Network Underlying Behaviors and Transition of Behaviors

As shown in Figures 4.10 and 4.11, in unstable behavior, neurons in a functional network interact with each other through one vast subnetwork with a large value of the clustering coefficient and the shortest path length. This result indicates that the transitions between behaviors or exploration of behavior occur via a functional network with a small value of the shortest path length, which can transmit information rapidly, and a large value of the clustering coefficient, which indicates high frequent interactions between neurons. On the other hand, in the case of a stable behavior, a functional network has less complex network properties and has a broad-range, distributed interaction neuron of neurons in subnetworks that locally interact with the body. Furthermore, as shown in the Figure 4.12, the transfer entropy in the functional network during stable behavior is low (i.e., interaction between neurons is less). These positive and negative relationships between the structural property of the network and the duration of the behavior indicate the probability of transition from the current behavior to a different behavior by examining the current structure of the functional network. This finding can suggest a mechanism of chaotic itinerancy in terms of the spontaneous activities of animal from aspects of neural activities, such as a default mode network [16] (a network consisting of activation signals among several brain areas of the cortex when a person is in a resting state). Hermundstad et al. [53] showed that the shortest path length decreased when the task to be concentrated on is given. Therefore, we speculate the functional network for stable and unstable behaviors corresponding to unfocused (unconscious) and focused states (conscious).

4.5.3 Influence of the Network Types on the Number and Duration of Behaviors

As shown in Figure 4.8, statistically significant differences were observed between the structure of synaptic networks. We speculate that these differences were caused by the existing the hub node, which has larger node degree than that other nodes, in the network. As shown in Figure 4.4, scale-free and random networks demonstrate a large value of maximum degree centrality than other network types (i.e. a hub node is existing in the network). Several studies showed that this hub node plays an important role in maintaining network dynamics [2]. In this regard, the hub node may help to maintain the chaotic dynamics in the network. This result may relate to the result in the Figure 3.5 that shows the large complexity at the large value of p_{WS}. That is, the random network, which has a hub node, shows large complexity. As shown in the Figure 4.8 (a), the value of sensor ratio at which start the rapid decreasing the number of behavior patterns on random and scale-free networks is larger than other networks. This result also supports our speculation.

Nevertheless, this result showed that the type of synaptic network affects the emergence of diverse behaviors. Furthermore, the simulation revealed differences between networks with the uniform and randomly distributed weights. We also consider that these results are due to the structural properties of the synaptic network. As shown in the Figure 4.3, a randomly distributed weighted network has a large shortest path length and a small clustering coefficient. Therefore, the network requires more time to transmit information from one neuron to another neuron, and has less interaction among the neighboring neurons.

Results obtained with the functional network showed that the functional network has common structural properties related to the stability of the behavior, regardless of the type of synaptic network. However, the structural properties of the synaptic network and the sensor ratio relate are related to the frequency of the emerging behaviors. This may be involved in how the connectivity between the body and brain dynamics is formed through the subplate; the structural properties of the synaptic network are important for the emergence of the diverse behaviors as we mentioned in the Section 2.3.1. Therefore, a balance of the two dynamics of

both the body and the network determines the property of the chaotic itinerancy of the behavior in an embodiment system. If either side of the coupled dynamics dominates the other, the diversity of the behavior disappears. In contrast, the number of emerging movements tended to increase as the sensor ratio is differed with respect to the structure of the non-linear oscillator networks, and particularly with the distribution of node degree. Moreover, the general movement, which is a diverse behavior in early childhood, and the change in diverse behaviors with age [105], may also be related to this finding in terms of behavioral dynamics. More analyses are needed to verify these speculations.

Chapter 5

Conclusion

5.1 Summary and Contributions

In this thesis, we presented insights into how neural activity changes according to the structural properties of the macroscopic network, and how it affects the emergence of behaviors through interaction with body dynamics. Furthermore, we also showed how coupled dynamics changes according to emerging behaviors and their transitions. We constructed a spiking neural network model with different macroscopic networks and compared structural properties and the complexity of neural activities in each neuron group in the model. We also investigated the dynamics underlying emergent behaviors and their transitions, which are derived from the coupled dynamics between the musculoskeletal model and the oscillator network model with different macroscopic networks.

In summary, the following contributions have been made in this thesis:

- **Relationship among the structural properties of a macroscopic anatomical network, the complexity of neural activity (Chapter 3):** We constructed a neural network using multiple neuron groups that consisted of spiking neurons and changed the clustering coefficient and shortest path length in the network using the WS model. Then, we analyzed their spontaneous activity using MSE. Using complex network theory analysis and neural activity for each neuron group in a synaptic network, we showed that the local over-connectivity in the synaptic network decreased complexity and enhanced the intensity of specific frequency components of brain activity.

- **Relationship between the brain and body dynamics for emergence of behaviors (Chapter 4):** We constructed a simulation using a musculoskeletal model and a nonlinear oscillator network to represent the body and brain dynamics, respectively. We showed that the number of emergent behaviors is increased and restricted by the sensor ratio, and the degree of increase is changed by the structural properties of the synaptic network, especially the degree centrality of the nodes.

- **Coupled dynamics within emergence of behaviors and their transitions (Chapter 4):** We analyzed the dynamics behind the emergent behaviors and their transitions from the embodiment model using information and complex network theories. Our results of the analysis of a functional network showed that the clustering coefficient and the shortest path length in the functional network have a negative and positive relation with the duration of the behavior, respectively, regardless of the structure of the synaptic network.

5.2 Directions for Future work

5.2.1 Extension of Parameters of Macro- and Microscopic Network Model

In order to focus on the topological structure of a macroscopic network, we used the WS model to construct a fundamental network in Chapter 3. However, it is well known that anatomical and functional network have other structural properties, such as being scale-free network [30] or rich-club network [55], which has connections between the high degree of nodes. As shown in Figure 3.9, our results showed that the degree centrality in a synaptic network strongly affects induction of differences in complexity of neural activity. Investigating neural activities when such network structures are used as a fundamental network would be interesting point. Furthermore, a neuron group in our model had a randomly connected structure; however, the cortex has various layer structures. Moreover, several studies on ASD have discussed that the atypical balance of excitatory to inhibitory neurons in the cortex induces atypical connectivity and activity in the brains with ASD [23, 80, 44]. In future, we should include these kinds of parameters or structures in our

model. We expect that using these approaches would be a step forward to increasing understanding of the relationship between the structure and activity of the brain.

5.2.2 Role of Subnetworks and Dynamical Changing

Even though we showed that a subnetwork with interface neurons locally interacts with the body in the case of a stable behavior, the roles of other subnetworks are not clear, as discussed in Chapter 4. As we have mentioned earlier in Chapter 2, based on fMRI studies, each local network in the brain has a variable connectivity to perform different tasks [3]. Cole et al. [25] showed that the frontoparietal brain network acts as a hub region with a wide variety of connectivity and could be used to identify the current task and could be involved in transiting to another state, to switch to a novel task. We expect that some subnetworks in our simulation to act as a hub or play a different role, such as inhibiting or suppressing the activation of other subnetworks. Furthermore, the result of this research shows that a different functional network with subnetworks emerges with each behavior in a behavioral chaotic itinerancy. Analyses of such networks, focusing on the temporal changes of multiple variables, using limited penetrable horizontal visibility graphs and multiscale analysis, have recently been conducted [39, 41, 40, 38, 42]. Investing the dynamic fluctuation of the subnetwork structure with reference to such a method would also be interesting. Understanding this type of relationship would shed light on the mechanism of chaotic itinerancy within neural and behavioral dynamics.

5.2.3 Learning Method and Self-organization of Networks for Tasks using Coupled Dynamics

In the current model, we have not yet introduced any learning methods to adapt to a new environment or task, because the purpose of our research was to understand the role and potential of the coupled dynamics of the body and the brain itself for the emergence of spontaneous behaviors. However, the brains of humans and animals, as self-organizing systems, might be reconstructed via their experiences and information from the external environment. These changes influence their behavior and induce different experiences. How synaptic and functional networks

change through the interplay between behavior and a self-organized system in an environment and how it influences behaviors are interesting topics in developmental science. Several studies have shown that changes in synaptic [5] and functional networks [77, 87] occur in the brain according to age. These changes may play an important role in the emergence of behavior and functions of a human [22]. Another important future issue is understanding how various spontaneously emerging behaviors observed in the current model can be used to adapt to the environment or help motor development. Several studies have shown that having access to a diversity of behavior is effective for rapid learning of a new behavior, rather than noise-like behaviors [54, 107, 46]. These studies also discussed the relationship between the diversity of the behavior in early infancy and subsequent motor development [50]. We expect that using our approach with learning methods, such as reinforcement of learning for goal-directed behaviors, or Hebbian learning to learn corresponding behavior to the environment, will not only provide new insights into development and higher cognitive functions, but could also be adapted to engineering applications, such as the generation of robot behavior.

5.2.4 Effect of Morphology of Body and Environment

We used a simplified body and environment in our attempt to reveal the role of the structural properties of synaptic and functional networks for the emergence of diverse behaviors. However, in a developmental process, both the brain and the body change, and different behaviors are observed according to age (e.g., crawling, standing, or grabbing an object using one or two hands in humans). Several studies have shown the importance of both the physical body and the environment for the emergence of behaviors. For example, in an experimental study, Thelen and Smith [109] demonstrated the reappearance of a stepping movement in an infant following change in the body and the environment. In a simulation-based study regarding the morphological aspects of the body, Mori and Kuniyoshi [78] showed that a human-like distribution of tactile sensors induces human-like behaviors. Therefore, we expect that implementing such morphological changes will induce different behaviors and lead to a deeper understanding of the relationship of the brain, body,

and environment. Furthermore, we also expect that using multiple sensors will induce the emergence of a subnetwork with a specific role, such as a motor area or a sensory area in the brain.

Appendix A

Relationship between complexity of neural activity and neuron groups with all p_{WS} and statistical test

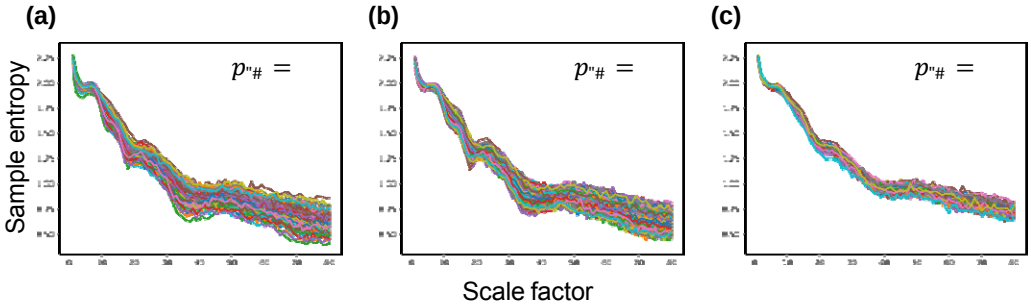

Figure A.1: Multiscale entropy (MSE)-based complexity curves of each neuron group in a synaptic network. (a) Lattice network ($p_{\mathrm{WS}} = 0.0$). (b) A small-world network ($p_{\mathrm{WS}} = 0.1$). (c) A random network ($p_{\mathrm{WS}} = 1.0$). The y-axis indicates sample entropy, and the x-axis indicates scale factor $\boldsymbol{\varepsilon}$.

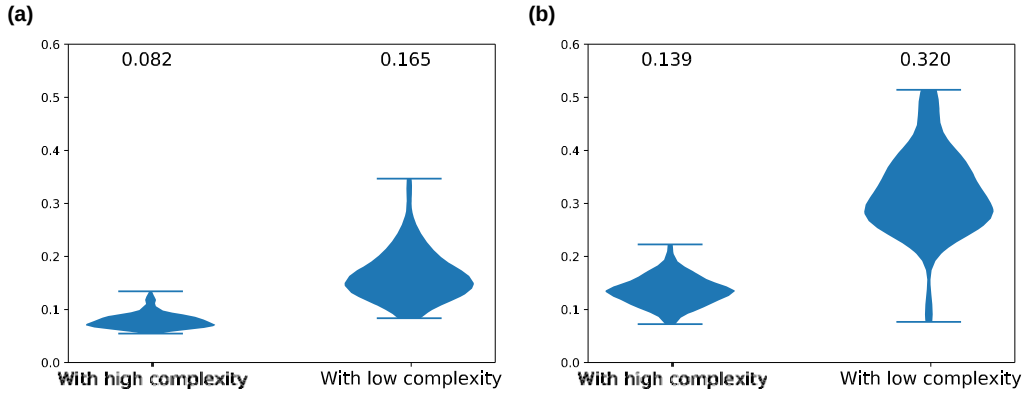

Figure A.2: The differences of peak amplitude of spontaneous neural activity in some frequency bands between neuron groups with low and high complexity when $p_{WS} = 0.0$. We used 10 neuron groups with high and low complexity in each simulation as comparison data. The number on above each violin plot denotes the average value for ten simulations. Wilcoxon signed-rank test was used for statistical test. (a) Amplitude in the 20-40 Hz band (Wilcoxon signed-rank test, statistic=6.0, p-value=4.6706e-18); (b)) Amplitude in the 40-60 Hz band (Wilcoxon signed-rank test, statistic=11.0, p-value=5.4302e-18).

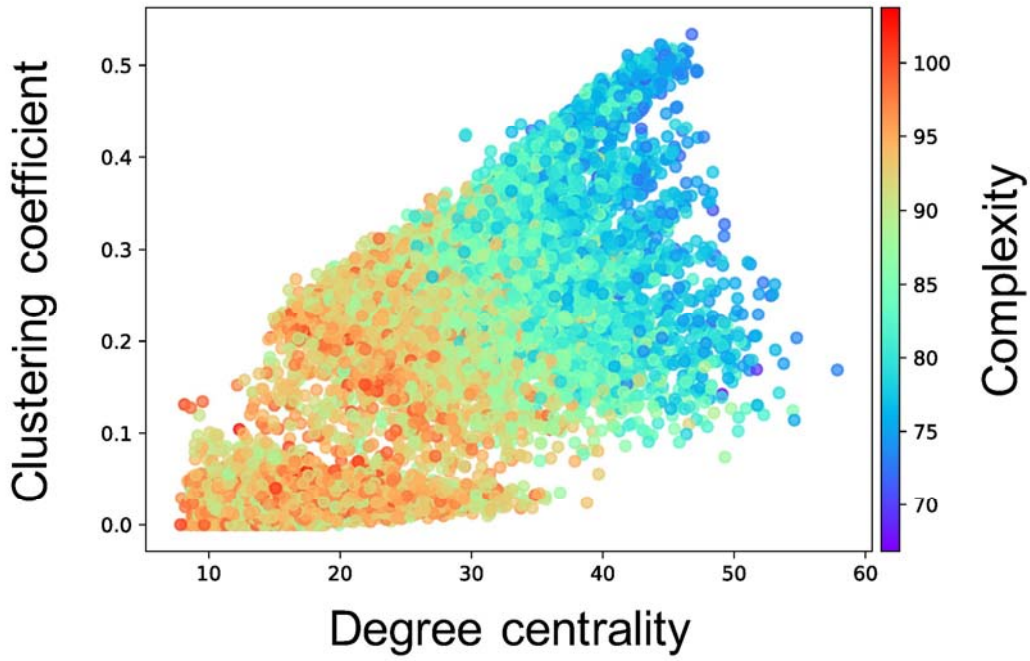

Figure A.3: Relationship between the connectivity structure and the complexity of neural activity. Each marker corresponds to a neuron group in the network, and its color indicates the summation of the sample entropy for all 80 scale factors. The x-axis indicates the degree centrality, and the y-axis indicates the clustering coefficient.

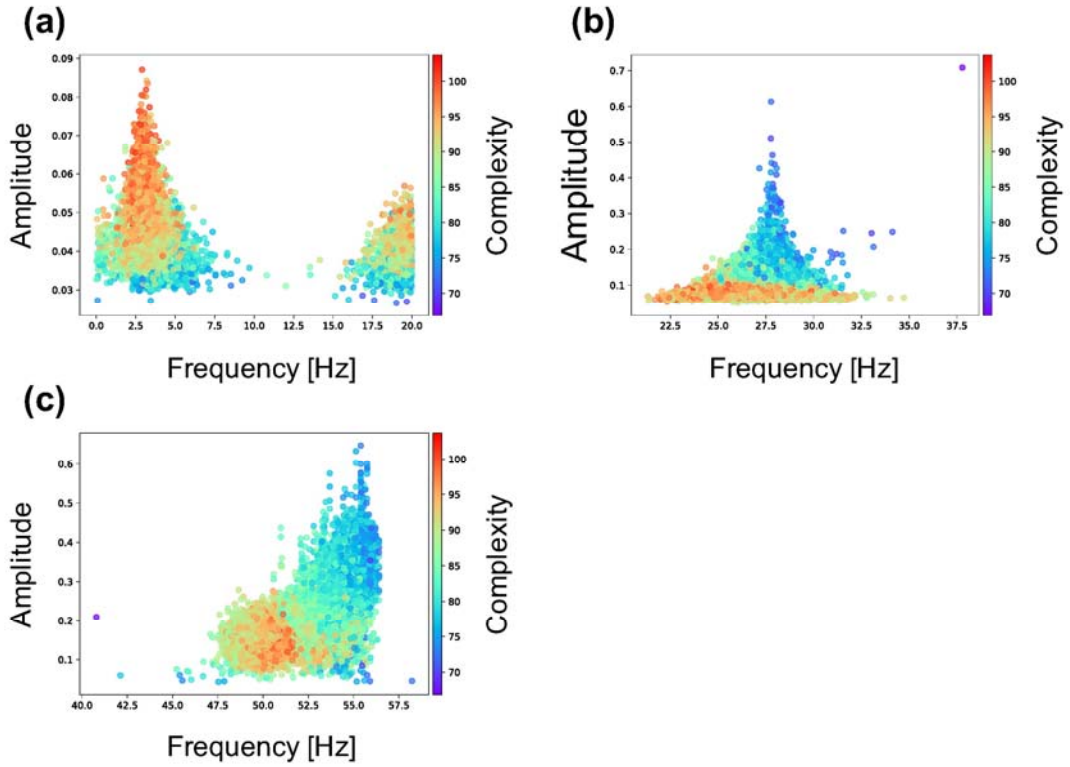

Figure A.4: Relationship between the peak frequency and the complexity of neural activity. (a) Relationship in the 0-20 Hz band. (b) Relationship in the 20-40 Hz band. (c) Relationship in the 40-60 Hz band. Each marker corresponds to a neuron group in the network, and its color indicates the summation of the sample entropy for all 80 scale factors. The x-axis indicates the peak frequency of the neural activity, and the y-axis indicates the amplitude.

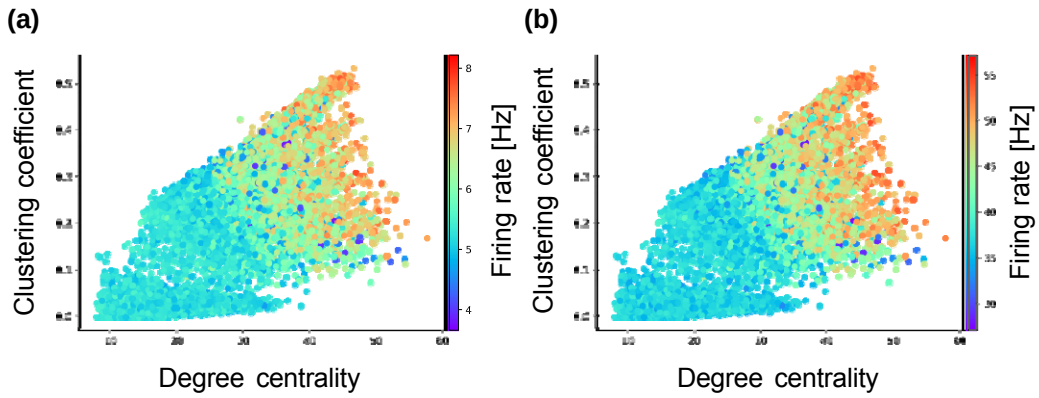

Figure A.5: Relationship between the connectivity structure and the firing rate of excitatory and inhibitory neurons. Each marker corresponds to a neuron group in the network, and its color indicates the average firing rate of excitatory and inhibitory neurons. The x-axis indicates the degree centrality, and the y-axis indicates the clustering coefficient. (a) Relationship between structural properties and firing rate of excitatory neurons. (b) Relationship between structural properties and firing rate of inhibitory neurons.

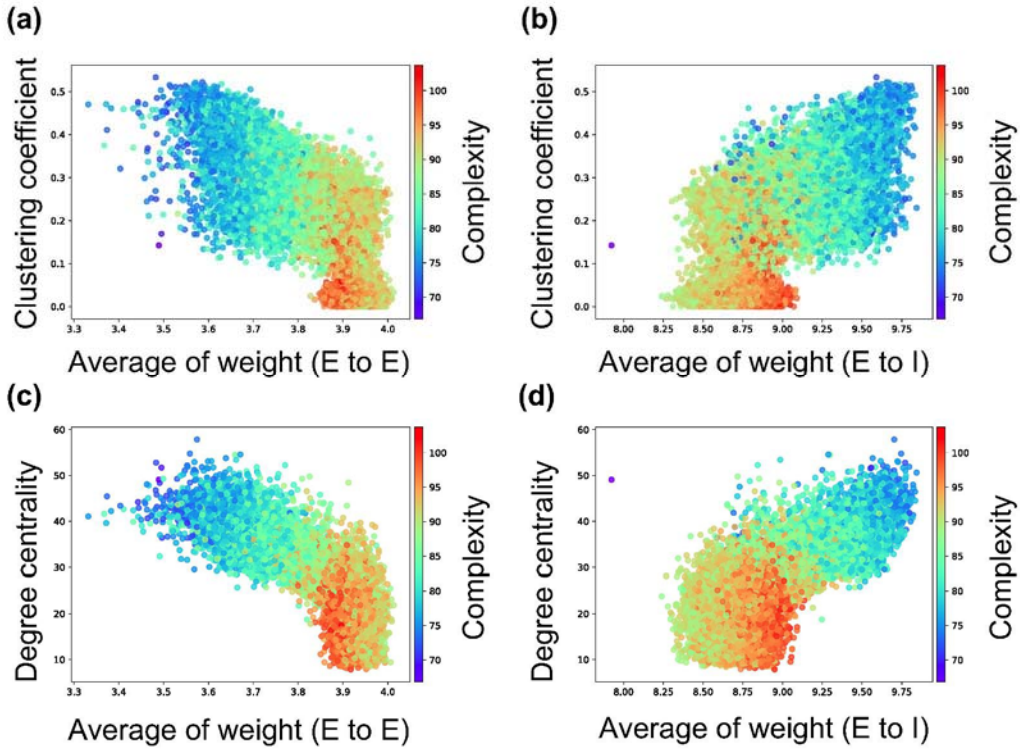

Figure A.6: Relationship among the weight of intraconnection, structural properties, and complexity of neural activity. (a) Relationship among the weight of intraconnection from excitatory to excitatory neuron, clustering coefficient based on the interconnection, and complexity. (b) Relationship among the weight of intraconnection from excitatory to inhibitory neuron, clustering coefficient based on the interconnection, and complexity. (c) Relationship among the weight of intraconnection from excitatory to excitatory neuron, degree centrality based on the interconnection, and complexity. (d) Relationship among the weight of intraconnection from excitatory to inhibitory neuron, degree centrality based on the interconnection, and complexity. Each marker corresponds to a neuron group in the network, and its color indicates the summation of the sample entropy for all 80 scale factors. The x-axis indicates the average of weight of interconnection, and the y-axis the structural properties of interconnection.

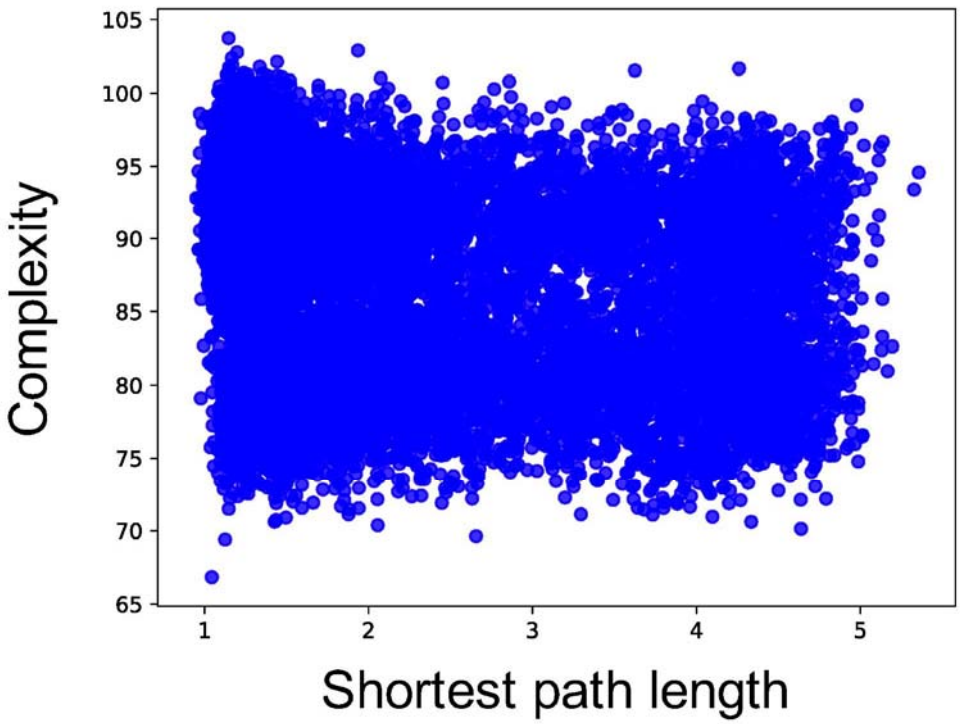

Figure A.7: Relationship between shortest path length and complexity for each neuron group. The x-axis is the shortest path length, and the y-axis is the summation of the sample entropy for all 80 scale factors.

Table A.1: Statistical comparisons with Tukey–Kramer test among MSE of LAP signals and MSE of band-pass randomized surrogate LAP signals in a specific frequency bands. In the table, Meandiff indicates the difference in mean value between the compared groups. Lower and Upper mean lower limit and upper limit of confidence interval, respectively.

Compared group1	Compared group2	Meandiff	Lower	Upper	p-value
0-20 Hz	20-40 Hz	-1.909	-2.179	-1.639	0.001
0-20 Hz	40-60Hz	-1.748	-2.018	-1.478	0.001
0-20 Hz	60-80Hz	-4.029	-4.299	-3.759	0.001
0-20 Hz	original	-4.037	-5.956	-2.119	0.001
20-40 Hz	40-60Hz	0.160	-0.109	0.430	0.482
20-40 Hz	60-80Hz	-2.120	-2.390	-1.850	0.001
20-40 Hz	original	-2.128	-4.046	-0.210	0.021
40-60Hz	60-80Hz	-2.281	-2.551	-2.011	0.001
40-60Hz	original	-2.289	-4.207	-0.371	0.009
60-80Hz	original	-0.008	-1.926	1.91	0.9

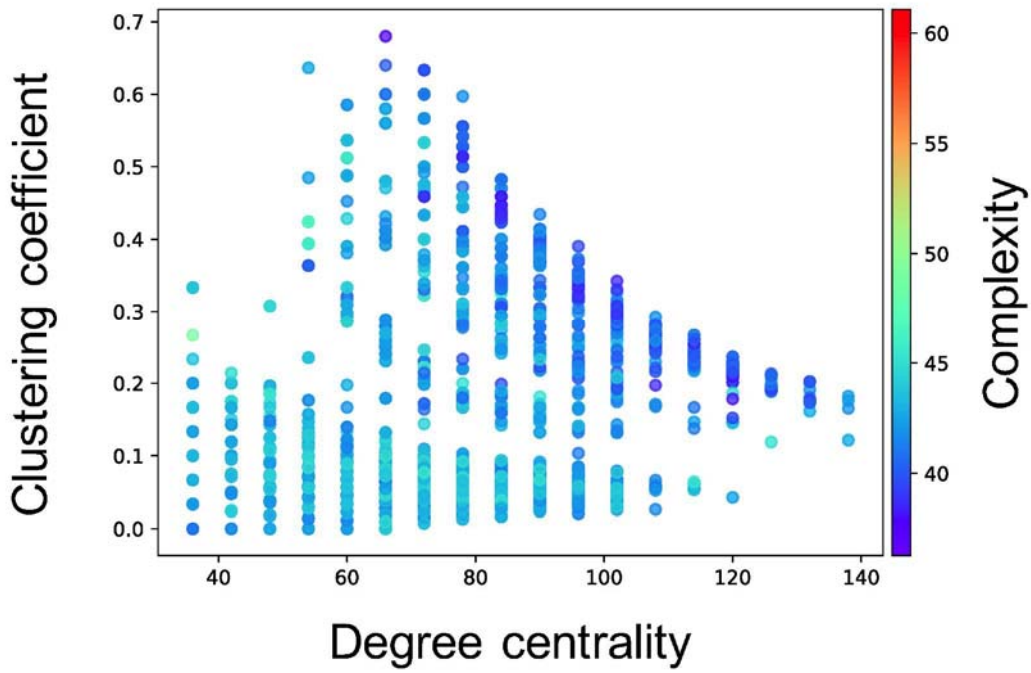

Figure A.8: Relationship between the connectivity structure without STDP and the complexity of neural activity with the tonic input. Duration for tonic input was set as 100 s. Here, we used the same initial weights of the synaptic networks in the Figure A.3 and fixed the weights during the tonic input. Each marker corresponds to a neuron group in the network, and its color indicates the summation of the sample entropy for all 80 scale factors. The x-axis indicates the degree centrality, and the y-axis indicates the clustering coefficient. There is no clear relationship between the complexity and structural properties of synaptic network compared to the Figure A.3.

Table A.2: Correlation coefficient among the complexity, structural properties of synaptic and functional networks for all values of p_{WS} of ten simulations. In the table, Clustering_S and Clustering_F represent clustering coefficient of synaptic and functional networks in each frequency bands, respectively. Degree_S and Degree_F represent degree centrality of synaptic and functional networks in each frequency bands, respectively. In all cases, p-value < 2.2e-16.

		Frequency bands of functional network			
Compared components1	Compared components2	0-20 Hz	20-40 Hz	40-60 Hz	0-1000 HZ
Complexity	Clustering_F	-0.6646089	-0.6583268	-0.282451	0.5503528
Complexity	Degree_F	-0.7022768	-0.6727727	-0.3539034	-0.7220229
Clustering_F	Clustering_S	0.5108812	0.7596675	0.256991	0.6164434
Degree_F	Degree_S	0.5223337	0.6506093	0.2799739	0.7126037

Appendix B

Effect of tonic input for emergence of behaviors

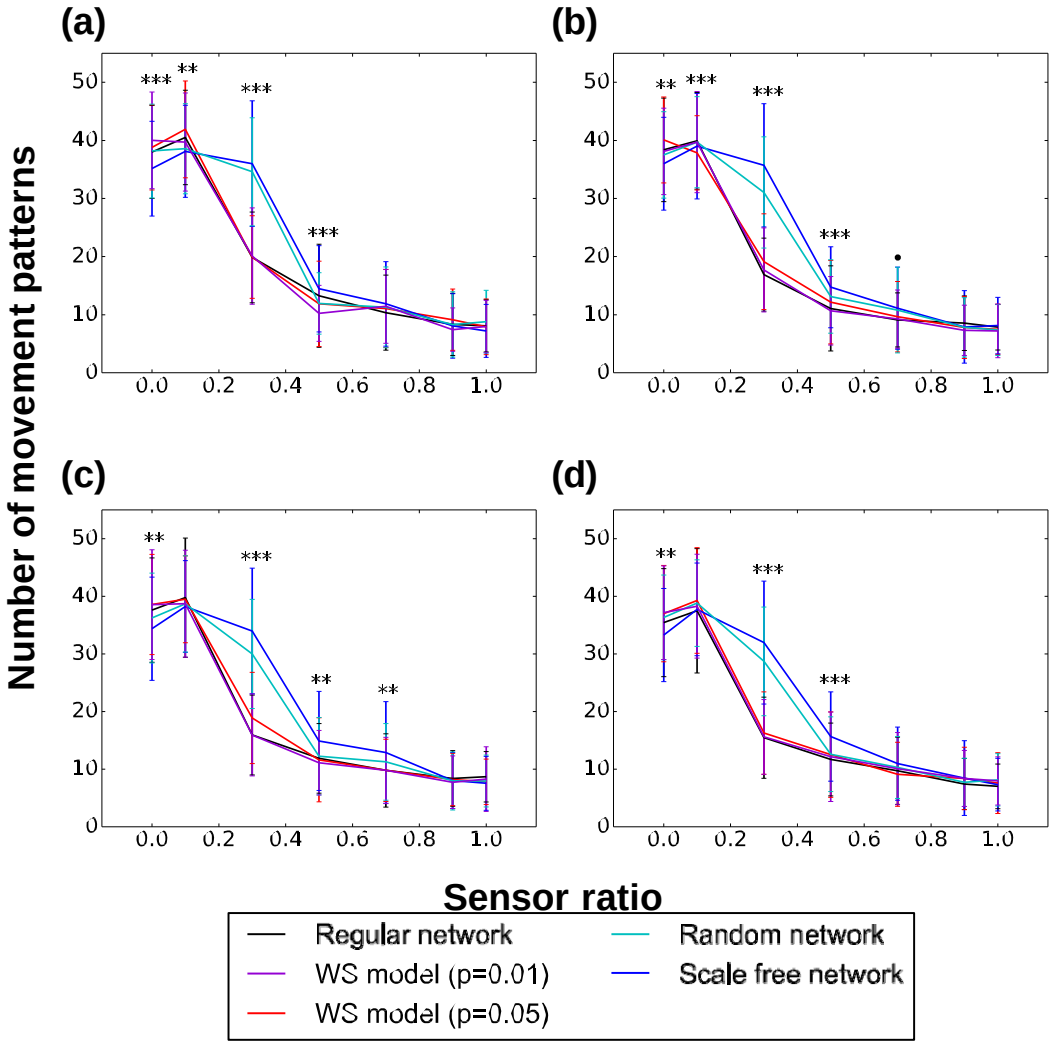

Figure B.1: Number of movement patterns for uniform weights. The tonic input for each graph is 0.4 (A), 0.45 (B), 0.5 (C),or 0.55 (D). The x-axis indicates the sensor ratio necessary α in Eq (4.3) to control the proportional influences between the body and the network. *** $p < 0.001$, ** $p < 0.01$, * $p < 0.05$ and $\cdot$ $p < 0.1$ indicate a statistically significant differences between the wired networks through the ANOVA test.

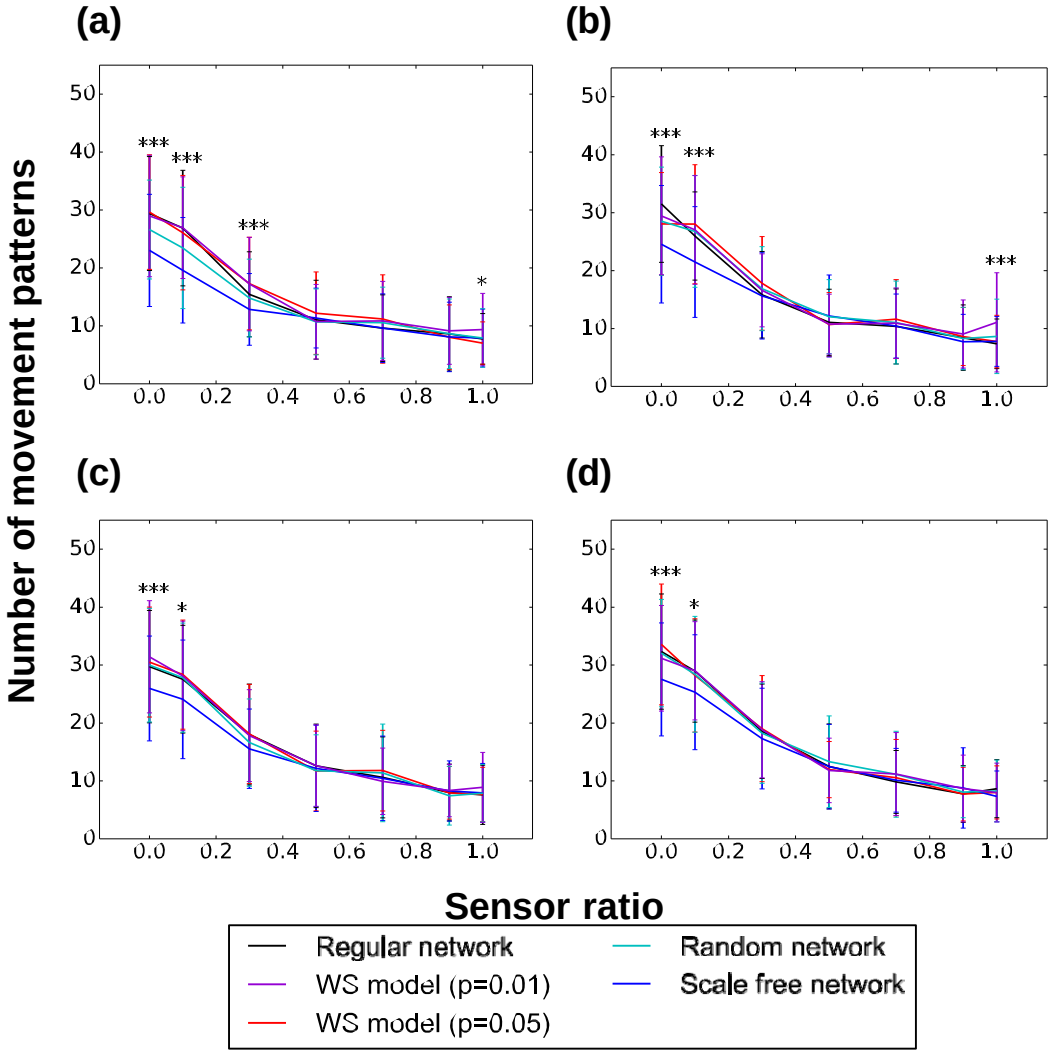

Figure B.2: Number of movement patterns for randomly distributed weights. The tonic input for each graph is 0.4 (A), 0.45 (B), 0.5 (C),or 0.55 (D). The x-axis indicates the sensor ratio necessary α in Eq (4.3) to control the proportional influences between the body and the network. *** $p < 0.001$, ** $p < 0.01$, * $p < 0.05$ and $\cdot$ $p < 0.1$ indicate a statistically significant differences between the wired networks through the ANOVA test.

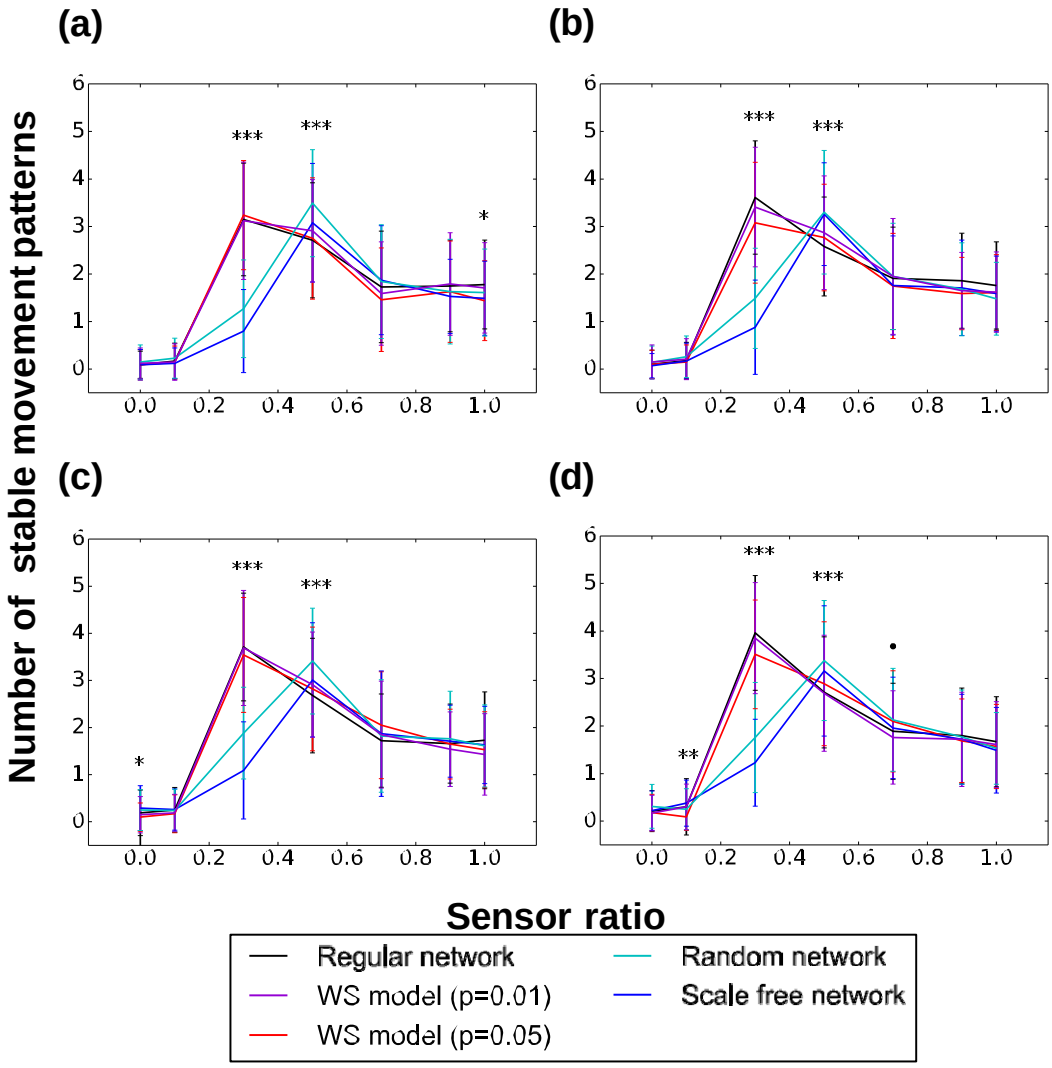

Figure B.3: Number of stable movement patterns for uniform weights. The tonic input for each graph is 0.4 (A), 0.45 (B), 0.5 (C),or 0.55 (D). The x-axis indicates the sensor ratio necessary α in Eq (4.3) to control the proportional influences between the body and the network. *** $p < 0.001$, ** $p < 0.01$, * $p < 0.05$ and $\cdot$ $p < 0.1$ indicate a statistically significant differences between the wired networks through the ANOVA test.

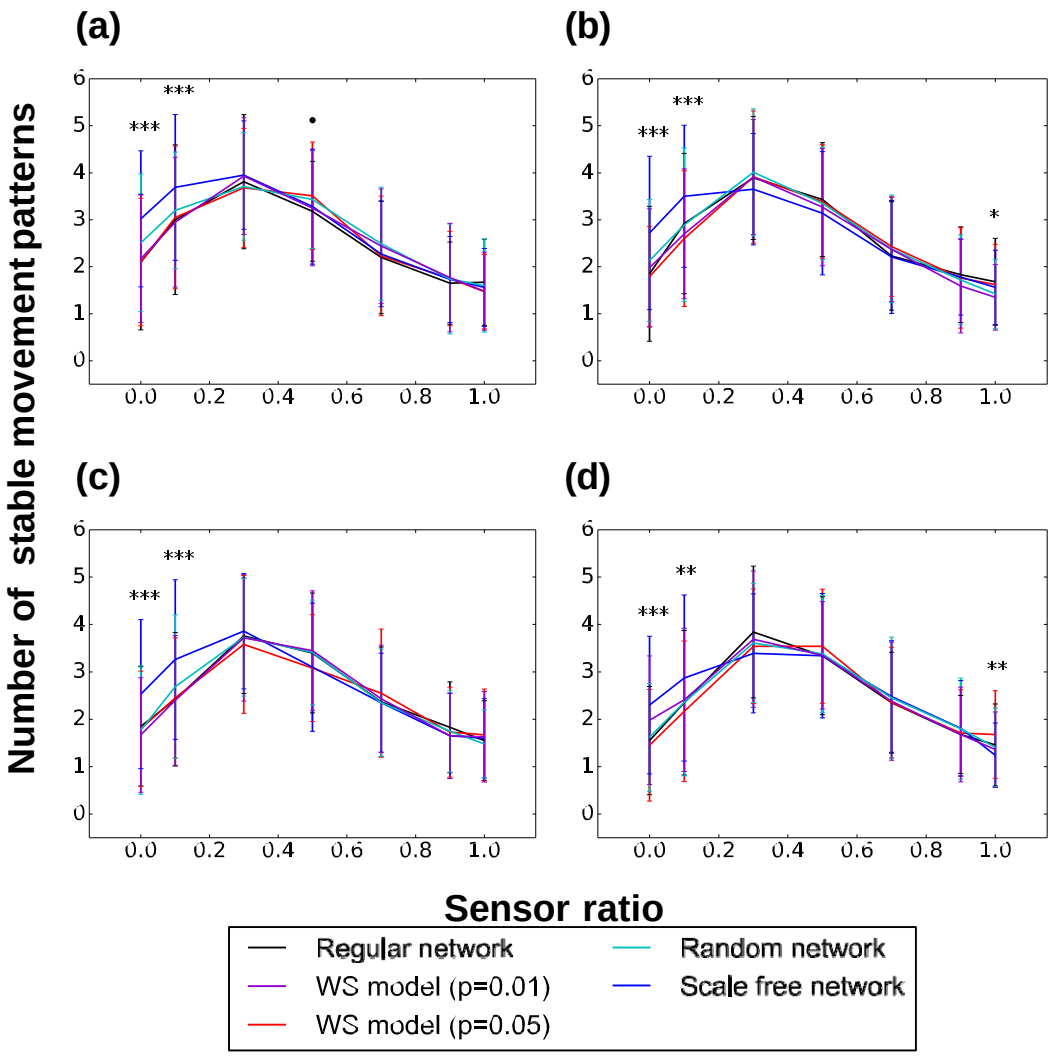

Figure B.4: Number of stable movement patterns for randomly distributed weights. The tonic input for each graph is 0.4 (A), 0.45 (B), 0.5 (C),or 0.55 (D). The x-axis indicates the sensor ratio necessary α in Eq (4.3) to control the proportional influences between the body and the network. *** $p < 0.001$, ** $p < 0.01$, * $p < 0.05$ and · $p < 0.1$ indicate a statistically significant differences between the wired networks through the ANOVA test.

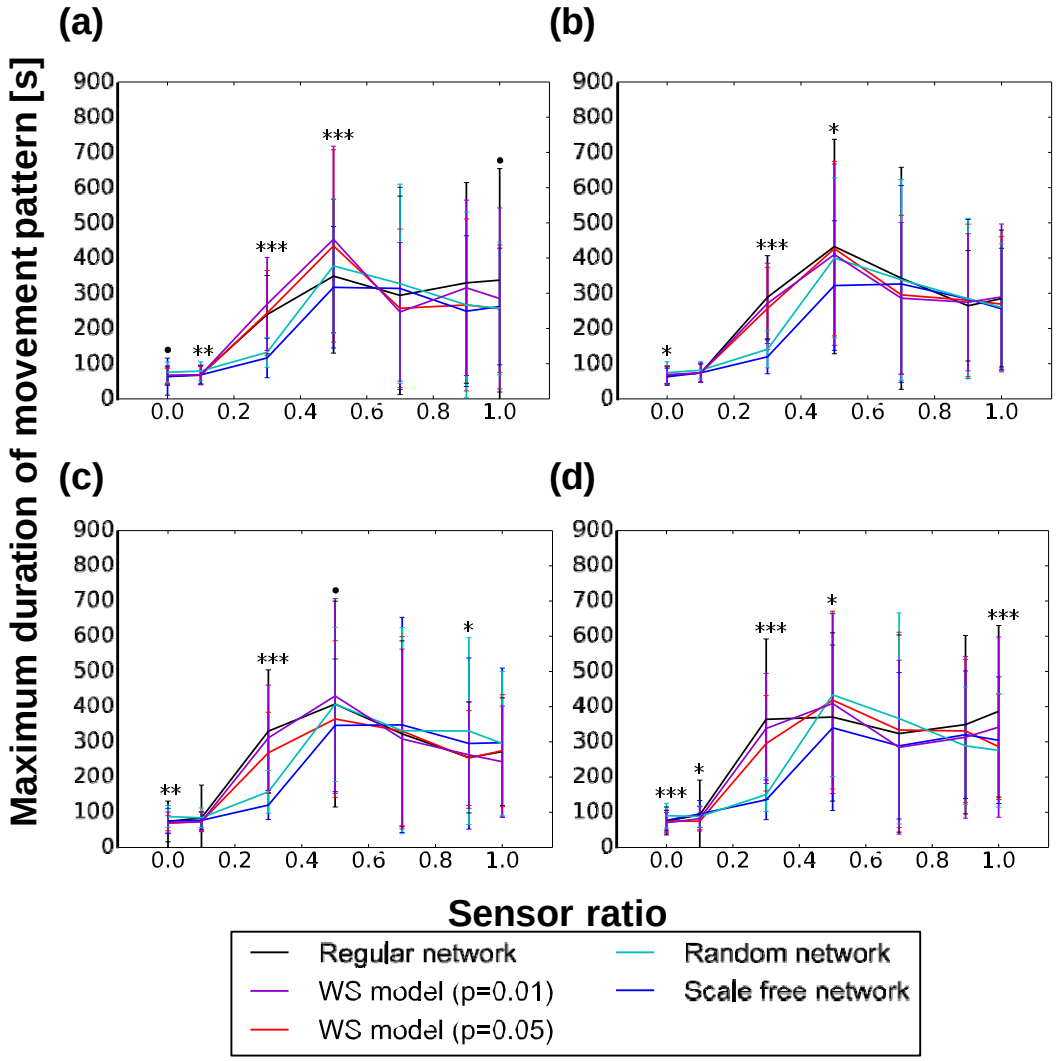

Figure B.5: Maximum duration of the movement pattern for uniform weights. The tonic input for each graph is 0.4 (A), 0.45 (B), 0.5 (C),or 0.55 (D). The x-axis indicates the sensor ratio necessary α in Eq (4.3) to control the proportional influences between the body and the network. *** $p < 0.001$, ** $p < 0.01$, * $p < 0.05$ and $\cdot$ $p < 0.1$ indicate a statistically significant differences between the wired networks through the ANOVA test.

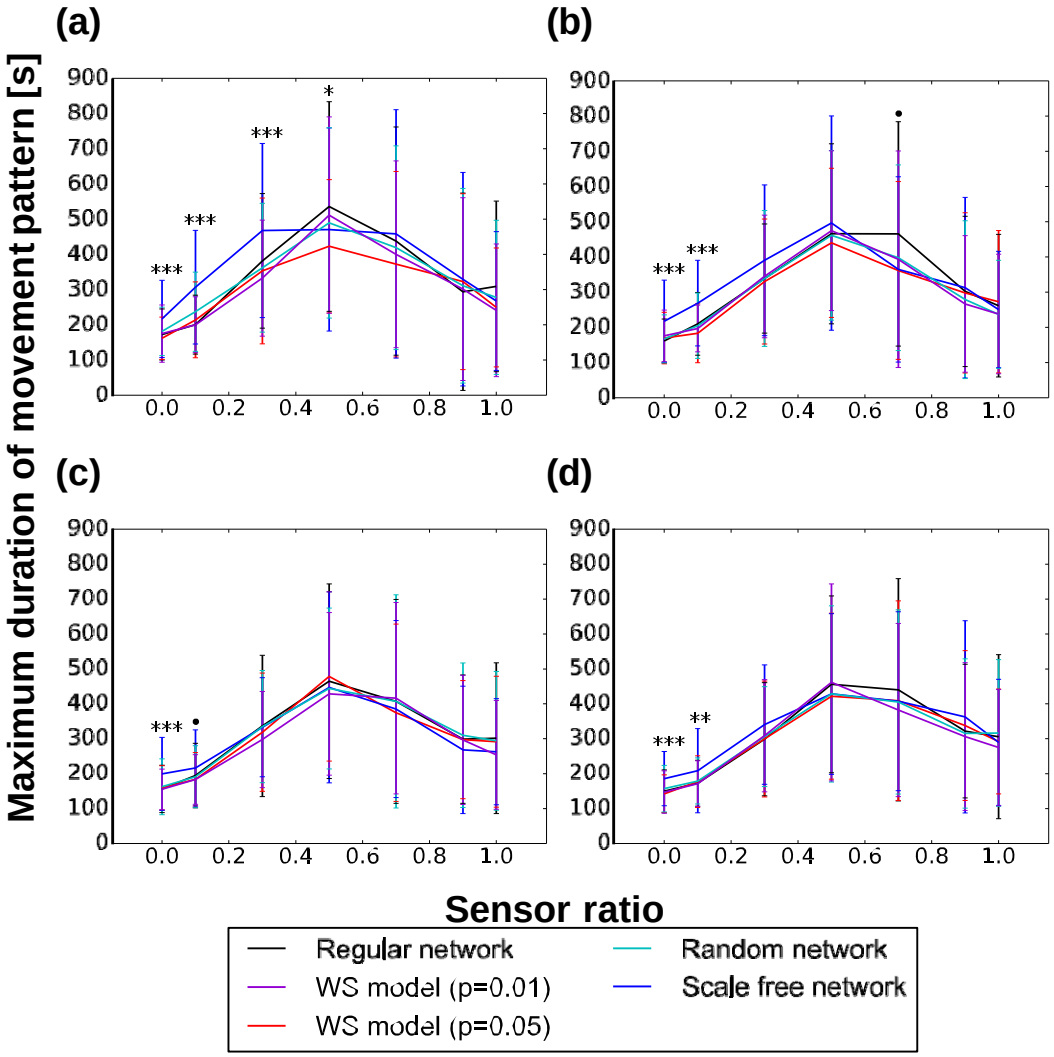

Figure B.6: Maximum duration of the movement patterns for randomly distributed weights. The tonic input for each graph is 0.4 (A), 0.45 (B), 0.5 (C),or 0.55 (D). The x-axis indicates the sensor ratio necessary α in Eq (4.3) to control the proportional influences between the body and the network. *** $p < 0.001$, ** $p < 0.01$, * $p < 0.05$ and $\cdot$ $p < 0.1$ indicate a statistically significant differences between the wired networks through the ANOVA test.

Bibliography

[1] Sophie Achard, Raymond Salvador, Brandon Whitcher, John Suckling, and ED Bullmore. "A resilient, low-frequency, small-world human brain functional network with highly connected association cortical hubs". In: *Journal of Neuroscience* 26.1 (2006), pp. 63–72.

[2] Réka Albert, Hawoong Jeong, and Albert-László Barabási. "Error and attack tolerance of complex networks". In: *nature* 406.6794 (2000), pp. 378–382.

[3] Michael L Anderson, Josh Kinnison, and Luiz Pessoa. "Describing functional diversity of brain regions and brain networks". In: *Neuroimage* 73 (2013), pp. 50–58.

[4] Yoshiyuki Asai, Taishin Nomura, and Shunsuke Sato. "Emergence of oscillations in a model of weakly coupled two Bonhoeffer–van der Pol equations". In: *BioSystems* 58.1 (2000), pp. 239–247.

[5] Gareth Ball, Paul Aljabar, Sally Zebari, Nora Tusor, Tomoki Arichi, Nazakat Merchant, Emma C Robinson, Enitan Ogundipe, Daniel Rueckert, A David Edwards, et al. "Rich-club organization of the newborn human brain". In: *Proceedings of the National Academy of Sciences* 111.20 (2014), pp. 7456–7461.

[6] Albert-László Barabási and Réka Albert. "Emergence of scaling in random networks". In: *science* 286.5439 (1999), pp. 509–512.

[7] Danielle S Bassett, Andreas Meyer-Lindenberg, Sophie Achard, Thomas Duke, and Edward Bullmore. "Adaptive reconfiguration of fractal small-world human brain functional networks". In: *Proceedings of the National Academy of Sciences* 103.51 (2006), pp. 19518–19523.

[8] Danielle Smith Bassett and Ed Bullmore. "Small-world brain networks". In: *Neuroscientist* 12.6 (2006), pp. 512–523.

[9] Randall D Beer. "A dynamical systems perspective on agent-environment interaction". In: *Artificial intelligence* 72.1-2 (1995), pp. 173–215.

[10] Randall D Beer. "Dynamical approaches to cognitive science". In: *Trends in cognitive sciences* 4.3 (2000), pp. 91–99.

[11] Mikhail Belkin and Partha Niyogi. "Laplacian eigenmaps for dimensionality reduction and data representation". In: *Neural computation* 15.6 (2003), pp. 1373–1396.

[12] Maxwell A Bertolero, B T Thomas Yeo, and Mark D'Esposito. "The modular and integrative functional architecture of the human brain". In: *Proceedings of the National Academy of Sciences* 112.49 (Dec. 2015), E6798–E6807.

[13] Viviana Betti, Stefania Della Penna, Francesco de Pasquale, Dante Mantini, Laura Marzetti, Gian Luca Romani, and Maurizio Corbetta. "Natural Scenes Viewing Alters the Dynamics of Functional Connectivity in the Human Brain". In: *Neuron* 79.4 (Aug. 2013), pp. 782–797.

[14] W. Bosl, A. Tierney, H. Tager-Flusberg, and C. Nelson. "EEG complexity as a biomarker for autism spectrum disorder risk". In: *BMC Med* 9 (2011), p. 18.

[15] Steven L Bressler and Vinod Menon. "Large-scale brain networks in cognition: emerging methods and principles". In: *Trends in Cognitive Sciences* 14.6 (June 2010), pp. 277–290.

[16] Randy L. Buckner, Jessica R. Andrews-Hanna, and Daniel L. Schacter. "The Brain's Default Network". In: *Annals of the New York Academy of Sciences* 1124.1 (2008), pp. 1–38.

[17] Randy L Buckner, Jorge Sepulcre, Tanveer Talukdar, Fenna M Krienen, Hesheng Liu, Trey Hedden, Jessica R Andrews-Hanna, Reisa A Sperling, and Keith A Johnson. "Cortical hubs revealed by intrinsic functional connectivity: mapping, assessment of stability, and relation to Alzheimer's disease". In: *Journal of Neuroscience* 29.6 (2009), pp. 1860–1873.

[18] Ed Bullmore and Olaf Sporns. "Complex brain networks: graph theoretical analysis of structural and functional systems". In: *Nature Reviews Neuroscience* 10.3 (2009), pp. 186–198.

[19] P. Bush and T. Sejnowski. "Inhibition synchronizes sparsely connected cortical neurons within and between columns in realistic network models". In: *J Comput Neurosci* 3.2 (1996), pp. 91–110.

[20] György Buzsáki and Andreas Draguhn. "Neuronal oscillations in cortical networks". In: *science* 304.5679 (2004), pp. 1926–1929.

[21] György Buzsáki and Brendon O Watson. "Brain rhythms and neural syntax: implications for efficient coding of cognitive content and neuropsychiatric disease". In: *Dialogues Clin Neurosci* 14.4 (2012), pp. 345–367.

[22] Lisa Byrge, Olaf Sporns, and Linda B Smith. "Developmental process emerges from extended brain–body–behavior networks". In: *Trends in cognitive sciences* 18.8 (2014), pp. 395–403.

[23] G. Cellot and E. Cherubini. "GABAergic signaling as therapeutic target for autism spectrum disorders". In: *Front Pediatr* 2 (2014), p. 70.

[24] Michael W Cole, Danielle S Bassett, Jonathan D Power, Todd S Braver, and Steven E Petersen. "Intrinsic and task-evoked network architectures of the human brain". In: *Neuron* 83.1 (2014), pp. 238–251.

[25] Michael W Cole, Jeremy R Reynolds, Jonathan D Power, Grega Repovs, Alan Anticevic, and Todd S Braver. "Multi-task connectivity reveals flexible hubs for adaptive task control". In: *Nature neuroscience* 16.9 (2013), pp. 1348–1355.

[26] M. Costa, A. L. Goldberger, and C. K. Peng. "Multiscale entropy analysis of biological signals". In: *Phys Rev E Stat Nonlin Soft Matter Phys* 71.2 Pt 1 (2005), p. 021906.

[27] M. Costa, A. L. Goldberger, and C. K. Peng. "Multiscale entropy analysis of complex physiologic time series". In: *Phys. Rev. Lett.* 89.6 (2002), p. 068102.

[28] E. Courchesne and K. Pierce. "Why the frontal cortex in autism might be talking only to itself: local over-connectivity but long-distance disconnection". In: *Curr. Opin. Neurobiol.* 15.2 (2005), pp. 225–230.

[29] Nicolas A Crossley, Andrea Mechelli, Petra E Vértes, Toby T Winton-Brown, Ameera X Patel, Cedric E Ginestet, Philip McGuire, and Edward T Bullmore.

"Cognitive relevance of the community structure of the human brain functional coactivation network." In: *Proceedings of the National Academy of Sciences of the United States of America* 110.28 (July 2013), pp. 11583–11588.

[30] V. M. Eguiluz, D. R. Chialvo, G. A. Cecchi, M. Baliki, and A. V. Apkarian. "Scale-free brain functional networks". In: *Phys. Rev. Lett.* 94.1 (2005), p. 018102.

[31] Victor M Eguiluz, Dante R Chialvo, Guillermo A Cecchi, Marwan Baliki, and A Vania Apkarian. "Scale-free brain functional networks". In: *Physical review letters* 94.1 (2005), p. 018102.

[32] Martin Ester, Hans-Peter Kriegel, Jörg Sander, Xiaowei Xu, et al. "A density-based algorithm for discovering clusters in large spatial databases with noise." In: *Kdd*. Vol. 96. 34. 1996, pp. 226–231.

[33] G. Fagiolo. "Clustering in complex directed networks". In: *Phys Rev E Stat Nonlin Soft Matter Phys* 76.2 Pt 2 (2007), p. 026107.

[34] Alex Fornito, Andrew Zalesky, Christos Pantelis, and Edward T Bullmore. "Schizophrenia, neuroimaging and connectomics". In: *Neuroimage* 62.4 (2012), pp. 2296–2314.

[35] Walter J Freeman. "Evidence from human scalp electroencephalograms of global chaotic itinerancy". In: *Chaos: An Interdisciplinary Journal of Nonlinear Science* 13.3 (2003), pp. 1067–1077.

[36] Walter J Freeman. "Simulation of chaotic EEG patterns with a dynamic model of the olfactory system". In: *Biological cybernetics* 56.2-3 (1987), pp. 139–150.

[37] K J Friston. "Theoretical neurobiology and schizophrenia". In: *Br. Med. Bull.* 52.3 (1996), pp. 644–655.

[38] Zhong-Ke Gao, Michael Small, and Jürgen Kurths. "Complex network analysis of time series". In: *EPL (Europhysics Letters)* 116.5 (2017), p. 50001.

[39] Zhong-Ke Gao, Yu-Xuan Yang, Peng-Cheng Fang, Yong Zou, Cheng-Yi Xia, and Meng Du. "Multiscale complex network for analyzing experimental multivariate time series". In: *EPL (Europhysics Letters)* 109.3 (2015), p. 30005.

[40] Zhong-Ke Gao, Qing Cai, Yu-Xuan Yang, Wei-Dong Dang, and Shan-Shan Zhang. "Multiscale limited penetrable horizontal visibility graph for analyzing nonlinear time series". In: *Scientific reports* 6 (2016), p. 35622.

[41] Zhong-Ke Gao, Peng-Cheng Fang, Mei-Shuang Ding, and Ning-De Jin. "Multivariate weighted complex network analysis for characterizing nonlinear dynamic behavior in two-phase flow". In: *Experimental Thermal and Fluid Science* 60 (2015), pp. 157–164.

[42] Zhong-Ke Gao, Qing Cai, Yu-Xuan Yang, Na Dong, and Shan-Shan Zhang. "Visibility Graph from Adaptive Optimal Kernel Time-Frequency Representation for Classification of Epileptiform EEG". In: *International Journal of Neural Systems* 27.04 (June 2017), pp. 1750005–12.

[43] Y. Ghanbari, L. Bloy, J. Christopher Edgar, L. Blaskey, R. Verma, and T. P. Roberts. "Joint analysis of band-specific functional connectivity and signal complexity in autism". In: *J Autism Dev Disord* 45.2 (2015), pp. 444–460.

[44] N. Gogolla, J. J. Leblanc, K. B. Quast, T. C. Sudhof, M. Fagiolini, and T. K. Hensch. "Common circuit defect of excitatory-inhibitory balance in mouse models of autism". In: *J Neurodev Disord* 1.2 (2009), pp. 172–181.

[45] G. Gonzalez-Burgos and D. A. Lewis. "GABA neurons and the mechanisms of network oscillations: implications for understanding cortical dysfunction in schizophrenia". In: *Schizophr Bull* 34.5 (2008), pp. 944–961.

[46] Shlomi Haar, Opher Donchin, and Ilan Dinstein. "Individual movement variability magnitudes are predicted by cortical neural variability". In: *bioRxiv* (2017), p. 097824.

[47] M. Hadders-Algra. "Early human brain development: Starring the subplate". In: *Neurosci Biobehav Rev* 92 (Sept. 2018), pp. 276–290.

[48] Mijna Hadders-Algra. "Early human motor development: From variation to the ability to vary and adapt". In: *Neuroscience Biobehavioral Reviews* 90 (2018), pp. 411 –427. ISSN: 0149-7634.

[49] Mijna Hadders-Algra. "Putative neural substrate of normal and abnormal general movements". In: *Neuroscience & Biobehavioral Reviews* 31.8 (2007), pp. 1181–1190.

[50] Mijna Hadders-Algra. "Variation and variability: key words in human motor development". In: *Physical therapy* 90.12 (2010), pp. 1823–1837.

[51] Jiping He, Mitchell G Maltenfort, Qingjun Wang, and Thomas M Hamm. "Learning from biological systems: Modeling neural control". In: *IEEE Control Systems* 21.4 (2001), pp. 55–69.

[52] Yong He, Zhang J Chen, and Alan C Evans. "Small-world anatomical networks in the human brain revealed by cortical thickness from MRI". In: *Cerebral cortex* 17.10 (2007), pp. 2407–2419.

[53] Ann M Hermundstad, Danielle S Bassett, Kevin S Brown, Elissa M Aminoff, David Clewett, Scott Freeman, Amy Frithsen, Arianne Johnson, Christine M Tipper, Michael B Miller, et al. "Structural foundations of resting-state and task-based functional connectivity in the human brain". In: *Proceedings of the National Academy of Sciences* 110.15 (2013), pp. 6169–6174.

[54] David J Herzfeld and Reza Shadmehr. "Motor variability is not noise, but grist for the learning mill". In: *nature neuroscience* 17.2 (2014), pp. 149–150.

[55] M. P. van den Heuvel and O. Sporns. "Rich-club organization of the human connectome". In: *J. Neurosci.* 31.44 (2011), pp. 15775–15786.

[56] E. M. Izhikevich. "Polychronization: computation with spikes". In: *Neural Comput* 18.2 (2006), pp. 245–282.

[57] E. M. Izhikevich. "Simple model of spiking neurons". In: *IEEE Trans Neural Netw* 14.6 (2003), pp. 1569–1572.

[58] E. M. Izhikevich and G. M. Edelman. "Large-scale model of mammalian thalamocortical systems". In: *Proc. Natl. Acad. Sci. U.S.A.* 105.9 (2008), pp. 3593–3598.

[59] Seung-Hyun Jin, Peter Lin, and Mark Hallett. "Reorganization of brain functional small-world networks during finger movements". In: *Human brain mapping* 33.4 (2012), pp. 861–872.

[60] Kunihiko Kaneko. "Clustering, coding, switching, hierarchical ordering, and control in a network of chaotic elements". In: *Physica D: Nonlinear Phenomena* 41.2 (1990), pp. 137–172.

[61] JA Scott Kelso. *Dynamic patterns: The self-organization of brain and behavior*. MIT press, 1997.

[62] Charles Kemp, Joshua B Tenenbaum, Thomas L Griffiths, Takeshi Yamada, and Naonori Ueda. "Learning systems of concepts with an infinite relational model". In: *AAAI*. Vol. 3. 2006, p. 5.

[63] Reka Kinney, Paolo Crucitti, Reka Albert, and Vito Latora. "Modeling cascading failures in the North American power grid". In: *The European Physical Journal B-Condensed Matter and Complex Systems* 46.1 (2005), pp. 101–107.

[64] Ivica Kostović, Goran Sedmak, Mario Vukšić, and Miloš Judaš. "The Relevance of Human Fetal Subplate Zone for Developmental Neuropathology of Neuronal Migration Disorders and Cortical Dysplasia". In: *CNS Neuroscience & Therapeutics* 21.2 (2015), pp. 74–82.

[65] Alexander Kraskov, Harald Stögbauer, and Peter Grassberger. "Estimating mutual information". In: *Physical review E* 69.6 (2004), p. 066138.

[66] Yasuo Kuniyoshi and Shinji Sangawa. "Early motor development from partially ordered neural-body dynamics: experiments with a cortico-spinal-musculoskeletal model". In: *Biological cybernetics* 95.6 (2006), pp. 589–605.

[67] Yasuo Kuniyoshi and Shinsuke Suzuki. "Dynamic emergence and adaptation of behavior through embodiment as coupled chaotic field". In: *Intelligent Robots and Systems, 2004.(IROS 2004). Proceedings. 2004 IEEE/RSJ International Conference On*. Vol. 2. IEEE. 2004, pp. 2042–2049.

[68] Yoshiki Kuramoto. "Cooperative Dynamics of Oscillator CommunityA Study Based on Lattice of Rings". In: *Progress of Theoretical Physics Supplement* 79 (1984), pp. 223–240.

[69] V. Latora and M. Marchiori. "Efficient behavior of small-world networks". In: *Phys. Rev. Lett.* 87.19 (2001), p. 198701.

[70] C. Li, G. H. Ding, G. Q. Wu, and C. S. Poon. "Band-phase-randomized surrogate data reveal high-frequency chaos in heart rate variability". In: *Conf Proc IEEE Eng Med Biol Soc* 2010 (2010), pp. 2806–2809.

[71] Joseph T Lizier. "JIDT: An information-theoretic toolkit for studying the dynamics of complex systems". In: *Frontiers in Robotics and AI* 1 (2014), p. 11.

[72] Annemarie B Lüchinger, Mijna Hadders-Algra, Colette M van Kan, and Johanna I P de Vries. "Fetal Onset of General Movements". In: *Pediatric Research* 63 (2008), p. 191.

[73] Artur Luczak, Peter Barthó, and Kenneth D Harris. "Spontaneous events outline the realm of possible sensory responses in neocortical populations". In: *Neuron* 62.3 (2009), pp. 413–425.

[74] H. Markram, J. Lubke, M. Frotscher, and B. Sakmann. "Regulation of synaptic efficacy by coincidence of postsynaptic APs and EPSPs". In: *Science* 275.5297 (1997), pp. 213–215.

[75] N. Masuda and K. Aihara. "Global and local synchrony of coupled neurons in small-world networks". In: *Biol Cybern* 90.4 (2004), pp. 302–309.

[76] P. N. McGraw and M. Menzinger. "Clustering and the synchronization of oscillator networks". In: *Phys Rev E Stat Nonlin Soft Matter Phys* 72.1 Pt 2 (2005), p. 015101.

[77] Vinod Menon. "Developmental pathways to functional brain networks: emerging principles". In: *Trends in Cognitive Sciences* 17.12 (2013), pp. 627–640.

[78] Hiroki Mori and Yasuo Kuniyoshi. "A human fetus development simulation: Self-organization of behaviors through tactile sensation". In: *Development and Learning (ICDL), 2010 IEEE 9th International Conference on*. IEEE. 2010, pp. 82–87.

[79] T. T. Nakagawa, V. K. Jirsa, A. Spiegler, A. R. McIntosh, and G. Deco. "Bottom up modeling of the connectome: linking structure and function in the resting brain and their changes in aging". In: *Neuroimage* 80 (2013), pp. 318–329.

[80] S. B. Nelson and V. Valakh. "Excitatory/Inhibitory Balance and Circuit Homeostasis in Autism Spectrum Disorders". In: *Neuron* 87.4 (2015), pp. 684–698.

[81] Jason S Nomi and Lucina Q Uddin. "Developmental changes in large-scale network connectivity in autism". In: *NeuroImage: Clinical* 7 (2015), pp. 732–741.

[82] Nobuo Okado. "Development of the human cervical spinal cord with reference to synapse formation in the motro nucleus". In: *Journal of Comparative Neurology* 191.3 (1980), pp. 495–513.

[83] Makito Oku and Kazuyuki Aihara. "Associative dynamics of color images in a large-scale chaotic neural network". In: *Nonlinear Theory and Its Applications, IEICE* 2.4 (2011), pp. 508–521.

[84] Nobuyuki Otsu. "A threshold selection method from gray-level histograms". In: *IEEE transactions on systems, man, and cybernetics* 9.1 (1979), pp. 62–66. [85] Jim Pitman. *Combinatorial stochastic processes*. Notes for Saint Flour Summer School. 2002.

[86] Jonathan D Power, Alexander L Cohen, Steven M Nelson, Gagan S Wig, Kelly Anne Barnes, Jessica A Church, Alecia C Vogel, Timothy O Laumann, Fran M Miezin, Bradley L Schlaggar, et al. "Functional network organization of the human brain". In: *Neuron* 72.4 (2011), pp. 665–678.

[87] Jonathan D Power, Damien A Fair, Bradley L Schlaggar, and Steven E Petersen. "The development of human functional brain networks". In: *Neuron* 67.5 (2010), pp. 735–748.

[88] Mikhail I Rabinovich, Alan N Simmons, and Pablo Varona. "Dynamical bridge between brain and mind". In: *Trends in cognitive sciences* 19.8 (2015), pp. 453–461.

[89] E. Salinas and T. J. Sejnowski. "Correlated neuronal activity and the flow of neural information". In: *Nat. Rev. Neurosci.* 2.8 (2001), pp. 539–550.

[90] R. Schmidt, K. J. LaFleur, M. A. de Reus, L. H. van den Berg, and M. P. van den Heuvel. "Kuramoto model simulation of neural hubs and dynamic synchrony in the human cerebral connectome". In: *BMC Neurosci* 16 (2015), p. 54.

[91] James M Shine, Patrick G Bissett, Peter T Bell, Oluwasanmi Koyejo, Joshua H Balsters, Krzysztof J Gorgolewski, Craig A Moodie, and Russell A Poldrack. "The Dynamics of Functional Brain Networks: Integrated Network States during Cognitive Task Performance". In: *Neuron* 92.2 (Oct. 2016), pp. 544–554.

[92] Linda B Smith and Esther Thelen. "Development as a dynamic system". In: *Trends in cognitive sciences* 7.8 (2003), pp. 343–348.

[93] Linda B Smith, Esther Thelen, Robert Titzer, and Dewey McLin. "Knowing in the context of acting: the task dynamics of the A-not-B error." In: *Psychological review* 106.2 (1999), pp. 235–260.

[94] Russell Smith and others. "Open dynamics engine". In: (2005).

[95] S. Solso, R. Xu, J. Proudfoot, D. J. Hagler, K. Campbell, V. Venkatraman, C. Carter Barnes, C. Ahrens-Barbeau, K. Pierce, A. Dale, L. Eyler, and E. Courchesne. "Diffusion Tensor Imaging Provides Evidence of Possible Axonal Overconnectivity in Frontal Lobes in Autism Spectrum Disorder Toddlers". In: *Biol. Psychiatry* 79.8 (2016), pp. 676–684.

[96] S. Song and L. F. Abbott. "Cortical development and remapping through spike timing-dependent plasticity". In: *Neuron* 32.2 (2001), pp. 339–350.

[97] S. Song, K. D. Miller, and L. F. Abbott. "Competitive Hebbian learning through spike-timing-dependent synaptic plasticity". In: *Nat. Neurosci.* 3.9 (2000), pp. 919–926.

[98] Sara Spadone, Stefania Della Penna, Carlo Sestieri, Viviana Betti, Annalisa Tosoni, Mauro Gianni Perrucci, Gian Luca Romani, and Maurizio Corbetta. "Dynamic reorganization of human resting-state networks during visuospatial attention". In: *Proceedings of the National Academy of Sciences* 112.26 (June 2015), pp. 8112–8117.

[99] A. J. Spittle, N. C. Brown, L. W. Doyle, R. N. Boyd, R. W. Hunt, M. Bear, and T. E. Inder. "Quality of general movements is related to white matter pathology in very preterm infants". In: *Pediatrics* 121.5 (2008), e1184–1189.

[100] O. Sporns, G. Tononi, and G. M. Edelman. "Theoretical neuroanatomy: relating anatomical and functional connectivity in graphs and cortical connection matrices". In: *Cereb. Cortex* 10.2 (2000), pp. 127–141.

[101] O. Sporns and J. D. Zwi. "The small world of the cerebral cortex". In: *Neuroinformatics* 2.2 (2004), pp. 145–162.

[102] Olaf Sporns and Jonathan D Zwi. "The small world of the cerebral cortex". In: *Neuroinformatics* 2.2 (2004), pp. 145–162.

[103] Cornelius J Stam. "Functional connectivity patterns of human magnetoencephalographic recordings: a 'small-world' network?" In: *Neuroscience letters* 355.1 (2004), pp. 25–28.

[104] H Supèr, E Soriano, and H B M Uylings. "The functions of the preplate in development and evolution of the neocortex and hippocampus". In: *Brain Research Reviews* 27.1 (1998), pp. 40–64. ISSN: 0165-0173.

[105] Gentaro Taga, Rieko Takaya, and Yukuo Konishi. "Analysis of general movements of infants towards understanding of developmental principle for motor control". In: *Systems, Man, and Cybernetics, 1999. IEEE SMC'99 Conference Proceedings. 1999 IEEE International Conference on*. Vol. 5. 1999, pp. 678–683.

[106] Jun Tani. *Exploring robotic minds: actions, symbols, and consciousness as self-organizing dynamic phenomena*. Oxford University Press, 2016.

[107] James TH Teo, Orlando BC Swayne, Binith Cheeran, Richard J Greenwood, and John C Rothwell. "Human theta burst stimulation enhances subsequent motor learning and increases performance variability". In: *Cerebral Cortex* 21.7 (2010), pp. 1627–1638.

[108] James Theiler, Stephen Eubank, André Longtin, Bryan Galdrikian, and J. Doyne Farmer. "Testing for nonlinearity in time series: the method of surrogate data". In: *Physica D: Nonlinear Phenomena* 58.1 (1992), pp. 77 –94. ISSN: 0167-2789.

[109] Esther Thelen and Linda B Smith. *A dynamic systems approach to the development of cognition and action*. MIT press, 1996.

[110] Esther Thelen, Gregor Schöner, Christian Scheier, and Linda B Smith. "The dynamics of embodiment: A field theory of infant perseverative reaching". In: *Behavioral and brain sciences* 24.01 (2001), pp. 1–34.

[111] Dardo Tomasi and Nora D Volkow. "Mapping small-world properties through development in the human brain: disruption in schizophrenia". In: *PloS one* 9.4 (2014), e96176.

[112] Ichiro Tsuda. "Hypotheses on the functional roles of chaotic transitory dynamics". In: *Chaos: An Interdisciplinary Journal of Nonlinear Science* 19.1 (2009), p. 015113.

[113] Ichiro Tsuda. "Toward an interpretation of dynamic neural activity in terms of chaotic dynamical systems". In: *Behavioral and Brain Sciences* 24.05 (2001), pp. 793–810.

[114] Ichiro Tsuda and Hiroshi Fujii. "Chaos reality in the brain". In: *Journal of integrative neuroscience* 6.02 (2007), pp. 309–326.

[115] Ichiro Tsuda, Hiroshi Fujii, Satoru Tadokoro, Takuo Yasuoka, and Yutaka Yamaguti. "Chaotic itinerancy as a mechanism of irregular changes between synchronization and desynchronization in a neural network". In: *Journal of integrative neuroscience* 3.02 (2004), pp. 159–182.

[116] Martijn P Van Den Heuvel and Hilleke E Hulshoff Pol. "Exploring the brain network: a review on resting-state fMRI functional connectivity". In: *European neuropsychopharmacology* 20.8 (2010), pp. 519–534.

[117] Martijn P Van Den Heuvel and Olaf Sporns. "Rich-club organization of the human connectome". In: *Journal of Neuroscience* 31.44 (2011), pp. 15775–15786.

[118] D. J. Watts and S. H. Strogatz. "Collective dynamics of 'small-world' networks". In: *Nature* 393.6684 (1998), pp. 440–442.

[119] Yasunori Yamada, Hoshinori Kanazawa, Sho Iwasaki, Yuki Tsukahara, Osuke Iwata, Shigehito Yamada, and Yasuo Kuniyoshi. "An Embodied Brain Model of the Human Foetus". In: *Scientific Reports* 6 (2016), p. 27893.

[120] Teruya Yamanishi, Jian-Qin Liu, Haruhiko Nishimura, and Sou Nobukawa. "Low-frequency in the Default Mode Brain Network from Spiking Neuron Model". In: *GSTF Journal on Computing (JoC)* 3.1 (2013), pp. 8–16.

[121] Lucia Zemanová, Changsong Zhou, and Jürgen Kurths. "Building a Large-Scale Computational Model of a Cortical Neuronal Network". In: *Lectures in Supercomputational Neurosciences: Dynamics in Complex Brain Networks*. Ed. by Peter beim Graben, Changsong Zhou, Marco Thiel, and Jürgen Kurths. Berlin, Heidelberg: Springer Berlin Heidelberg, 2008, pp. 251–266. ISBN: 978-3-540-73159-7.

Published Papers by the Author

Papers related to the thesis

Journal papers with review

1. Jihoon Park, Hiroki Mori, Yuji Okuyama, and Minoru Asada. Chaotic itinerancy within the coupled dynamics between a physical body and neural oscillator networks. PLOS ONE, Vol.12, No.8, e0182518, 2017.

2. Jihoon Park, Koki Ichinose, Yuji Kawai, Junichi Suzuki, Minoru Asada, and Hiroki Mori. Macroscopic Cluster Organizations Change the Complexity of Neural Activity. Entropy, 21(2), 2019.

Workshop and conference papers with review

1. Koki Ichinose, Jihoon Park, Yuji Kawai, Junichi Suzuki, Hiroki Mori, and Minoru Asada. Why does neural activity in ASD have low complexity?: from a perspective of a small-world network model. Proceedings of the 26th Annual Computational Neuroscience Meeting, 2017.

2. Koki Ichinose, Jihoon Park, Yuji Kawai, Junichi Suzuki, Minoru Asada, and Hiroki Mori. Local over-connectivity reduces the complexity of neural activity: toward a constructive understanding of brain networks of autism spectrum disorder. Proceedings of the 7th Joint IEEE International Conference on Development and Learning and on Epigenetic Robotics, pp.233–238, 2017.

Workshop and conference papers without review

1. Jihoon Park, Hiroki Mori, Minoru Asada. Graph analysis of information network within embodied system, The 2nd International Symposium on Cognitive Neuroscience Robotics, 2016.

2. Jihoon Park, Hiroki Mori and Minoru Asada. Analysis of causality network from interactions between nonlinear oscillator networks and musculoskeletal system, Late Breaking Proc. European Conf. on Artificial Life 2015, pp.25-26, 2015.

Other papers

Journal papers with review

1. Yuji Kawai, Jihoon Park, and Minoru Asada. A small-world topology enhances the echo state property and signal propagation in reservoir computing, Neural Networks, 112, 15–23, 2019.

International workshop and conference papers with review

1. Yuji Kawai, Tomohiro Takimoto, Jihoon Park, and Minoru Asada. Efficient reward-based learning through body representation in a spiking neural network. the 8th Joint IEEE International Conference on Development and Learning and on Epigenetic Robotics, pp.198–203, 2018.

2. Tomohiro Miki, Yuji Kawai, Jihoon Park, and Minoru Asada. Intrinsically bursting neurons enlarge timescales of fluctuations in firing rates. the 27th Annual Computational Neuroscience Meeting, 2018

3. Motohiro Ogura, Jihoon Park, Yuji Kawai, and Minoru Asada. An excitation / inhibition ratio impacts on organization of neural connectivity and information transfer. the 27th Annual Computational Neuroscience Meeting, 2018.

4. Tomohiro Takimoto, Yuji Kawai, Jihoon Park, and Minoru Asada. Self-organization based on auditory feedback promotes acquisition of babbling. Proceedings of the 7th Joint IEEE International Conference on Development and Learning and on Epigenetic Robotics, pp.120–125, 2017.

5. Yuji Kawai, Tatsuya Tokuno, Jihoon Park, and Minoru Asada. Echo in a small-world reservoir: time-series prediction using an economical recurrent neural

network. Proceedings of the 7th Joint IEEE International Conference on Development and Learning and on Epigenetic Robotics, pp.126–131, 2017.

6. Yuji Kawai, Jihoon Park, Takato Horii, Yuji Oshima, Kazuaki Tanaka, Hiroki Mori, Yukie Nagai, Takashi Takuma and Minoru Asada. Throwing Skill Optimization through Synchronization and Desynchronization of Degree of Freedom, RoboCup 2012: Robot Soccer World Cup XVI, Springer, pp.178-189, 2013.

Workshop and conference papers without review

1. Jihoon Park, Yuji Kawai, Minoru Asada. Neural representation of behavioral transitions emerged from an oscillator network, The 1st International Symposium on Systems Intelligence Division, 2017.

2. Jihoon Park, Yuji Kawai, Minoru Asada. Self-organization of a Network Structure and Emergence of Behaviors under Body Constraints in the Embodied System, The 1st International Symposium on Symbiotic Intelligent Systems, 2019

3. 河合祐〕, 瀧本友弘, 朴志勲, 浅田稔. スパイクニューラルネットワークの自己組織化と身体運動の相互作用を通した報酬学習. 第 32 回人工知能学会全国大会, 2L2-OS-6a-05, 2018.

4. 三宅智仁, 河合祐〕, 朴志勲, 島谷二郎, 高橋英之, 浅田稔. 人工物との共同作業における心の知覚と責任帰属の関係. 第 32 回人工知能学会全国大会, 1F2-OS-5a-02, 2018.

5. 立川和樹, 河合祐〕, 朴志勲, 浅田稔. 脳波特徴の階層性を利用した効率的なシャープしイ値推定による脳波識別の根拠の定量化. 第 32 回人工知能学会全 国大会, 1N2-05, 2018.

6. 河合祐〕, 朴志勲, 浅田稔. スモールワールド性を有するエコース子ートネットワークのロバストな記憶容量. 電子情報通信学会 ニューロコンピュー子イング研究会, pp.1–6, 2017.

7. 瀧本友弘, 河合祐〕, 朴志勲, 浅田稔. 聴覚フイードバックに基づくスパイク神経網の自己組織化による南語獲得の促進. 電子情報通信学会 ニューロコンビュー子イング研究会, pp.7–12, 2017.

8. 一瀬公輝, 朴志勲, 河合祐〕, 鈴木淳一, 森裕紀, 浅田稔. 大域-局所の結合のバランスか神経活動の複雑性に与える影響 自閉スペクトラム症における特異な神 経活動の構成論的考案. 電子情報通信学会 ニューロコンビュー子イング研究会, pp.13–18, 2017.

9. 立川和樹, 河合祐〕, 朴志勲, 高橋哲也, 池田尊〕, 吉村優子, 菊知充, 浅田稔. 深層学習を用いた脳磁図計測による子どもの自閉スペクトラム症識別. 日本神経発達科学学会 第 6 回学術集会, pp.28, 2017.

10. 朴志勲，森裕紀, 浅田稔・非線形振動子ネットワークと身体の相互作用から現れるダイ十ミクな情報的ネットワーク. 日本発達神経科学学会第 4 回学術集会, 2015.

11. Jihoon Park, Yuji Kawai, Takato Horii, Yuji Oshima, Kazuaki Tanakam, Hiroki Mori, Yukie Nagai, Takashi Takuma and Minoru Asada, Differentiation within Coordination in Acquisition of skilled Throwing. 第 35 回人工知能学会 AI チャ しンジ研究会, pp.19 — 24, 2012.

Awards

1. Babybot Challenge Paper Award, ICDL-EpiRob 2018
2. 人工知能学会 全国大会優秀賞, 第 32 回人工知能学会全国大会, 2018
3. Babybot Challenge participation award, ICDL-EpiRob 2017
4. 人工知能学会研究会優秀賞，2013 年度人工知能学会全国大会, 2013
5. 日本ロボット学会特別賞，RoboCup JapanOpen 2013, 2013